

Editor-in-Chief B.E.Paton

Editorial board:

Yu.S.Borisov V.F.Grabin
Yu.Ya.Gretskii A.Ya.Ishchenko
B.V.Khitrovskaya V.F.Khorunov
I.V.Krivtsun
S.I.Kuchuk-Yatsenko
Yu.N.Lankin V.K.Lebedev
V.N.Lipodaev L.M.Lobanov
V.I.Makhnenko A.A.Mazur
V.F.Moshkin O.K.Nazarenko
I.K.Pokhodnya I.A.Ryabtsev
Yu.A.Sterenbogen N.M.Voropai
K.A.Yushchenko V.N.Zamkov
A.T.Zelnichenko

International editorial council:

N.P.Alyoshin (Russia)
B.Braithwaite (UK)
C.Boucher (France)
Guan Qiao (China)
U.Diltey (Germany)
P.Seyffarth (Germany)
A.S.Zubchenko (Russia)
T.Eagar (USA)
K.Inoue (Japan)
N.I.Nikiforov (Russia)
B.E.Paton (Ukraine)
Ya.Pilarczyk (Poland)
D. von Hofe (Germany)
Zhang Yanmin (China)
V.K.Sheleg (Belarus)

Promotion group:

V.N.Lipodaev, V.I.Lokteva
A.T.Zelnichenko (exec. director)
Translators:
A.V.Gorskaya, Fomina S.A.,
I.N.Kutianova, T.K.Vasilenko
Editor
N.A.Dmitrieva
Electron galley:
I.S.Batasheva, T.Yu.Snegiryova

Address:

E.O. Paton Electric Welding Institute,
International Association «Welding»,
11, Bozhenko str., 03680, Kyiv, Ukraine
Tel.: (38044) 287 67 57
Fax: (38044) 528 04 86
E-mail: journal@paton.kiev.ua
http://www.nas.gov.ua/pwj

State Registration Certificate
KV 4790 of 09.01.2001

Subscriptions:

\$324, 12 issues per year,
postage and packaging included.
Back issues available.

All rights reserved.

This publication and each of the articles
contained herein are protected by copyright.
Permission to reproduce material contained in
this journal must be obtained in writing from
the Publisher.

Copies of individual articles may be obtained
from the Publisher.

CONTENTS

SCIENTIFIC AND TECHNICAL

**Yushchenko K.A., Savchenko V.S., Chervyakova L.V.,
David S. and Vitek J.** Investigation of weldability of nickel
superalloys and development of repair technology for gas
turbine blades 2

Borisov Yu.S., Zatserkovny A.S. and Krivtsun I.V.
Convective-conductive and radiation heat exchange of
plasma flow with particles of dispersed materials in plasma
spraying 6

**Pentegov I.V., Petrienko O.I., Pustovojt S.V.,
Sidorets V.N. and Lavrenyuk A.V.** Determination of
voltage drop in the area of electrode wire contact with the
welding torch nozzle under mechanized methods of arc
welding 10

**Shlepakov V.N., Kotelchuk A.S., Naumejko S.M. and
Bilinets A.V.** Influence of the composition of flux-cored
wire core and shielding gas on the stability of arc welding
process 16

**Shejko P.P., Zhernosekov A.M., Lozovskaya A.V. and
Shimanovsky Yu.O.** Application of a two-channel system
of automatic stabilization of pulsed-arc welding to improve
the welded joint quality 21

Ryzhov R.N. and Kuznetsov V.D. Choice of optimal
parameters of external electromagnetic action in arc
methods of welding 24

INDUSTRIAL

Bernadsky V.N. Steel and welding in construction
engineering 28

Ryabtsev I.A. High-efficiency wide-layer surfacing using
electrode wires and strips (Review) 31

Matveev V.V. Surfacing of train wheel flanges after
annealing of the tread surface in car-repair plants of
Ukraine 36

Skulsky V.Yu. and Moravetsky S.I. Filler materials for
automatic submerged-arc welding of heat-resistant
9 % Cr steels 42

BRIEF INFORMATION

**Orlov L.N., Golyakevich A.A., Upyr V.N. and
Giyuk S.P.** Flux-cored wire for welding in shipbuilding 44

Thesis for a candidate of technical sciences degree 45

NEWS 46



INVESTIGATION OF WELDABILITY OF NICKEL SUPERALLOYS AND DEVELOPMENT OF REPAIR TECHNOLOGY FOR GAS TURBINE BLADES

K.A. YUSHCHENKO¹, V.S. SAVCHENKO¹, L.V. CHERVYAKOVA¹, S. DAVID² and J. VITEK²

¹E.O. Paton Electric Welding Institute, NASU, Kiev, Ukraine

²Oak Ridge National Laboratory, Oak Ridge, USA

The paper describes studies on evaluation of weldability of nickel-base superalloys applied in manufacture of gas turbine blades. The content of the strengthening γ -phase in the alloys reaches 60 %. A technology is proposed for repair of blades by plasma powder cladding.

Keywords: plasma powder cladding, nickel superalloys, gas turbine blades, strengthening γ -phase, ductility dip, repair technology

Nickel-base superalloys characterised by high mechanical properties at high temperatures are the key alloys used to manufacture gas turbine engines. As requirements to service temperature of engines have been greatly increased in the last years, modifications of alloys have led to increase (more than 45 %) in the strengthening γ -phase content of microstructure of nickel alloys. Having a satisfactory performance, these materials feature poor weldability (they are sensitive to hot cracking during welding and heat treatment).

This study was conducted under the Ukrainian-American Partnership Project «Welding and Brazing for Repair of Aircraft and Ground Gas Turbine Components» funded by the Science and Technology Centre in Ukraine. The Project participants were the United States Department of Energy's Oak Ridge National Laboratory (Oak Ridge, Tennessee), Pratt & Whitney-Paton (Kiev, Ukraine), E.O. Paton Electric Welding Institute (Kiev, Ukraine) and International Association INTERM (Kiev, Ukraine).

The goal of the Project was to improve and apply technologies for repair welding and brazing of components of nickel-base superalloys used to manufacture ground gas turbines and aircraft engines, thus

leading to reduction of costs for their reconditioning and manufacture. Alloys ChS-70 and JS-26 used currently to manufacture blades of ground gas turbine plants and aircraft engines were chosen for the studies.

Alloy ChS-70 is a nickel-base superalloy strengthened by the γ -phase, the content of which amounts to 50–55 %. Casting provides an equiaxed structure of the alloy, which guarantees high strength properties (including at increased temperatures) after appropriate heat treatment (austenising and ageing).

Alloy JS-26 is a nickel-base alloy with a high content of γ -forming elements. Mean content of the γ -phase reaches 60–65 %. The special casting technology provides oriented solidification of blades. Heat treatment consists of austenising to eliminate interdendritic heterogeneity (at 1265 °C) and ageing. Ageing results in formation of γ -phases with the fcc lattice and optimal size of 0.3–0.5 μm , primarily of a cubic form.

Chemical composition and mechanical properties of alloys ChS-70 and JS-26 are given in the Table. Nickel superalloys are multicomponent materials containing a number of elements that have a limited solubility in γ -solid solution. Substantial chemical heterogeneity of metal and development of thermal-deformation processes lead to formation of defects of the type of hot cracks in fusion welding of the alloys [1]. Dynamic deformation of welded specimens using the Vareststraint Test type machine was employed for quantitative evaluation of weldability [2]. In this case it is possible to evaluate ductility of the weld metal within a temperature range from solidification to room temperature. The generalising curve of variations in ductility is shown in Figure 1. Given that structural elements of the materials under consideration can be formed only in casting and have limited sizes, the studies were conducted on composite specimens.

Appearance of a working unit of the machine used to conduct experiments on evaluation of weldability of the alloys is shown in Figure 2. Thickness of the test specimens was 1.7 mm. The TIG welding method under the following conditions: $I_w = 70 \text{ A}$, $U_a =$

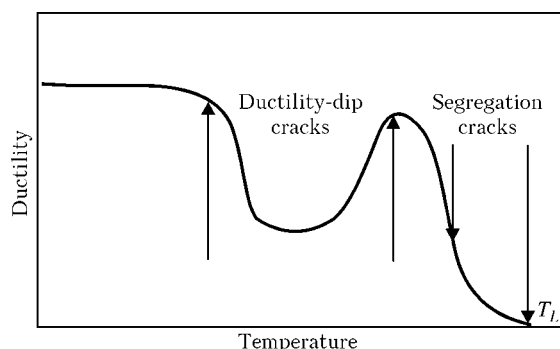


Figure 1. Temperature dependence of ductility of the weld metal with zones of segregation and ductility-dip cracks



Chemical composition and mechanical properties of alloys ChS-70 and JS-26 in short-time tension

Alloy grade	Content of elements, wt. %											
	Ni	C	Cr	Co	Mo	W	Al	Ti	Nb	Ce	Fe	B
ChS-70	Base	0.60–0.12	15.0–16.7	9.5–12.5	1.5–2.5	4.5–6.5	2.4–3.2	4.2–5.0	0.10–0.25	0.050	≤ 0.8	≤ 0.2
JS-26	Same	0.13–1.18	4.3–5.6	8.0–10.0	0.8–1.4	10.9–12.5	5.5–6.2	0.8–1.2	1.1–1.8	0.025	1.0	0.015

Cont.

Alloy grade	$T_{test}, ^\circ C$	Mechanical properties			
		σ_v, MPa	σ_y, MPa	$\delta_5, \%$	$\psi, \%$
ChS-70	20	850	750	3	ND
	600	960	ND	6	9.3
	900	ND	Same	ND	ND
JS-26	20	860–930	790	8–16	11–13
	800	910–1030	760–890	8–18	9–20
	900	850–880	840	16–21	19–23

= 10.5 V, $v_w = 8.5$ m/h, and argon flow rate --- 10 l/min, was used for penetration of the specimens during the tests.

Cast specimens of alloy JS-26 with oriented solidification used for the investigations contained single crystal with orientation {001} in the weld and HAZ metal. High-temperature mechanical properties of the metal were evaluated using the ALA-TOO machine, the principle of operation of which is similar to the Gleeble type testing machine.

The tests were conducted in a vacuum chamber. Appearance of a specimen after the tests is shown in

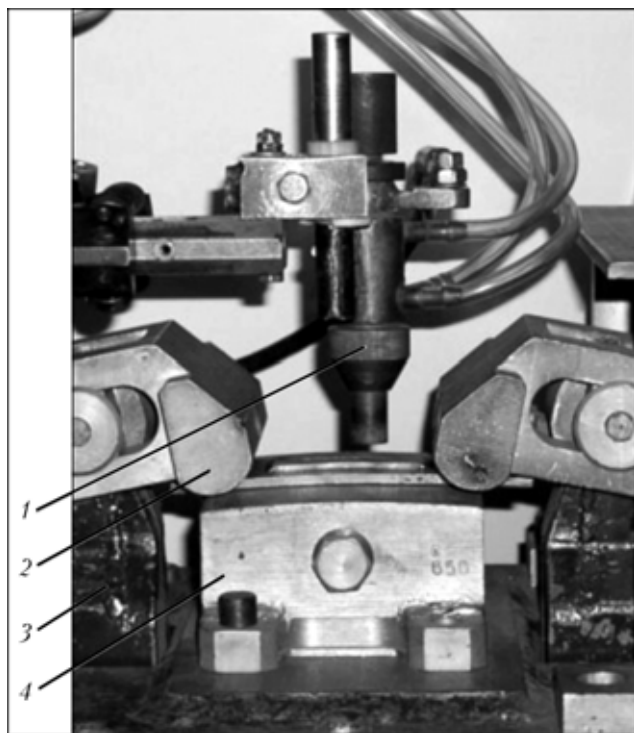


Figure 2. Appearance of the working unit of testing machine (mandrel for bending with a radius of 650 mm) and composite specimen: 1 --- TIG torch; 2 --- clamp; 3 --- specimen; 4 --- mandrel

Figure 3. The gauge part of specimens of the materials studied was welded into flat grips. This design of a specimen makes it possible to evaluate, if necessary, properties of metal of a real airfoil. Examinations of the used blades were conducted by subjecting them to preliminary restoration heat treatment, thus evaluating weldability of their metal.

The most important characteristic determining kinetics of thermal-deformation state within the weld pool region is a linear thermal expansion coefficient of metal, which affects its volumetric changes in heating and residual stresses. The linear thermal expansion coefficient was estimated using a specialised dilatometry unit by the non-contact method, which ensures high accuracy of measurements at temperatures of up to a melting point.



Figure 3. Appearance of ChS-70 specimen after high-temperature tests

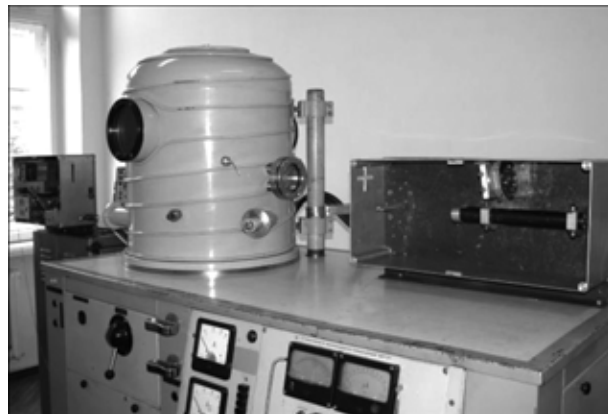


Figure 4. General view of the unit to study linear thermal expansion of metals

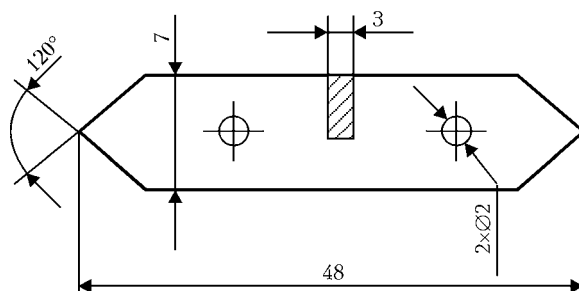


Figure 5. Schematic of specimen for dilatometry examinations

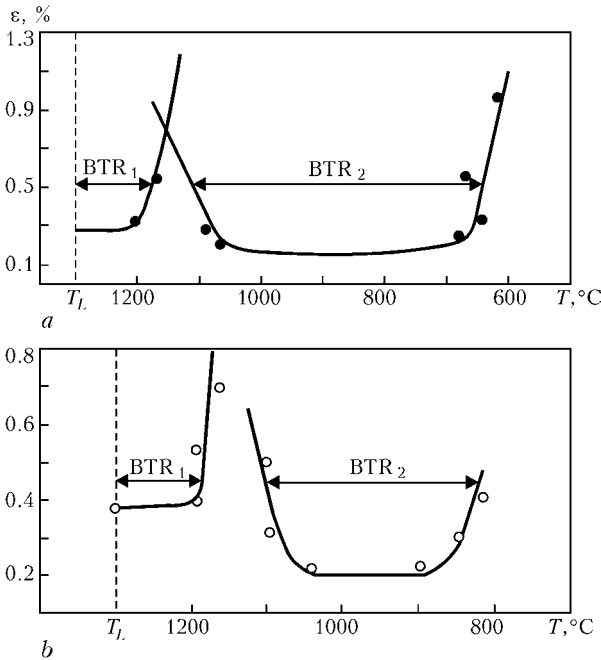


Figure 6. Brittle high- (BTR₁) and low-temperature (BTR₂) ranges for alloys ChS-70 (a) and JS-26 (b)

Appearance of the unit and schematic of a specimen for dilatometry examinations are shown in Figures 4 and 5, respectively. Brittle temperature ranges (BTR) were determined as a result of metallography performed by the optical and electron scanning microscopy methods for alloys ChS-70 and JS-26 (Figure 6). Analysis of the curves plotted for alloy ChS-70 with equiaxed structure shows the trends to increase of critical deformation value in BTR₁. Weldability of the alloy in this case determines behaviour of the weld metal in BTR₂. This peculiarity is even more pro-

nounced for alloy JS-26 in evaluation of its weldability. Moreover, the threshold values of deformation in BTR₁ and BTR₂ for alloy JS-26 are higher than the corresponding parameters of alloy ChS-70, despite a more complex alloying system of alloy JS-26. Supposedly, this is associated with solidification conditions of both alloys. On alloy ChS-70 with an equiaxed structure, the weld has a conventional structure of equiaxed crystals with elongated grains that grow from half-fused grains of the base metal. Here the high-angle grain boundaries are present, which are the preferential propagation paths for hot cracks.

In welding alloy JS-26 with an oriented structure, where the weld zone is practically a single crystal, the weld inherits structure of the base metal. The grain boundaries acting as sources of intergranular brittle fracture are absent [3, 4]. This results in increase of ductility of the weld metal in BTR₁ and BTR₂. Characteristic structures of the weld metal proving these assumptions are shown in Figure 7. They are additionally confirmed by comparative studies of high-temperature mechanical properties of the weld metal (Figure 8) in ChS-70 and JS-26 welded joints performed by using the Gleeble type testing machine ALA-TOO.

The tests performed on the alloys studied by depositing beads on plates 5 × 50 × 80 mm in size show that alloy JS-26 is less sensitive to hot cracking, compared with alloy ChS-70, which is proved by the data on weldability of these alloys.

Large scope of investigations under the Project was dedicated to computer modelling of thermal-deformation processes occurring in weld regions during welding of nickel superalloys ChS-70 and JS-26, as well as contribution to the dynamics of changes in

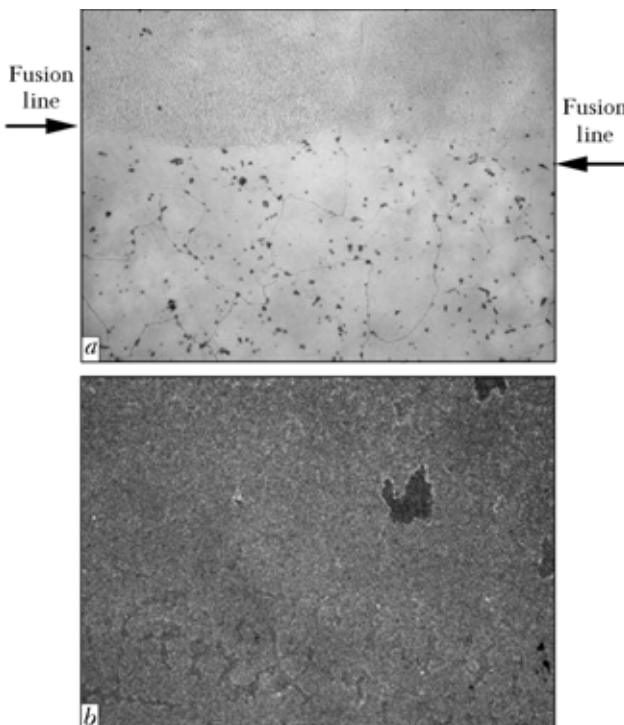


Figure 7. Microstructure of weld metal on alloys ChS-70 (a) and JS-26 (b) (×100)

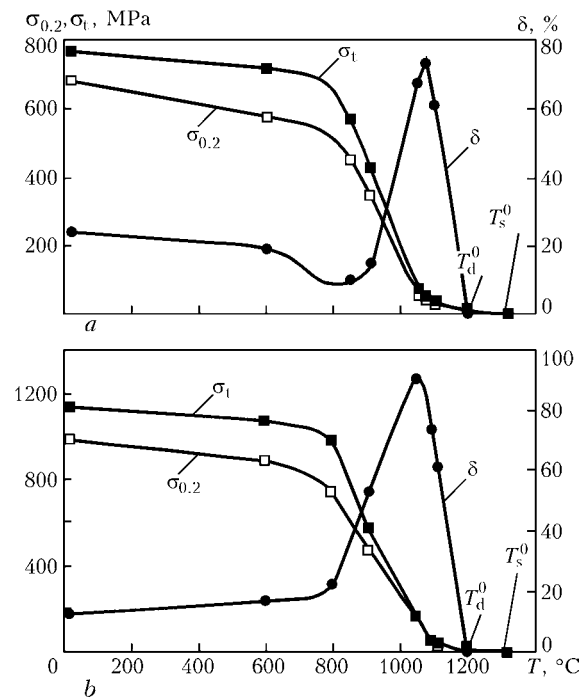


Figure 8. Temperature dependence of strength and ductility of the weld metal in joints on alloys ChS-70 (a) and JS-26 (b) (T_s^0 , T_d^0 — zero strength and zero ductility temperatures, respectively)



such processes by structural transformations in the HAZ metal. Structural examinations were conducted using a high-temperature laser dilatometer.

Results of measurement of the thermal expansion coefficient of the alloys show that $\gamma \rightarrow \gamma' \rightarrow \gamma$ transformations accompanied by increase in volume contribute greatly to thermal expansion of metal during heating. This mechanism is possible to occur, provided that interplanar spacings of the γ' -phase are smaller than the corresponding parameters of the matrix with austenitic structure. Maximal values of the thermal expansion coefficient at temperatures close to T_S are $60 \cdot 10^{-6}$ and $44 \cdot 10^{-6} \text{ K}^{-1}$ for alloys ChS-70 and JS-26, respectively. These real values markedly exceed the table data and determine development of substantial elasto-plastic strains.

These strains were computed using the PWI software, which allows for the values of real physical properties, including the above values of the thermal expansion coefficient. The computations were made for superalloy ChS-70 and, to compare, for stable austenitic high-alloy steel that experiences no phase transformations in heating and cooling. Analysis of the results shows that substantial plastic strains develop in the HAZ metal under the effect of the thermal welding cycle, and that the total value of these strains allowing for the biaxial stressed state may exceed the values of ductility of the alloy and lead to cracking during welding [5].

Repair welding was tried out on gas turbine blades of alloy ChS-70 (Figure 9). Examinations of microstructure of the deposited metal revealed no defects. Mechanical tests of the repaired regions of model samples showed that properties of the weld metal were close to those of the base metal.

A sample batch of the blades repaired by the developed technology was subjected to cyclic tests using the dynamic rig to determine fatigue limit of these blades. Fatigue tests conducted at a resonance frequency of airfoil proved a good performance of the repaired blades.

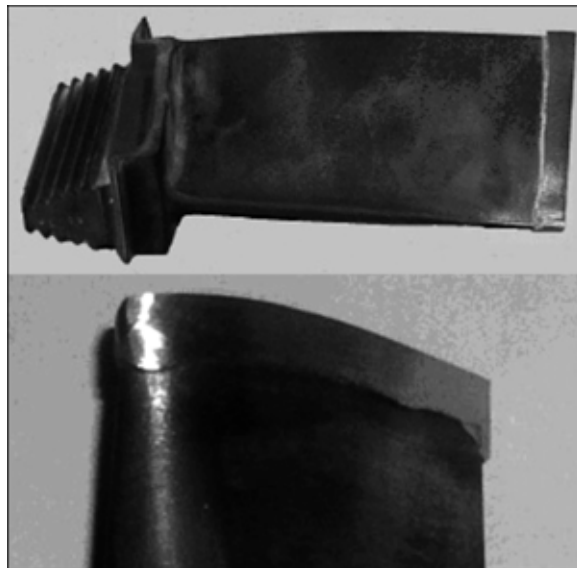


Figure 9. Appearance of gas turbine blades after repair welding

CONCLUSIONS

1. Investigations of weldability of nickel-base superalloys were conducted on gas turbine blades.
2. Commercial technology was developed to repair gas turbine blades using plasma powder cladding.

Acknowledgement. Participants of the Project express their special gratitude to associates of the Science and Technology Centre in Ukraine for their sustained support in accomplishment of this Project.

1. Sims, C.T., Stoloff, N.S., Hagel, W.C. (1995) *Superalloys II*. New York: Wiley-Interscience Publ.
2. Savage, W.F., Lundin, G.D. (1965) The Varestreint test. *Welding J.*, 44(10), 433–442.
3. Bukhanova, A.A., Toloraja, V.N. (1984) On structure and properties of single crystals of heat-resistant nickel-base alloys. In: *High-temperature and heat-resistant steels and nickel-base alloys*. Moscow: Nauka.
4. Park, I.W., Babu, S.S., Vitek, I.M. et al. (2003) Stray grain formation in single crystal Ni-base superalloy welds. *J. Appl. Phys.*, 94(6), 4203–4209.
5. Savchenko, V.S., Yushchenko, K.A., Makhnenko, V.I. et al. (1993) Effect of physical characteristics of cast heat-resistant nickel alloys on development of thermal-deformation processes in fusion welding. *Avtomatich. Svarka*, 11, 6–9.



CONVECTIVE-CONDUCTIVE AND RADIATION HEAT EXCHANGE OF PLASMA FLOW WITH PARTICLES OF DISPERSED MATERIALS IN PLASMA SPRAYING

Yu.S. BORISOV, A.S. ZATSERKOVNY and I.V. KRIVTSUN

E.O. Paton Electric Welding Institute, NASU, Kiev, Ukraine

Physical processes are described, which determine the thermal impact of the plasma jet on dispersed material particles in plasma spraying of coatings. Various criterial dependencies are analysed, which are used for calculation of the convective-conductive component of the heat flow through the surface of a spherical particle in the flow of a low-temperature plasma at atmospheric pressure. A procedure is proposed for calculation of characteristics of radiation heat exchange of dense plasma with the metal particle surface. Numerical analysis of the considered components of the heat flow into a particle has been conducted in a broad range of parameters of a non-disturbed plasma flow (argon plasma) and temperature of the particle (aluminium) surface. It is shown that the radiation heat exchange has a significant influence on the resulting heat flow through the surface of a spraying particle.

Keywords: plasma spraying, dispersed material, particle, plasma jet, plasma, heat exchange, heat flow, radiation

Complexity of an experimental study of processes occurring in the plasma jet–dispersed material system during plasma spraying of coatings leads to the need to theoretically investigate and numerically analyse the set of factors that determine the thermal and dynamic impact on particles of a spraying material by the flow of ionised gas (plasma). Many approaches and models for calculation of the heat flow from plasma into an individual particle it surrounds are available. They allow for different mechanisms of heat exchange within the system considered [1–5]. The choice of this or that model of heat exchange providing an acceptable agreement between the calculation and experimental data is based in many respects on pressure, temperature and velocity of the oncoming plasma flow, temperature of the surface of particle, its shape and size. Under the plasma spraying conditions, these characteristics may undergo substantial changes as the spraying particle moves in the plasma jet. As a result, the contribution of each heat exchange mechanism to the resulting heat flow from plasma to the particle surface may substantially change with the spraying distance. Therefore, it is of interest to conduct comparative analysis of these mechanisms over a broad range of variations in temperature of plasma and, hence, the degree of its ionisation and particle temperature, as well as their relative velocities.

The purpose of this study is to analyse individual processes of thermal impact on a particle of the dispersed material by the ionised gas flow for the ranges of temperatures of plasma (from 3,000 to 15,000 K) and particle surface (from room temperature to a material boiling point or higher), as well as relative rates of these processes (from 0 to 600 m/s) that are characteristic of the sub-sonic plasma spraying conditions.

Consider the basic mechanisms of energy exchange between the isothermal atmospheric-pressure plasma

flow and spherical particle of the dispersed material placed into it. Assume that radius of the particle, a , is much larger than characteristic length of free path, $\bar{\lambda}$, of particles of the surrounding plasma (Knudsen number $Kn = \bar{\lambda}/a \ll 1$). For example, this condition is met at $a > 25 \mu\text{m}$ for the atmospheric-pressure argon plasma with a temperature of about 10,000 K [2]. Under the conditions under consideration the energy exchange between the plasma and dispersed material particle is determined by a combination of the following physical processes:

- convective-conductive heat exchange of the on-going flow with the particle surface caused by transfer of the energy of heat (chaotic) motion of the plasma particles to the material surface;
- exchange of the heat radiation energy between the plasma and particle;
- transfer to the material surface of the potential energy of charged particles of the plasma (energy released in ion recombination), energy of a directed movement of electrons reaching the surface, as well as additional kinetic energy of ions, which they acquire in the electric field formed near the particle surface;
- and cooling of the particle surface due to entraining the energy of evaporation of atoms of the particle material with the vapour flow.

In a case of flow of the molecular gas plasma around the particle, it is necessary to allow also for the transfer of the potential energy of gas atoms released in formation of molecules to the material surface. If further on the consideration is limited to atomic (inert) gas plasma, the local energy balance of a spherical particle in the plasma flow can be written down as follows:

$$-\left(\chi_m \frac{\partial T_m}{\partial r}\right)_{r=a} = Q_c + Q_r + Q_i + Q_e - Q_v,$$

where χ_m is the thermal conductivity coefficient of a particle material; $T_m(r)$ is the temperature field in



the particle which is assumed to be spherically symmetric; r is the distance from the particle centre; Q_c is the convective-conductive heat flow from plasma to the particle; Q_r is the resulting density of the thermal radiation energy flow (it is assumed that thermal radiation of plasma is absorbed in a thin sub-surface layer of the particle material); Q_i and Q_e are the densities of the flows of energy carried to the particle surface by plasma ions and electrons, respectively; and Q_v is the density of the flow of the evaporation energy carried from the particle surface by a vapour jet.

Study the convective-conductive and radiation heat exchange in the system under consideration. When describing the convective-conductive component of heat exchange, the plasma can be regarded as a continuum characterised at a preset temperature by certain values of thermal-physical parameters and transfer coefficients. In this case, the Newton model of heat exchange can be used to calculate Q_c [6]:

$$Q_c = \alpha(T_p - T_{ms}), \quad (1)$$

where α is the heat exchange coefficient; T_p is the temperature of the non-disturbed plasma flow; and T_{ms} is the temperature of the particle surface.

The heat exchange coefficient for a spherical particle can be calculated provided that the Nusselt number is known [7]:

$$Nu = (\alpha d) / \chi, \quad (2)$$

where $d = 2a$ is the particle diameter; and χ is the thermal conductivity coefficient of plasma calculated at a temperature of the non-disturbed flow.

There are many criterial dependencies which can be used to determine the Nusselt number (e.g. [8]), and they may differ under the same conditions of a flow around a particle. The most characteristic of them can be written down in the following generalised form:

$$Nu = A + BRe^m Pr^n, \quad (3)$$

where Re is the Reynolds number having the form of $(\rho u d) / \eta$; Pr is the Prandtl number having the form of $(C_p \eta) / \chi$; u is the non-disturbed velocity of the plasma flow with respect to a particle; ρ , η and C_p are the density, coefficient of dynamic viscosity and specific heat of plasma at a temperature of the non-disturbed flow, respectively. The augend in the right part of expression (3) describes the heat exchange between the plasma and particle due to a conductive transfer, while the addend describes that due to a convective transfer of energy of thermal movement of the plasma particles. Values A and B , as well as exponents m and n at the Re and Pr numbers, vary over rather broad ranges [1, 8]. For example, the following criterial dependence is suggested in study [9]:

$$Nu = 2 + 0.6Re^{1/2} Pr^{1/3}, \quad (4)$$

which provides a good description of the convective-conductive heat exchange for the system under con-

sideration at a small difference between the temperature of the non-disturbed plasma flow and that of the particle surface. Study [1] suggests that a correction allowing for variations in density and viscosity of the plasma through thickness of the thermal boundary layer around a particle should be added to the convective component of the given dependence to estimate the Nu number at a substantial difference between T_p and T_{ms} and high values of velocity of the ongoing flow ($Re = 45$):

$$Nu = 2 + 0.6Re^{1/2} Pr^{1/3} \left(\frac{\rho \eta}{\rho_s \eta_s} \right)^{0.2}, \quad (5)$$

while study [10] suggests that such a correction should be used for entire expression (4):

$$Nu = (2 + 0.6Re^{1/2} Pr^{1/3}) \left(\frac{\rho \eta}{\rho_s \eta_s} \right)^{0.6}. \quad (6)$$

Here and below the values with index s stand for the corresponding properties of the plasma determined at a temperature of the particle surface.

Analysis of heating of spherical particles in a high-temperature plasma flow conducted in [1, 11] shows that expressions (4) and (5) for a range of low values of the Re number can yield overstated values of the Nu number, compared with the values determined experimentally. The cause is a substantial variation of the thermal conductivity coefficient of the plasma that determines the conductive heat exchange within the limits of the boundary thermal layer. To eliminate this inaccuracy, study [1] suggests adding a correction to the conductive component of criterial dependence (5) in the form of a ratio of the thermal conductivity coefficients of the plasma at a temperature of the particle surface to that of the non-disturbed flow:

$$Nu = 2 \frac{\chi_s}{\chi} + 0.6Re^{1/2} Pr^{1/3} \left(\frac{\rho \eta}{\rho_s \eta_s} \right)^{0.2}. \quad (7)$$

Similar dependence derived on the basis of processing of the experimental data on a transverse flow of the atmospheric-pressure argon plasma around cylinders and spheres was suggested earlier in study [11]:

$$Nu = 2 \frac{\chi_s}{\chi} + 0.5Re^{0.5} Pr^{0.4} \left(\frac{\rho \eta}{\rho_s \eta_s} \right)^{0.2}. \quad (8)$$

Figures 1--3 show the results of numerical analysis of dependencies of heat flow Q_c introduced into a particle with radius $a = 30 \mu m$ by the isothermal atmospheric-pressure argon plasma upon the temperature and velocity of the non-disturbed plasma flow, as well as upon the temperature of the particle surface. Calculations were made on the basis of (1) and (2) using different forms of writing of the Nu number, (4)--(8), and the required values of thermal-physical properties and transfer coefficients for the argon plasma were taken from study [12]. The resulting calculation data show that at a small difference in values of T_p and T_{ms} all of the above criterial dependencies yield low and similar values of the heat flow

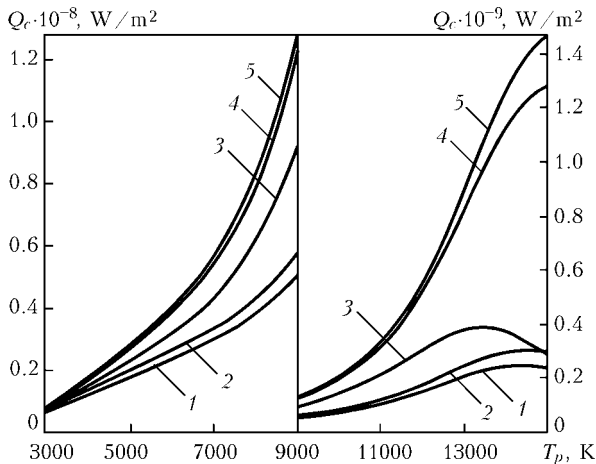


Figure 1. Dependence of convective-conductive component of heat flow to a particle upon the temperature of plasma at $u = 300$ m/s and $T_{ms} = 2,000$ K calculated on the basis of different expressions for Nu number: 1 — formula (8); 2 — (7); 3 — (6); 4 — (5); 5 — (4)

to a particle (see Figure 1). The values of Q_c first increase with increase in difference between the T_p and T_{ms} temperatures. Then the calculated values of the heat flow decrease to some extent when using criterial dependencies (6)–(8), the effect of correction coefficients in formulae (5)–(8) on Q_c being substantial (see Figures 1 and 3). This is associated with considerable variations in density, thermal conductivity coefficients and dynamic viscosity of argon within the considered range of variations in T_{ms} and T_p . As far as u is concerned, increase in this value is accompanied by a monotonous increase in values of the heat flow to a particle that occurs approximately identically for all of the considered forms of writing of the Nu number (see Figure 2). Further on in this study, Q_c was calculated using criterial dependence (8), which yields the best agreement with the experimental data for the case of flow of the argon plasma around a particle [11].

Thermal-physical processes in plasma spraying occur over a temperature range where the radiation heat exchange between the plasma jet and particles of a spraying material may play an important role. Consider this component of energy exchange allowing for the earlier assumption that the radiation of plasma falling on a particle is absorbed in a thin sub-surface

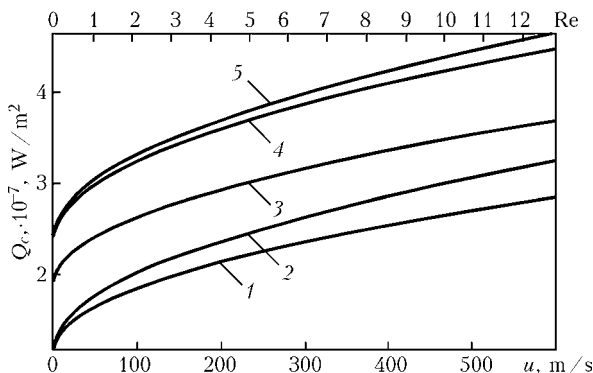


Figure 2. Dependence of convective-conductive component of heat flow upon the velocity of plasma relative to a particle at $T_p = 6,000$ K and $T_{ms} = 2,000$ K (see designations in Figure 1)

layer of its material (this assumption is justifiable, e.g. for metallic particles with a radius of more than $1 \mu\text{m}$ [13]). In the case under consideration, Q_r can be calculated using the following known relationship [6]:

$$Q_r = \xi \sigma_0 (T_p^4 - T_{ms}^4), \quad (9)$$

where ξ is the reduced emissivity, averaged over the thermal radiation spectrum, for the plasma-particle surface system; and σ_0 is the Stefan-Boltzmann constant.

The formula of study [14], describing the radiation heat exchange between two surfaces, i.e. metal surface that can be considered almost flat and having temperature T_{ms} under the considered conditions ($a > 25 \mu\text{m}$), and adjoining plasma surface assumed to be half-bounded and space-homogeneous, having temperature T_p , can be used to estimate the reduced emissivity ξ determining the efficiency of the radiation heat exchange between the dense plasma (atmospheric-pressure plasma) and a metal particle placed into it:

$$Q_r = \frac{\bar{h}}{4\delta^3 c^2} \int_0^\infty \hat{h}_u \hat{u}^3 \left[\frac{1}{\exp\left(\frac{\bar{h}\hat{u}}{kT_p}\right) - 1} - \frac{1}{\exp\left(\frac{\bar{h}\hat{u}}{kT_{ms}}\right) - 1} \right] d\hat{u}, \quad (10)$$

where \bar{h} is the Plank constant divided by 2π ; c is the velocity of light; ω is the radiation frequency; k is the Boltzmann constant; and ξ_ω is the spectral distribution of the reduced emissivity, which can be determined using the following relationship for the case of two plane-parallel surfaces:

$$\hat{h}_u = \int_0^{\delta/2} (\hat{h}_u^\perp + \hat{h}_u^\parallel) \cos J \sin J dJ, \quad (11)$$

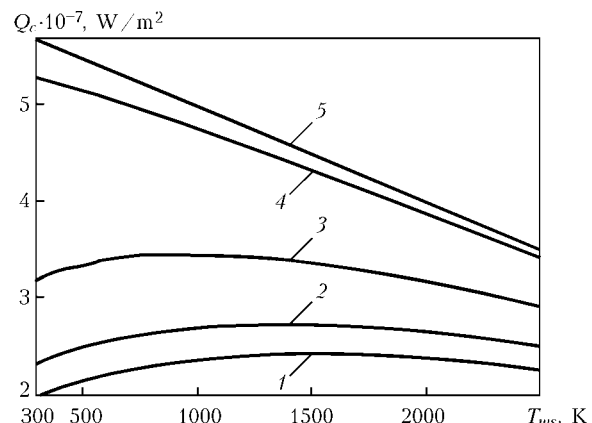


Figure 3. Dependence of convective-conductive component of heat flow to a particle upon the temperature of its surface at $T_p = 6,000$ K and $u = 300$ m/s (see designations in Figure 1)



where

$$\mathbf{x}_{\dot{u}}^{\perp, \parallel} = \frac{\Gamma_{m \dot{u}}^{\perp, \parallel} \Gamma_{p \dot{u}}^{\perp, \parallel}}{\Gamma_{m \dot{u}}^{\perp, \parallel} + \Gamma_{p \dot{u}}^{\perp, \parallel} - \Gamma_{m \dot{u}}^{\perp, \parallel} \Gamma_{p \dot{u}}^{\perp, \parallel}} \quad [15];$$

ϑ is the incidence angle; $\Gamma_{m, p \dot{u}}^{\perp, \parallel}(T_{ms}, p, \mathbf{J})$ are the coefficients of absorption of plane electromagnetic waves by the half-bounded isotropic plasma-like medium (index m stands for metal, and index p stands for plasma), corresponding to the above values of temperature and incidence angle, for two independent polarisations which are calculated as [15]:

$$\Gamma_{m, p \dot{u}}^{\perp, \parallel} = - \frac{4 \operatorname{Re}(r_{m, p \dot{u}}^{\perp, \parallel})}{|1 - r_{m, p \dot{u}}^{\perp, \parallel}|^2}, \quad (12)$$

signs \perp and \parallel corresponding to the case of incidence of a wave with the electric field vector normal and parallel to the incidence plane, respectively. Values $r_{m, p \dot{u}}^{\perp, \parallel}$ proportional to surface impedance of a half-bounded metal (plasma) [15] can be written down as follows, the spatial dispersion of dielectric permittivity being neglected:

$$\begin{aligned} r_{m, p \dot{u}}^{\perp} &= - \frac{\cos \mathbf{J}}{\sqrt{\hat{a}_{m, p}(\dot{u}) - \sin^2 \mathbf{J}}}; \\ r_{m, p \dot{u}}^{\parallel} &= - \frac{\sqrt{\hat{a}_{m, p}(\dot{u}) - \sin^2 \mathbf{J}}}{\hat{a}_m(\dot{u}) \cos \mathbf{J}}, \end{aligned} \quad (13)$$

where $\varepsilon_{m, p}(\omega)$ is the complex dielectric permittivity of an unbounded metal (plasma) at frequency ω , which in the used approximation of a «cold» plasma-like medium has the following form:

$$\varepsilon_{m, p}(\omega) = 1 - \frac{\omega_{m, pe}^2}{\omega(\omega + i\nu_{m, pe})}, \quad (14)$$

where $\omega_{m, pe} = \left(\frac{4\pi e^2 n_{m, pa}}{m_e} \right)^{1/2}$ and $\nu_{m, pe}$ are the plasma and effective frequency of collisions of electrons in metal (plasma); $n_{m, pe}$ is their concentration depending upon the temperature of a corresponding environment; and e and m_e are the charge and mass of an electron.

Before conducting quantitative analysis of the role of the radiation component of heat transfer in the total energy balance of the surface of a spraying particle, let us determine the value of ξ by equating the results of calculation of heat flow Q_r from (9) and (10) using expressions (11)–(14). For example, for the case of an aluminium particle in the atmospheric-pressure argon plasma, we find that for a given system the reduced emissivity ξ changes from 0.11 at $T_{ms} = 1,000$ K to 0.17 at $T_{ms} = 2,500$ K, and that it insignificantly depends upon the plasma temperature in

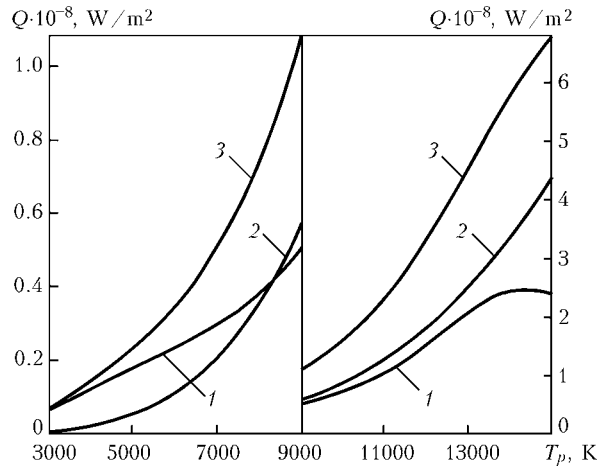


Figure 4. Effect of radiation heat exchange on density Q of heat flow from plasma to an aluminium particle with radius of $30 \mu\text{m}$ at $u = 300 \text{ m/s}$ and $T_{ms} = 2,000 \text{ K}$: 1 — $Q_c(T_p)$; 2 — $Q_r(T_p)$; 3 — sum thereof

a range of $T_p = 5,000\text{--}15,000 \text{ K}$ (temperature dependencies $n_{m, pe}$ and $\nu_{m, pe}$ used for the calculations are taken from [16, 17]).

The results of calculations of Q_r for the system under consideration are shown in Figure 4. To compare, this Figure also shows dependencies of Q_c and total heat flow into a particle having the fixed surface temperature $T_{ms} = 2,000 \text{ K}$ upon the temperature of a non-disturbed plasma flow, T_p . As it follows from the shown calculation curves, at $T_p > 8,000 \text{ K}$ the radiation heat exchange contributes much more to the total heat flow than its convective-conductive component. This effect is especially pronounced at high plasma temperatures, as at $T_p > 14,000 \text{ K}$ the values of Q_c decrease to some extent due to correction coefficient χ_s/χ in the expression for the Nu number (8), whereas the values of Q_r continue growing.

CONCLUSIONS

1. Numerical analysis of the convective-conductive component of the heat flow from the atmospheric-pressure argon plasma into a dispersed material spherical particle located in this flow indicates that there is a substantial scatter of data obtained using different criterial dependencies. At high values of a relative velocity, as well as difference in temperatures of the non-disturbed plasma flow and particle surface, the best agreement with the experimental data is provided by the criterial dependence that allows for the variations in density, coefficients of viscosity and thermal conductivity of the plasma through thickness of the boundary heat layer around a particle.

2. The radiation heat exchange between the atmospheric-pressure plasma jet and surface of a spraying particle at high plasma temperatures may play an important role in a total energy balance, and it should be taken into account in analysis of the process of heating of powder materials under the plasma spraying conditions. In particular, when aluminium particles are heated by the flow of argon plasma having a temperature of above $8,000 \text{ K}$, the radiation compo-



ment of the heat flow into a particle is larger than the convective-conductive one.

- Donskoj, A.V., Klubnikin, V.S. (1979) *Electroplasma processes and units in mechanical engineering*. Leningrad: Mashinostroenie.
- Gnedovets, A.G., Lokhov, Yu.N., Uglov, A.A. (1979) Thermal-physical problems of treatment of refractory metal particles in hot gas. *Fizika i Khimiya Obrab. Materialov*, **6**, 36–43.
- Bourdin, E., Fauchais, P., Boulos, M. (1983) Transient heat conduction under plasma conditions. *Int. J. Heat Mass Transfer*, **26**(4), 567–582.
- Vardelle, A., Vardelle, M., Zhang, H. et al. (2002) Volatilization of metal powders in plasma sprays. *J. Thermal Spray Technology*, **11**(2), 244–252.
- Shimanovich, V.D., Smyaglikov, I.P., Zolotovskiy, A.I. (2003) An effect of near-cathode region plasma of an argon arc on metal particles. In: *Proc. of 7th Europ. Conf. on Thermal Plasma Processes: Progress in Plasma Processing of Materials* (Strasbourg, June 18–21, 2003). New York: Begell House Inc.
- Kutateladze, S.S. (1979) *Fundamentals of the theory of heat exchange*. Moscow: Atomizdat.
- Landau, L.D., Lifshits, E.M. (1986) *Theoretical physics*. Vol. 6: Hydrodynamics. Moscow: Nauka.
- Burov, I.S. (1979) Calculation of heat exchange between dispersed material particles and plasma flows. *Fizika i Khimiya Obrab. Materialov*, **4**, 42–49.
- Ranz, W.E., Marshall, W.R. (1952) Evaporation from drops. *Chem. Eng. Progr.*, **48**, 141–146, 173–180.
- Fiszdon, J.K. (1979) Melting of powder grains in a plasma fume. *Int. J. Heat Mass Transfer*, **22**, 749–761.
- Dresvin, S.V., Donskoj, A.V., Goldfarb, V.M. et al. (1972) *Physics and technique of low-temperature plasma*. Moscow: Atomizdat.
- Boulos, M.I., Fauchais, P., Pfender, E. (1997) *Thermal plasmas: Fundamentals and applications*. Vol. 1. New York-London: Plenum Press.
- Bushma, A.I., Krivtsun, I.V. (2003) Peculiarities of absorption and scattering of different wavelength laser radiation by fine spherical particles. In: *Proc. of Int. Conf. on Laser Technologies in Welding and Materials Processing* (Katsiveli, Crimea, May 19–23, 2003). Kiev: PWI.
- Khair, K. (1976) *Statistical mechanics, kinetic theory and stochastic processes*. Moscow: Mir.
- Gvozdetsky, V.S., Zagorodny, A.G., Krivtsun, I.V. et al. (1987) Effect of laminated dielectric coatings on absorption properties of restricted plasma-like media. *Radiotekhnika i Elektronika*, **32** (11), 2372–2381.
- Miller, J.C. (1969) Optical properties of liquid metals at high temperatures. *Phil. Mag.*, **20**, 1115–1132.
- Gvozdetsky, V.S., Korshinsky, G.M., Krivtsun, I.V. et al. (1986) Calculation of energy factors of absorption and electromagnetic emission in laser welding. *Avtomatich. Svarka*, **5**, 33–37.

DETERMINATION OF VOLTAGE DROP IN THE AREA OF ELECTRODE WIRE CONTACT WITH THE WELDING TORCH NOZZLE UNDER MECHANIZED METHODS OF ARC WELDING

I.V. PENTEGOV, O.I. PETRIENKO, S.V. PUSTOVOJT, V.N. SIDORETS and A.V. LAVRENYUK

E.O. Paton Electric Welding Institute, NASU, Kiev, Ukraine

Experiments are described on determination of voltage drop in the area of electrode wire contact with the welding torch nozzle. Results of computer processing of experimental data were the basis to suggest empirical formulas of contact voltage drop dependence on different welding parameters.

Keywords: arc welding, contact voltage drop, contact resistance

A mathematical model of heat and electrical processes in gas-shielded arc welding with consumable electrode in the power supply–welding arc system is described in the works [1, 2]. Value of the voltage drop U_{con} in the area of electrode wire contact with the welding torch nozzle assumed as known is used in the model.

Many works are devoted to determination of the voltage and resistance drop in the area of electrode wire contact with the welding torch nozzle [3–10], however, most of them do not permit using these data in the developed mathematical model because of their drawbacks. For example, in the work [3] the values of U_{con} were established not experimentally but by the method of extrapolation of the experimentally obtained dependences on the «zero» extension. According to the data of this work the drop of the voltage between the nozzle and electrode wire at the 350 A

current is 0.6–0.9 V and it inconsiderably increases with a decrease of the electrode wire diameter. However, it is not clear from the work [3] at what wire feed rate these results were recorded. Therefore, it is not possible to obtain a functional dependence between U_{con} and wire feed rate v_f .

A method of the study described in the work [4] is based on oscillograph recording of the drop of voltage between the nozzle and sliding tungsten probe displacing on the surface of the electrode towards the article. In the process of oscillograph recording the probe consecutively passes the extension itself, «hot» end of the electrode and the arc zone, which allows determining distribution of voltages in these sites. The method allowed obtaining a considerable number of oscillograms showing that the voltage drop on the extension decreases non-linearly as approaching the «hot» end with a sharp increase on the «hot» end boundary. However, these data give only indirect in-



formation of the U_{con} values obtained by extrapolation of the curves to the beginning of the electrode wire extension.

Measurements of U_{con} made in the works [5, 6] showed that the electrode wire curvature and a shape of the current-carrying tip also affect the level of U_{con} . So, the values of U_{con} in welding with wire Sv-08Kh20N9G7T 2 mm in diameter vary in the range from 2 to 4 V while in welding with preliminary aligned wire with a cylindrical current-carrying tip the values of U_{con} in 1–2 h of the welding process may achieve 10–15 V. The authors of the work [5] state that a deviation of the U_{con} values increases as against the set one with the wear of the tip. However, they did not indicate the value of either feed rate of the electrode wire v_f or welding current I at which the experiments were conducted.

The results of the measurements of U_{con} in the works [3, 5] differ by an order.

The work [7] determines a resistance of the nozzle–wire contact and presents the data on conditions (feed rate, welding current, wire diameter) under which the values of the contact resistances are obtained. These values are widely spread, thus making them inappropriate for using in the mathematical model. Therefore, obtaining reliable data on the level of the voltage drop in the nozzle–wire contact, which can be then used in the mathematical models of heat and electrical process in gas-shielded arc welding with consumable electrodes is an urgent task.

This work describes the experiments on determination of the voltage drop in the area of electrode wire contact with the welding torch nozzle using the computer methods for processing of the experimental data. The measurements were carried out by the scheme presented in Figure 1.

Non-straightened wire Sv-08G2S 0.8 mm (copper-plated) and 1.2 mm (without copper-plating) in diameter was used for the experiment with different values of feed rate of the welding wire (opposite polarity) in CO_2 . Power source with external flat characteristic VDU-506 was used for power supply of the welding arc. The experimental data were processed on the computer with the built-in board L-154 (LCARD, Russia) where the A/D conversion (ADC) of input signals was implemented. The ADC used two channels with current values of the drop of contact voltage U_{con} and welding current I being sent to the input of the channels through the unit of amplification and galvanic decoupler. Signal U_{con} was received by the unit of galvanic decoupler through the voltage divider while signal I was read from the shunt.

Then the experimental data were processed by the program PowerGraph intended for registration, processing and storage of analog signals recorded by the ADC in the digital form. This allows using PC as an ordinary strip-chart recorder with a possibility to employ the methods for computer processing of the data. Frequency of measuring U_{con} and I was 20 kHz. Values

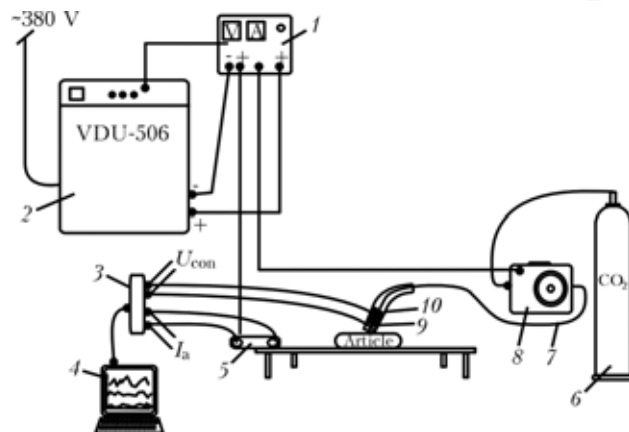


Figure 1. Scheme of switching equipment and devices for carrying out the experiments: 1 — control desk; 2 — power supply VDU-506; 3 — voltage divider and galvanic decoupler unit; 4 — PC with installed A/D converter (L-154); 5 — shunt; 6 — torch; 7 — nozzle; 8 — feeder; 9 — welding wire; 10 — bottle with CO_2

of R_{con} were obtained as a result of mathematical processing of the U_{con} and I data.

Tungsten probe installed at a distance of 1 mm from the face of the welding torch nozzle was used for reading the values of the contact voltage drop. The probe was fixed spring-loaded in the cut of the welding torch extension by a specially produced device (Figure 2) and then the sliding contact with the wire was achieved. The second lead of the measuring circuit was soldered to the copper nozzle.

Oscillogram fragments of the drop of voltage and current as well as resistance in the area of contact of the electrode wire with the welding torch nozzle obtained by the described method with different diameters of the wire and wire feed rates are presented in Figures 3 and 4. It is necessary to note that pure contact voltage drop plus voltage drop in the hidden site of the electrode extension were measured in the experiments. It is impossible to separate these two voltages and there is no need to do so because a sum of these voltages is required for heat calculations.

Dotted digital arrays of values of welding current, contact drop of voltage and resistance recorded by means of the program PowerGraph in equal time in-

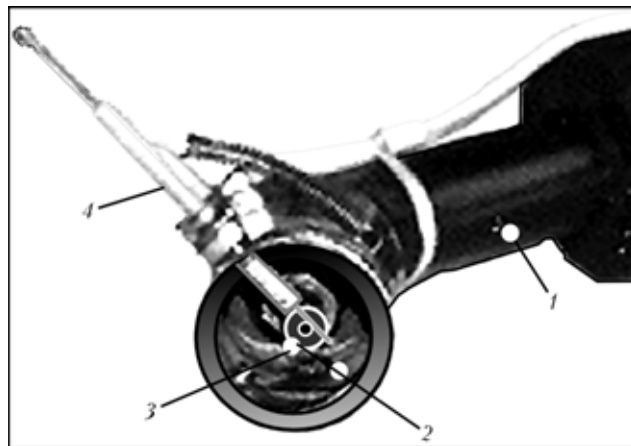


Figure 2. Appearance of welding torch nozzle with the probe installed on it: 1 — welding torch; 2 — welding torch orifice; 3 — probe; 4 — nozzle

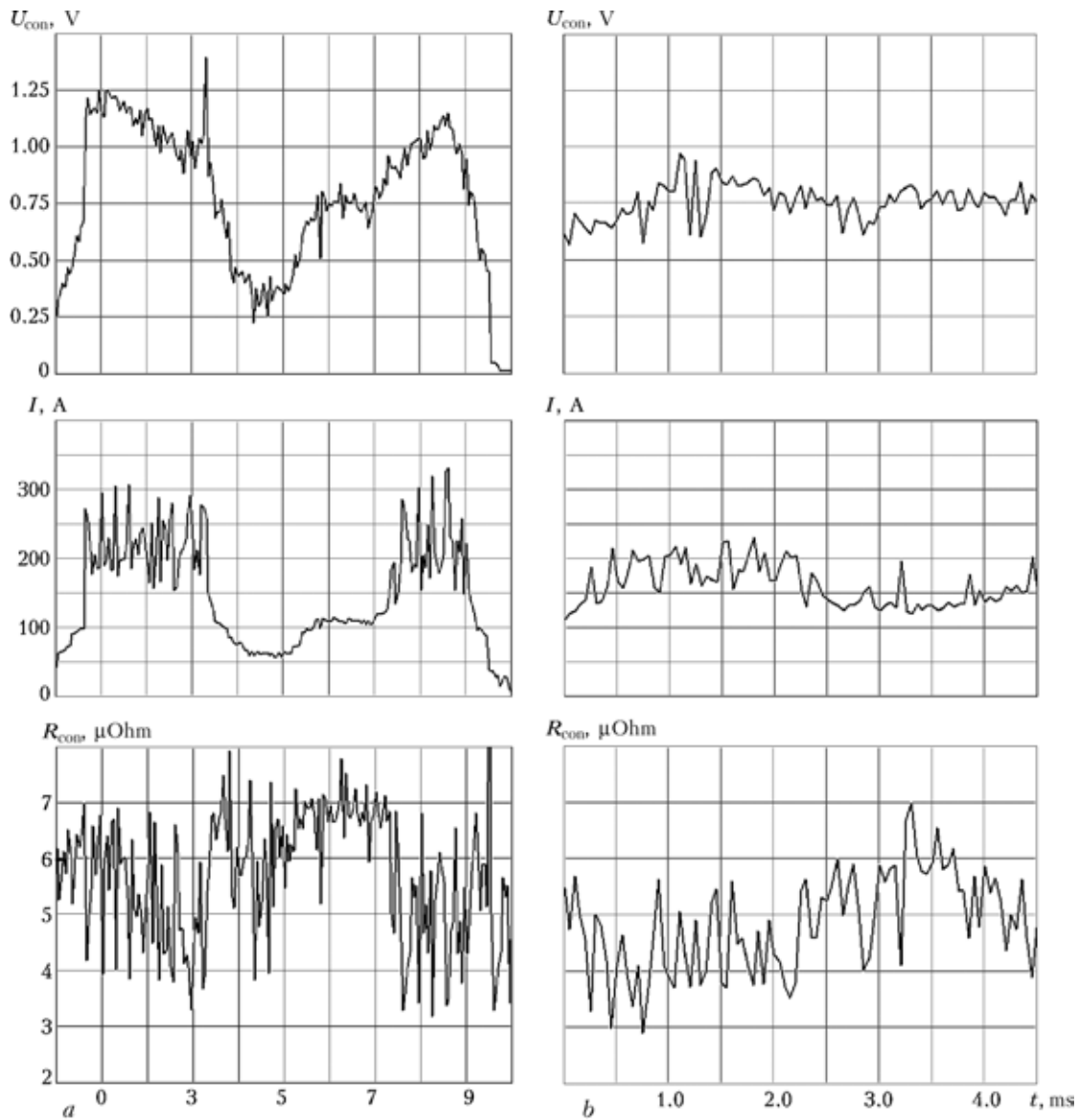


Figure 3. Fragments of processed oscillograms in welding with (a) and without (b) short circuit at $d = 0.8$ mm, $v_f = 0.053$ m/s

tervals (0.05 s) allow constructing volt-ampere (VAC) and ohm-ampere (OAC) characteristics of the nozzle-wire contact with different diameters and feed rates of the wire and studying a character of their changes in the process of arc welding in inert gases. These dotted dependences are presented in Figure 5. Here the areas of a selected series of instant U_{con} and I values in welding with and without short circuits are shown for electrode wire of different diameters (0.8 and 1.2 mm) and different values of v_f .

Consideration of the presented dotted arrays allows a conclusion that VAC of the contact does not depend on the welding conditions (with or without short circuit). All dots with the same currents are arranged in the narrow area irrespective of the conditions. This is explained by the fact that the contact is a low-inertia object and its state is specified by the values of the current at this point in time and does not depend on the prehistory of the process. Therefore, VAC of the contact depends neither on conditions nor on parameters of the welding circuit (inductivity of

the welding choke, power supply voltage and length of the extension). A dependence of the contact VAC on diameter of the electrode wire d and its feed rate v_f is traced. The parameter U_{con} grows together with the v_f and drops with increase of wire diameter d . When d and v_f are fixed the average value of U_{con} is determined only by the instant value of the welding current I . Voltage U_{con} smoothly grows together with the current increase through the contact and is within the range 0.2–1.5 V for the non-worn-down copper nozzle within the working current range. Copper plating of the wire or its absence does not practically affect U_{con} .

Spread of U_{con} values is caused by stochastic changes in both contact resistance and a length of the «hidden» section of the electrode extension specified by the wanderings of the contact point.

For using the arrays of the obtained data in the mathematical model it is required to carry out approximation of VAC of the nozzle-wire contact. In this case we use a power form of approximation of

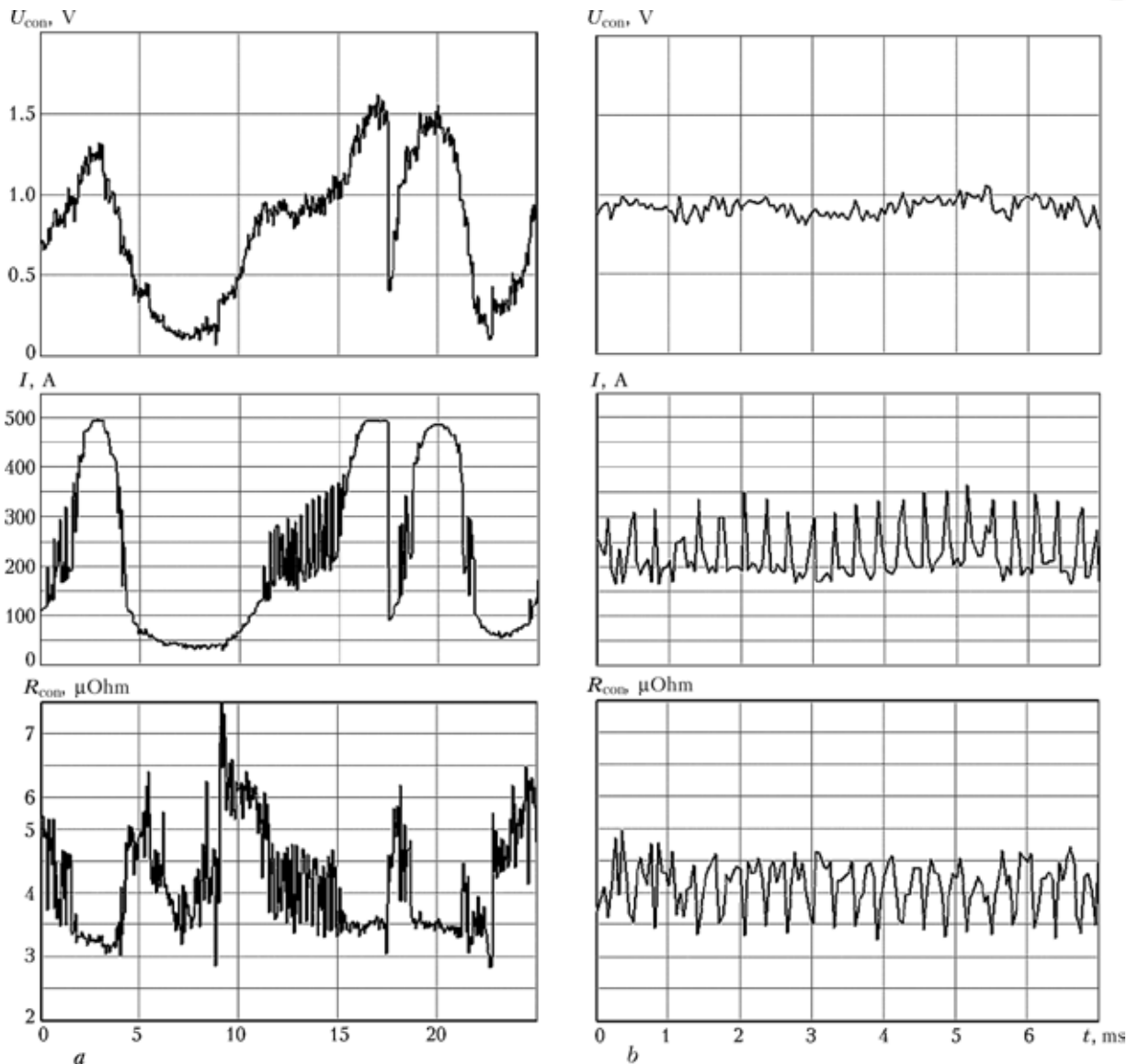


Figure 4. Fragments of processed oscillograms in welding with (a) and without (b) short circuit at $d = 1.2$ mm, $v_f = 0.085$ m/s

the dependences of U_{con} expectation on current, wire feed rate and wire diameter, which with the non-worn-down copper nozzle has the following form:

$$U_{con}(d, v_f, I) = \left[2.55 \left(\frac{I d_b}{I_b d} \right)^{0.2} - 1.78 \right] \left(\frac{v_f}{v_b} \right)^{0.2} \text{ [V]}, \quad (1)$$

where I_b , d_b , v_b are the basic values of welding current, diameter of the electrode and feed rate, respectively, which were selected as support values with the power index being 0.2:

$$I_b = 180 \text{ A}, \quad d_b = 1 \text{ mm}, \quad v_b = 0.035 \text{ m/s}.$$

The formula (1) may be used for the range of changes in parameters under which $U_{con} > 0$.

The obtained mathematical dependences of U_{con} on I in gas-shielded arc welding with consumable electrodes may serve as the elements of the mathematical model of heat processes in the electrode extension partially described in the works [1, 2].

Possible maximal deviation of the experimental data ΔU_{con} (maximal spread of U_{con} values) on aver-

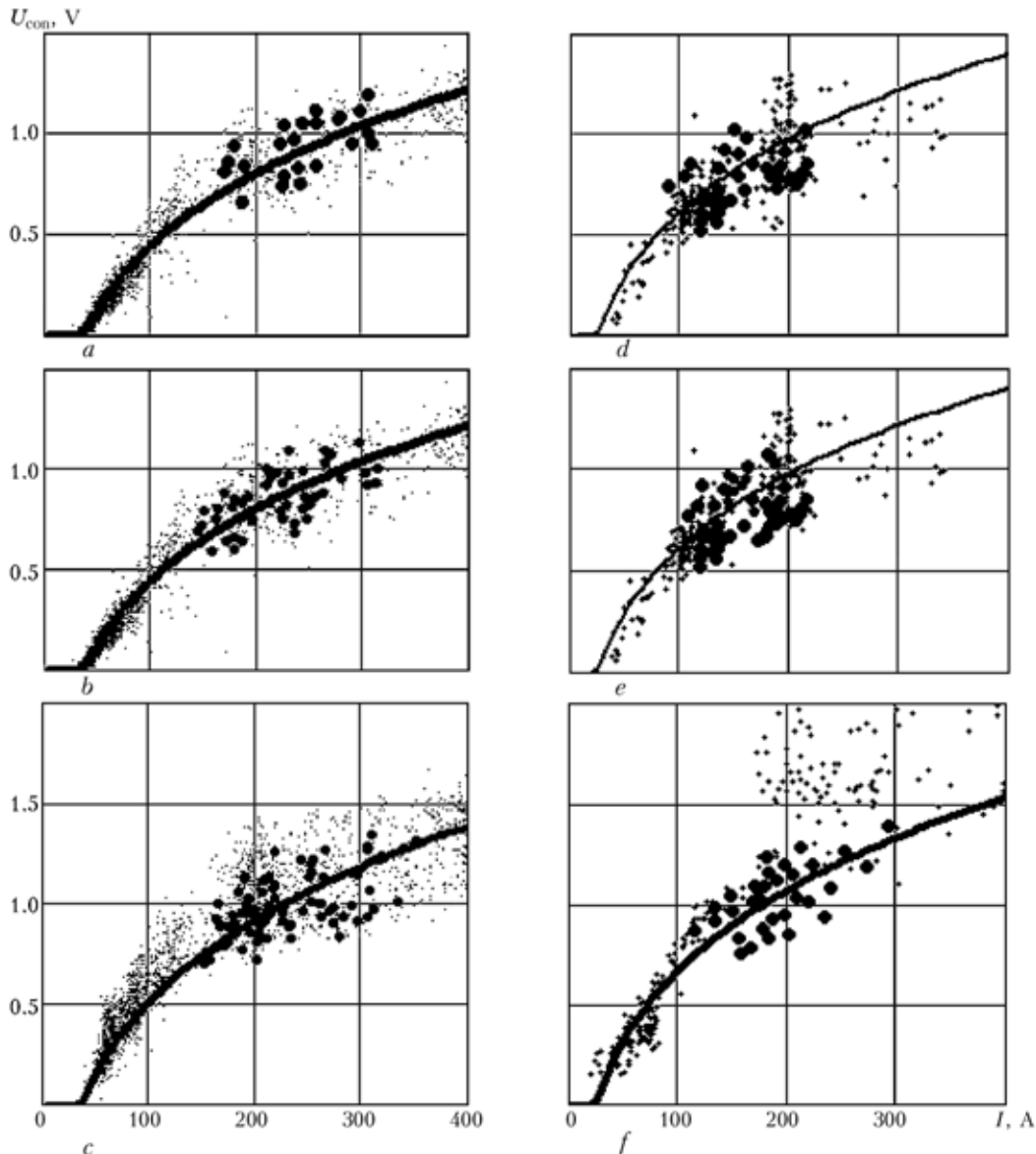
age values of U_{con} calculated by the formula (1) for the whole admissible range of the changes of welding current I with non-worn-out copper nozzle does not exceed

$$\Delta U_{con} = (d, v_f, I) = \pm 0.33 \left(\frac{I d_b v_f}{I_b d v_b} \right)^{0.2} \text{ [V]}. \quad (2)$$

The formula is valid at $U_{con} > \Delta U_{con}$.

Approximation curves of the averaged dependence of the experimental data U_{con} on I by the formula (1) in welding with and without short circuit are given in Figure 5. As it is followed from the Figure, approximation of the contact VAC correctly reflects all peculiarities of the dotted data arrays and it may be used for estimation of the average value of the voltage drop in the area of nozzle-wire contact.

Dotted arrays of the experimental data have their peculiarities with small and large currents. With currents smaller than 30–40 A a stochastically repeated decrease of U_{con} down to 0.01–0.04 V is observed both for wire with and without copper-plating. This



Figures 5. Arrays of experimental data of U_{con} and I in welding with (pluses) and without (dots) short circuit and VAC approximation (curve): *a* — $d = 1.2$ mm, $v_f = 0.055$ m/s; *b* — $d = 0.8$ mm, $v_f = 0.041$ m/s; *c* — $d = 1.2$ mm, $v_f = 0.085$ m/s; *d* — $d = 0.8$ mm, $v_f = 0.053$ m/s; *e* — $d = 1.2$ mm, $v_f = 0.108$ m/s; *f* — $d = 0.8$ mm, $v_f = 0.066$ m/s

can be explained by the fact that a stable copper interlayer of the nozzle material is formed on the wire with small currents while resistance of the copper-copper contact is much smaller than resistance of the copper-steel contact. This issue requires a separate investigation.

With large current densities in the electrode wire exceeding 400 A/mm^2 a nature of the contact becomes sparking, which leads to a sharp increase of the U_{con} level (Figure 5, *f*). It is desirable to avoid such conditions since they are accompanied by an increased wear of the nozzle and appearance of the heat waves moving together with extension and leading to destruction of stability of the welding process.

All this imposes limitation from above on selection of the admissible welding current, the smaller being the diameter of the electrode wire, the smaller being the admissible welding current. For example, with $d = 0.8$ mm and $v_f = 0.066$ m/s a critical current

density is achieved with current 180 A while with $d = 1.2$ mm it is not achieved even with current 400 A irrespective of the feed rate.

A boundary of the spark contact appearance shifts towards smaller current densities in the wire with the nozzle wear. In this case U_{con} can sharply increase achieving the values up to 6–10 V. That is why working with a worn-down nozzle it is impossible to receive quality welded joints.

Figure 6 shows a dotted array R_{con} and typical averaged OAC of the contact determined as a tangent of the slope of straight line drawn from the beginning of the coordinate to the current VAC dot and constructed using the expression (1) by the formula:

$$R_{con}(d, v_f, I) = \frac{U_{con}(d, v_f, I)}{I} \text{ [Ohm]}. \quad (3)$$

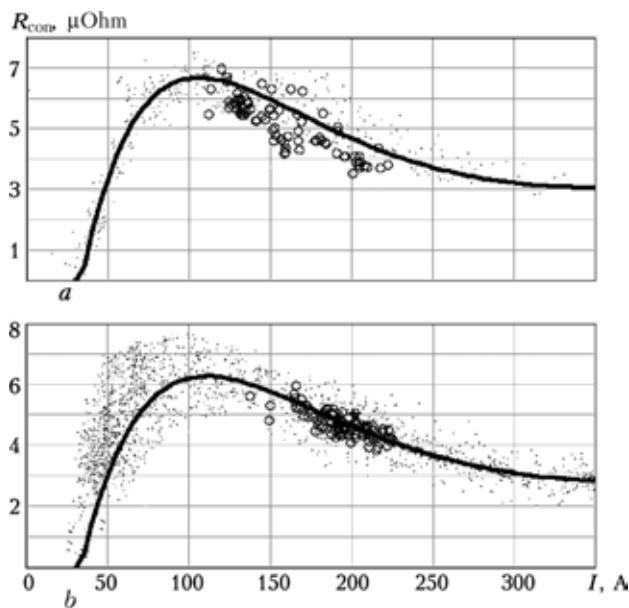


Figure 6. Arrays of experimental data of R_{con} and I in welding with (dots) and without (circles) shot circuit and typical averaged OAC at $d = 0.8$ (a) and 1.2 (b) mm

Maximum of this curve is determined by the point of tangency of the ray drawn from the beginning of the coordinate tangential to the VAC of the contact.

CONCLUSIONS

1. Experiments are carried out for determination of the voltage drop in the area of electrode wire contact with the welding torch nozzle using the computer methods for processing of the experimental data. Arrays of the experimental values of voltage drop, current and resistance in the zone of electrode wire and welding torch nozzle contact are obtained.

2. VAC and OAC of the nozzle-wire contact are constructed for different diameters of the wire and different feed rates. It is established that VAC of the

contact does not depend on the welding conditions (with or without short circuit) and parameters of the welding circuit.

3. A dependence of VAC of the contact on the diameter of the electrode wire d and feed rate v_f is established.

4. Approximations of the averaged dependence of the experimental data U_{con} on I in welding with and without short circuit are obtained. It is established that approximation of VAC of the contact reflects all peculiarities of the dotted data arrays and it can be used for estimation of the average value of the voltage drop in the area of the nozzle-wire contact.

5. Recommendations are given on selection of the admissible welding conditions.

1. Pentegov, I.V., Petrienko, O.I. (2002) Method of calculation of voltage drop in electrode stickout length with allowance for non-linearity of thermophysical parameters. *The Paton Welding J.*, **4**, 27-30.
2. Pentegov, I.V., Petrienko, O.I. (2003) Calculation of temperature distribution along the electrode extension taking into account the heat contributed by the drop. *Ibid.*, **7**, 19-24.
3. Koshkarev, B.T., Mikhajlov, A.N., Budnik, N.M. (1971) Influence of the stickout on process of electrode melting in CO_2 welding. *Svarochn. Proizvodstvo*, **11**, 30-32.
4. Kutepov, Yu.N. (1970) *Analysis and development of systems of automatic control of electrode stickout in CO_2 welding*. Syn. of Thesis for Cand. of Techn. Sci. Degree. Kiev.
5. Brigidin, V.Ya. (1979) Operation of current contact tips in arc welding. *Svarochn. Proizvodstvo*, **8**, 20-21.
6. Brigidin, V.Ya., Konotop, D.A. (1977) Current distribution in contact pair electrode wire-tip of welding automatic or semi-automatic machine. *Avtomatich. Svarka*, **6**, 21-24.
7. Chubukov, A.A. (1980) Resistance in contact tip-electrode wire in CO_2 welding. *Svarochn. Proizvodstvo*, **12**, 31-32.
8. Vakhalin, V.A. (1971) On problem of current carrying by sliding contact. *Ibid.*, **1**, 2-3.
9. Zwickert, H. (1987) Untersuchung der Kontaktverhältnisse bei der Stromuebertagung auf den Schweissdraht. In: *Wissenschaftliche Zeitschrift der Technischen Universitaet Otto von Guericke*, **4**, 96-102.
10. Berger, H., Pfeiffer, G. (1986) Kontaktduesen beim MAG-Schweissen. *ZIS-Mitt.*, **28**(6), 641-643.



INFLUENCE OF THE COMPOSITION OF FLUX-CORED WIRE CORE AND SHIELDING GAS ON THE STABILITY OF ARC WELDING PROCESS

V.N. SHLEPAKOV, A.S. KOTELCHUK, S.M. NAUMEJKO and A.V. BILINETS

E.O. Paton Electric Welding Institute, NASU, Kiev, Ukraine

The paper presents the results of studying the process of gas-shielded arc welding with flux-cored wires of metal-core type. The influence of mineral components of the flux-cored wire core and shielding gas composition on arcing stability and nature of metal transfer has been established, proceeding from the data of monitoring electrical signals.

Keywords: arc welding, metal-core wire, shielding gas, electric signals, statistical processing, investigation of process stability

Features of arcing, melting and transfer of metal in gas-shielded welding with solid and flux-cored wires are described in sufficient detail in [1–3]. It is reported in them that stability of the welding process and nature of electrode metal transfer essentially depend on the wire composition, welding mode, current polarity and applied shielding gas [1, 2]. Gas-shielded welding using metal-core wire [3] with a small (up to 2 %) weight fraction of non-metallic inclusions has been introduced in the last decade. However, the features of the process of arc welding with wires of this type have not been studied well enough.

Welding in CO_2 and in $\text{Ar} + 20\% \text{CO}_2$ mixture with metal-core wires of different composition was studied to evaluate the influence of small additives of non-metallic mineral components in the core on technological properties. Flux-cored wire of the above type of 1.2 mm diameter, having no mineral components in its core, was taken as the basic one. Influence of additives of such mineral components as titanium oxide, alkali and alkali-earth metal fluorides to the wire core was studied. Weight fraction of the mineral component of wire core was equal to 0.6 % for the four studied compositions, namely rutile (TiO_2), rutile and fluorite mixture ($\text{TiO}_2:\text{CaF}_2$ --- 3:1), mixture of rutile and sodium hexafluorosilicate (component ratio $\text{TiO}_2:\text{Na}_2\text{SiF}_6$ --- 3:1) and mixture of rutile, sodium hexafluorosilicate and cesium fluoride ($\text{TiO}_2 + \text{Na}_2\text{SiF}_6 + \text{CsF}$ --- 6:2:1).

DCRP welding was performed using a wire feed mechanism with maximum rate deviations of $\pm 1.5\%$ and welding arc power source VS-500 with a flat external characteristic. Shielding gas composition (CO_2 and $\text{Ar} + 20\% \text{CO}_2$ mixture) met the requirements of the currently valid standards as to impurity content. When test welds were made, the arc voltage was $U_a = 24\text{--}26$ V, welding current --- $I_w = 260\text{--}290$ A, shielding gas composition --- 18 l/min.

The main parameters of arc welding process were measured using a system of recording and analysis of

electric signals, namely the Hannover AN-XII analyzer [4, 5]. Probability distribution density of arc voltage and welding current, as well as short-circuiting frequency and weighted average arcing time were determined during measurement. Date reading frequency was $5 \cdot 10^5 \text{ s}^{-1}$, and duration of continuous parameter recording in test welding was 2 s in all the cases. Measurement results were processed by the mathematical statistics methods [6].

Analysis of the results was performed using calculated average values of arc voltage and welding current together with their root mean square deviations and coefficients of variation. These data were used to plot the probability density curves and to derive the time characteristics (in particular, short-circuiting duration, weighted average arcing time). Results of statistical processing of arc welding parameters (welding current I_w , arc voltage U_a and short-circuiting duration $\tau_{s.c.}$) with metal-core wires, obtained using Hannover AN-XII analyzer, are given in the Table and in Figures 1–5.

Comparison of the data obtained in welding in CO_2 and mixture of $\text{Ar} + 20\% \text{CO}_2$ showed that the nature of melting and transfer of electrode metal changes essentially, irrespective of the composition of mineral additive in the flux-cored wire core. From the Table and Figures 1–5 it is seen that replacement of CO_2 by its mixture with argon leads to reduction of average short-circuiting duration from 0.4 to 11 ms up to their practically complete disappearance. A change of the mode of electrode metal transfer from fine-drop to jet mode is also observed. Metal spatter is markedly reduced, and amplitudes of welding current and voltage fluctuations become smaller. Standard deviations of voltage drop from 1.1 to 2.4 V (CO_2 welding) to 0.5 to 0.7 V ($\text{Ar} + \text{CO}_2$ mixture), and those of welding current decrease 2 to 3 times. It was practically impossible to obtain jet transfer of electrode metal in test welding in pure CO_2 with wires of the studied type.

Tabulated data indicate that addition of titanium oxide (rutile) to the flux-cored wire core only slightly influences the stability of the welding process, and a



Statistical characteristics of gas-shielded welding with metal-core wires in different modes

Mineral component of core	Shielding atmosphere	U_a^{av} , V	S_U , V	K_U , %	I_w^{av} , A	S_I , A	K_I , %	τ^{sum} , ms	τ^{av} , μ s	K_τ
No	CO ₂	24.8	1.8	0.07	268.2	39.6	0.15	0.8	400.0	1.24
		24.7	1.9	0.08	272.5	43.2	0.16	0.4	100.0	0.58
	80 % Ar + 20 % CO ₂	24.9	0.7	0.03	261.7	15.8	0.06	0	0	∞
TiO ₂	CO ₂	24.9	2.2	0.09	285.0	45.0	0.16	2.0	177.3	1.04
		25.4	2.1	0.08	270.6	43.0	0.16	0.6	183.3	0.31
	80 % Ar + 20 % CO ₂	24.8	0.7	0.03	275.4	16.8	0.06	0	0	∞
TiO ₂ + Na ₂ SiF ₆	CO ₂	25.0	2.4	0.10	276.9	40.9	0.15	11.0	423.1	1.73
	80 % Ar + 20 % CO ₂	25.4	0.7	0.03	295.6	18.9	0.06	0	0	∞
TiO ₂ + CaF ₂	CO ₂	24.4	1.5	0.06	293.3	25.6	0.09	0	0	∞
		24.8	1.5	0.06	277.9	30.2	0.11	0	0	∞
	80 % Ar + 20 % CO ₂	24.2	0.5	0.02	231.0	21.5	0.09	0	0	∞
TiO ₂ + Na ₂ SiF ₆ + CsF	CO ₂	25.1	1.6	0.06	301.3	31.8	0.11	2.1	210.0	1.29
		24.9	1.1	0.07	266.8	22.0	0.08	0	0	∞
	80 % Ar + 20 % CO ₂	24.6	0.5	0.02	278.2	15.0	0.05	0	0	∞

Note. U_a^{av} , I_w^{av} , τ^{av} are the average values of arc voltage, welding current and short-circuiting duration, respectively; S_U , S_I are the standard deviations of the values of arc voltage and welding current, respectively; τ^{sum} is the total short-circuiting duration; K_U , K_I , K_τ are the coefficients of variation of arc voltage, welding current and short-circuiting duration, respectively; two typical parameter sets are given for CO₂ welding as with this method the process is less stable than in welding in a mixture of Ar + 20 % CO₂.

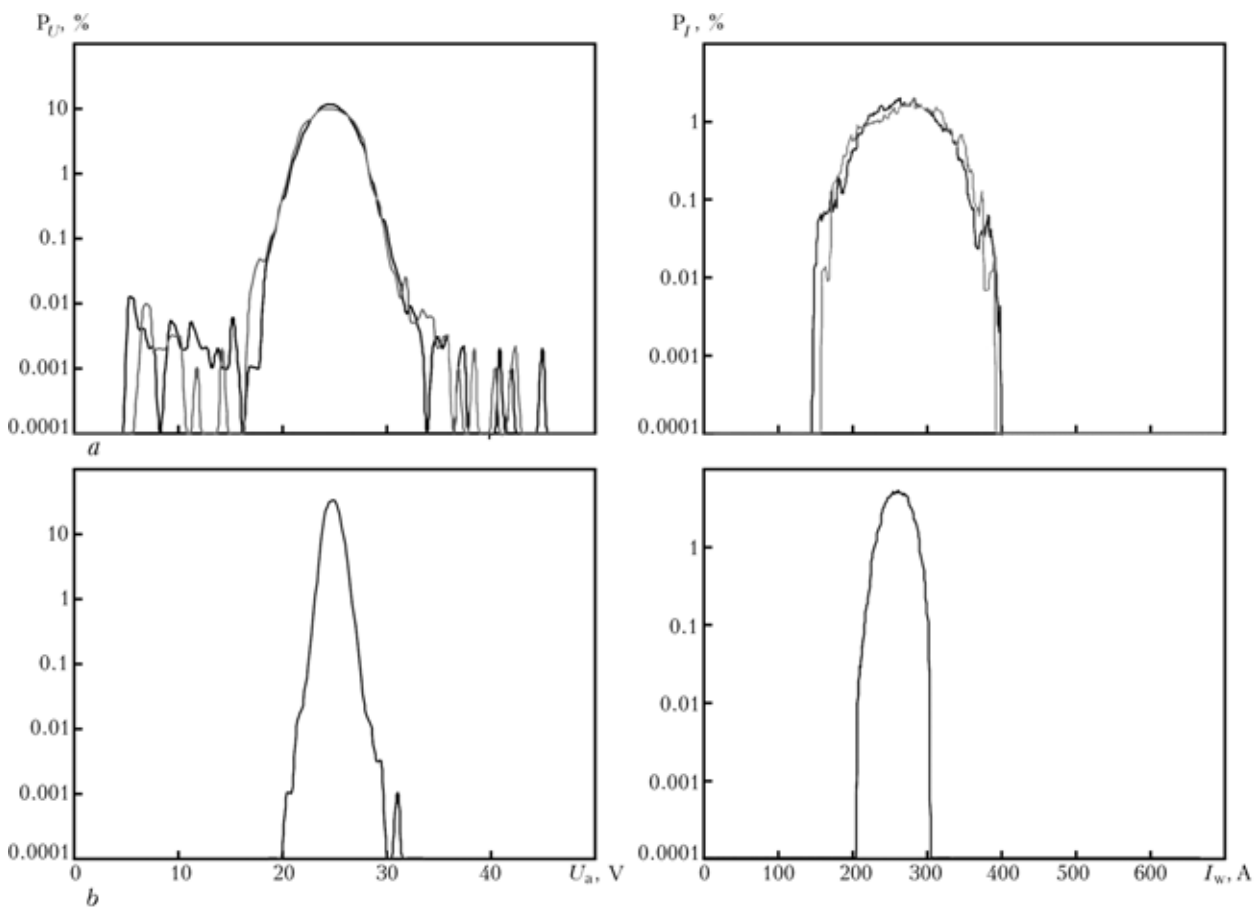


Figure 1. Curves of distribution of probability density of voltage P_U and welding current P_I in arc welding with metal-core wire, not containing any mineral components. Here and in Figures 2-5: a --- CO₂; b --- Ar + 20 % CO₂ mixture; two curves are the results of two measurements

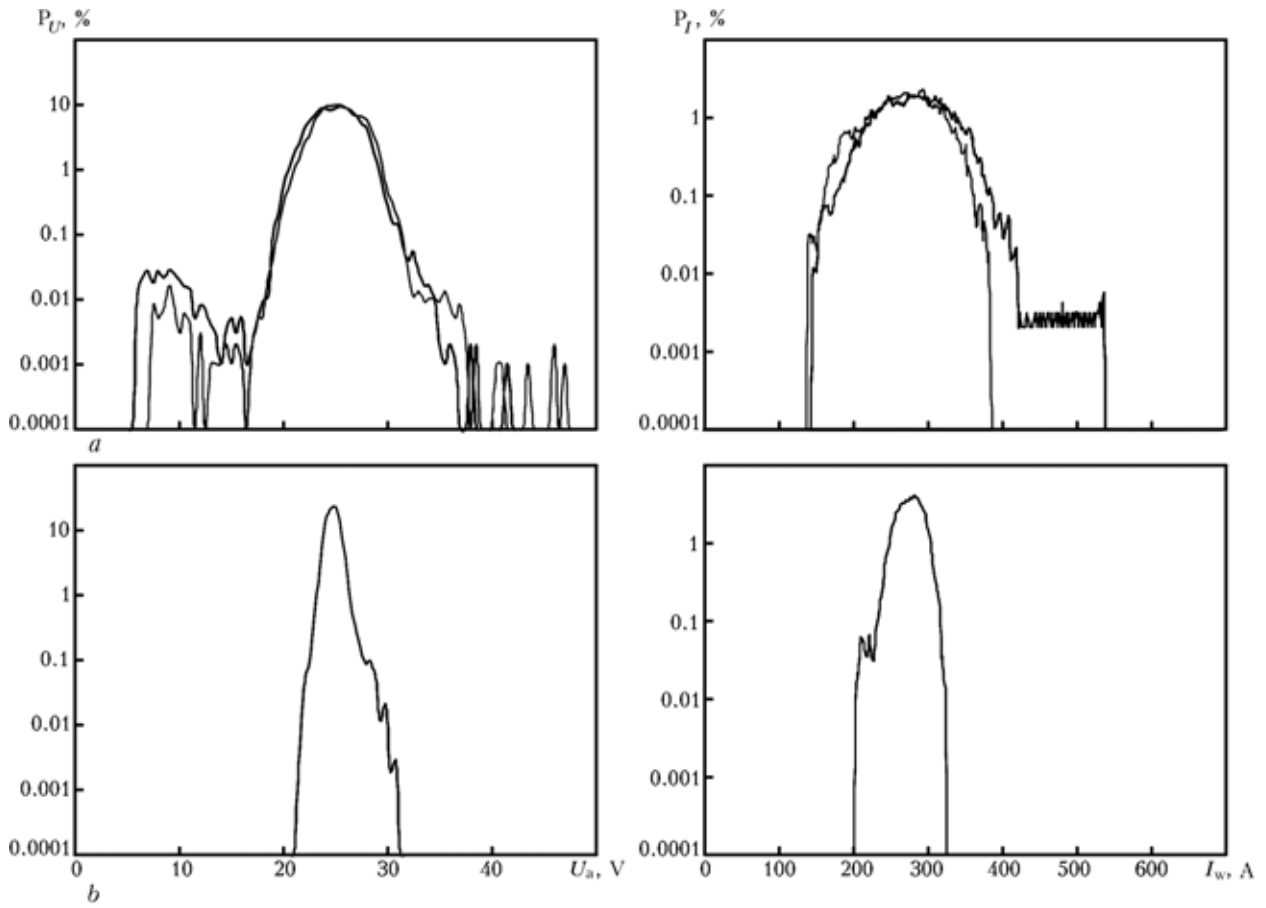


Figure 2. Same as in Figure 1, but for rutile-containing wire

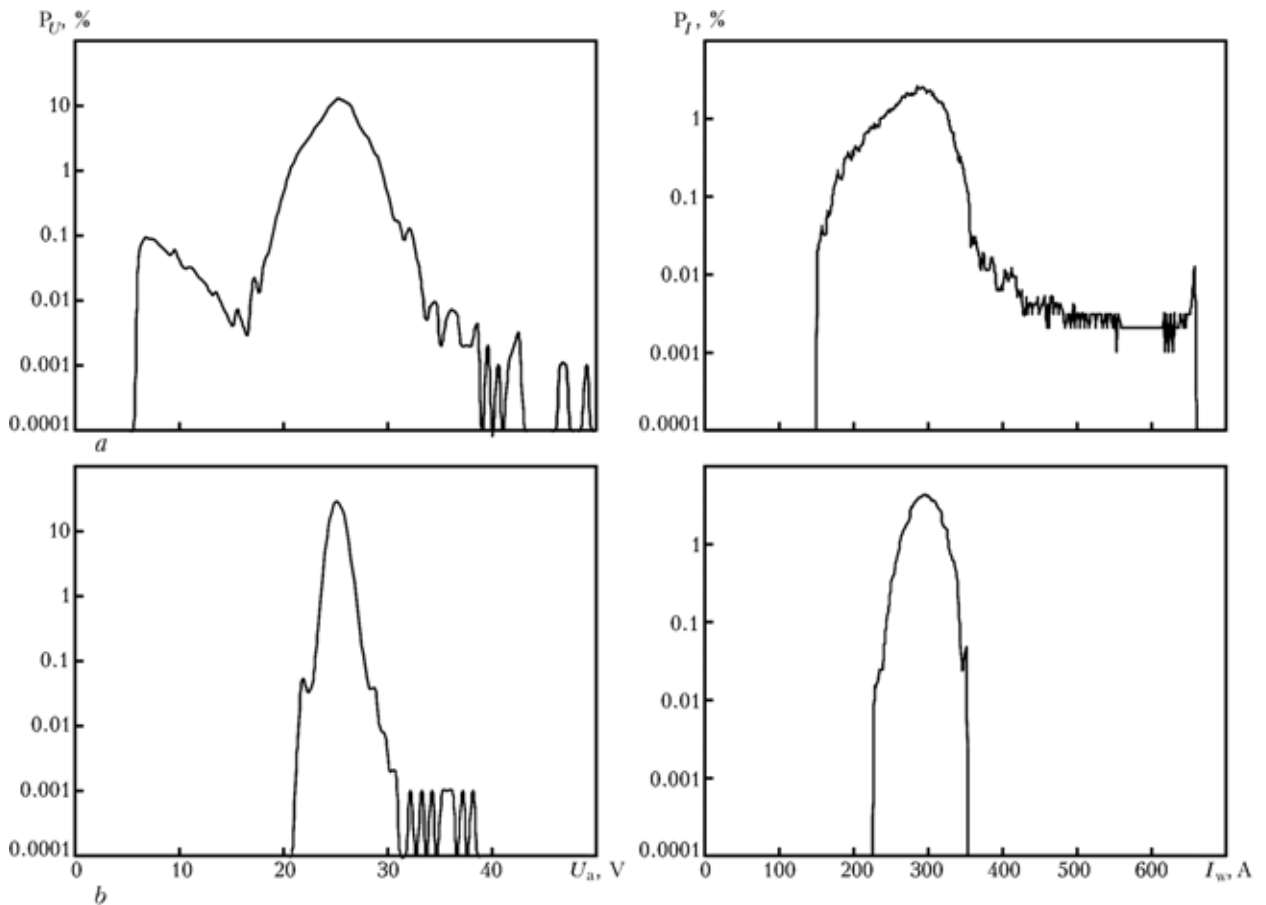


Figure 3. Same as in Figure 1, but for wire containing a mixture of rutile and sodium hexafluorosilicate

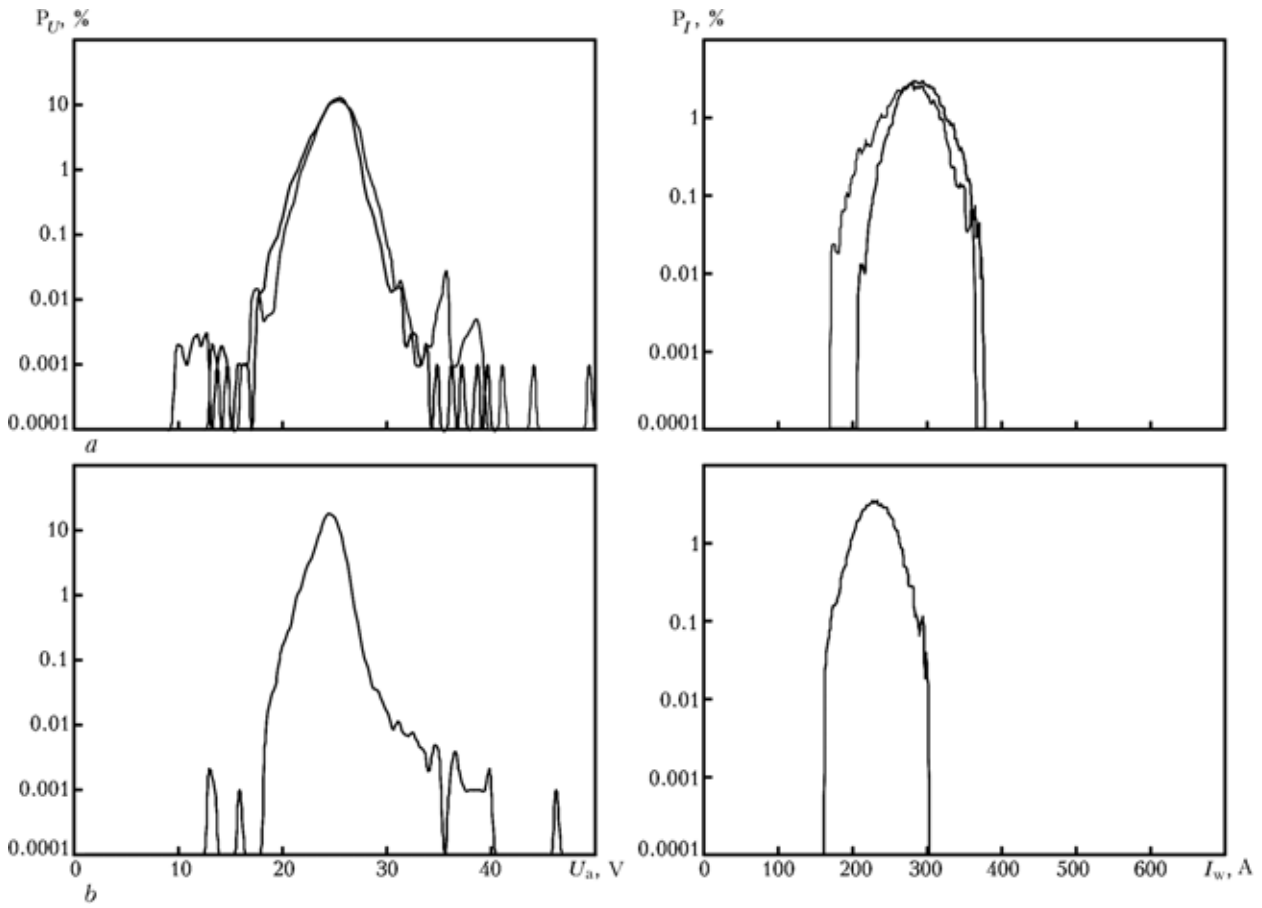


Figure 4. Same as in Figure 1, but for wire with a mixture of rutile and fluorite

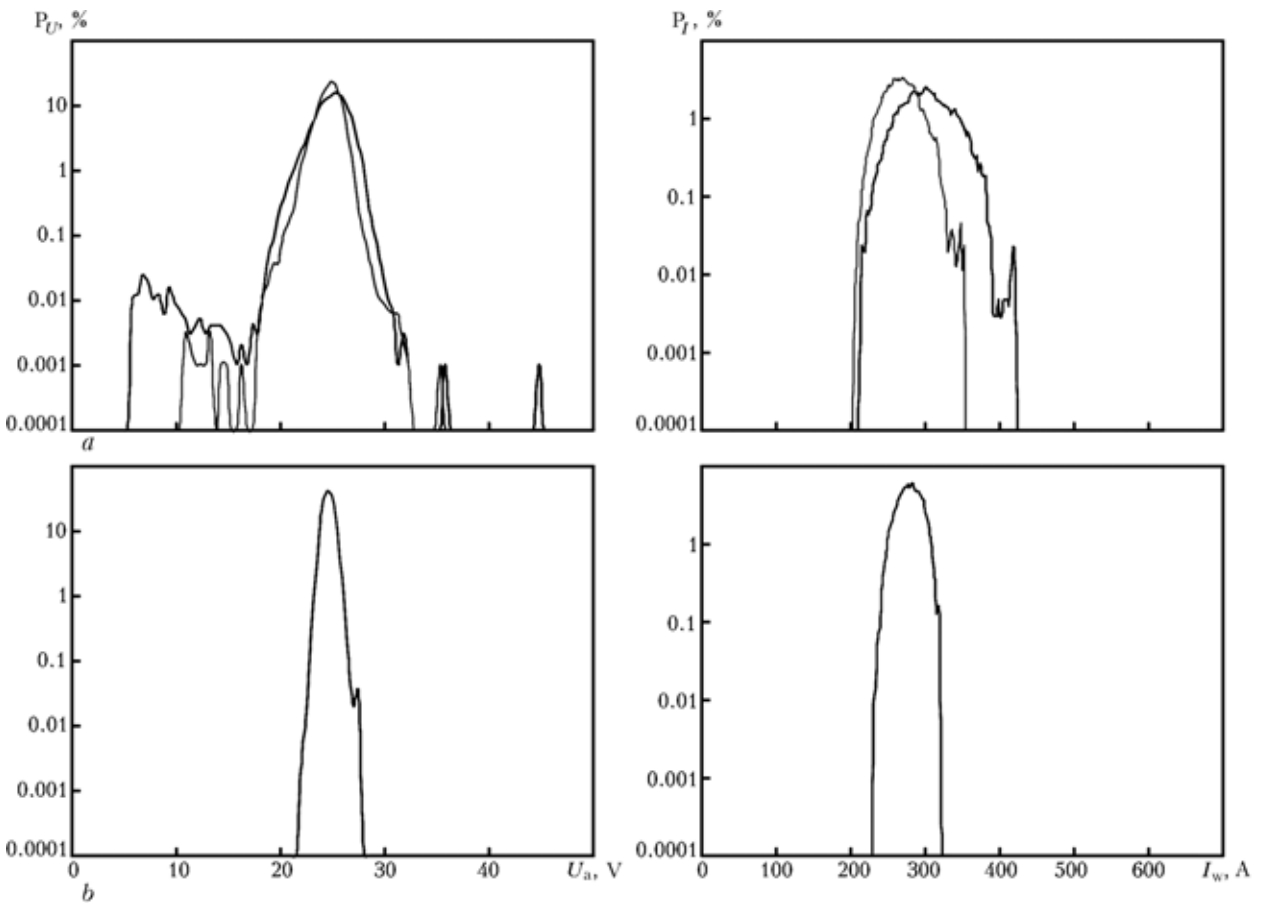


Figure 5. Same as in Figure 1, but for wire with a mixture of rutile, sodium hexafluorosilicate and cesium fluoride



small additive of mineral components containing fluoride compounds, has a significant influence on the welding process stability. However, even at a small (approximately up to 0.3 wt.%) content of fluorine compounds in the flux-cored wire core the welding process stability depends on the type of these compounds. This is indicated by a change in the overall number of short-circuits and amplitude of welding current and arc voltage fluctuations. In welding in a mixture of Ar + CO₂ jet transfer of electrode metal is observed at addition of fluorite to the core, while addition of sodium hexafluorsilicate leads to individual short-circuits (see the Table and Figure 3, 4). Intensive evolution of gas from the flux-cored wire core at thermal destruction of sodium hexafluorsilicate causes a non-uniformity of electrode metal transfer. Addition of a mixture of rutile with fluorite in the studied weight fractions to the wire core leads to a certain stabilization of the welding process and transition from the drop to jet transfer of electrode metal in CO₂ welding (see Figure 4). Presence of fluorite is favourable for titanium oxide melting and eliminates the non-uniformity of wire melting.

Addition of a small amount of ionizing component (cesium fluoride) promotes stabilization of the welding process. Irrespective of the composition of mineral components of the wire core, use of a mixture of Ar with CO₂ has a stabilizing influence on the process of its melting and causes transition from a fine-drop to jet transfer of electrode metal.

CONCLUSIONS

1. Investigation of the process of welding with test metal-core wire using CO₂ and its mixture with Ar

as a shielding medium showed that at weight fraction of mineral components in the wire below 2 %, the process of welding in a mixture of Ar + 20 % CO₂ features stable melting and a transition from a fine-drop to jet transfer of electrode metal without short-circuiting.

2. In arc welding the melting process of wires containing thermally unstable fluorides as mineral component in the core, is characterized by a lower stability and greater metal spatter. Oxide-type components (rutile) in a combination with non-volatile fluorides (in the studied range of their content in the wire core) stabilized the process of CO₂ welding.

3. Results of studying the arcing stability in welding with metal-core wires enabled determination of the composition of the core mineral component providing high indices of stability of the welding process and reduction of electrode metal losses in gas-shielded welding.

1. Dyatlov, V.I. (1964) Elements of theory of electrode metal transfer in electric arc welding. In: *New problems of welding engineering*. Kiev: Tekhnika.
2. Pokhodnya, I.K., Gorpenyuk, V.N., Milichenko, S.S. et al. (1990) *Metallurgy of arc welding: Processes in the arc and melting of electrodes*. Kiev: Naukova Dumka.
3. Bilinets, A.V. (2004) Metal-cored wires for mechanized shielded-gas welding. In: *Proc. of Int. Conf. on Welding Consumables of CIS Countries: Welding Consumables. Development. Technology. Production. Quality* (Dnepropetrovsk, July 1-4, 2004). Dnepropetrovsk.
4. Blakeley, P.J., Hass, B. (1991) A new approach to arc weld monitoring. *Welding Rev. Int.*, August, 157-160.
5. Rehfeldt, D., Schmitz, Th., Behrens, S.M. (1995) Report on the use of quality monitoring systems. *IIW Doc. XII-1420-95*.
6. Shlepakov, V.N., Kotelchuk, A.S., Suprun, S.A. (1999) Identification of flux-cored wire composition by electric signals of arc welding. *Avtomatich. Svarka*, **8**, 37-42.



APPLICATION OF A TWO-CHANNEL SYSTEM OF AUTOMATIC STABILIZATION OF PULSED-ARC WELDING TO IMPROVE THE WELDED JOINT QUALITY

P.P. SHEJKO, A.M. ZHERNOSEKOV, A.V. LOZOVSKAYA and Yu.O. SHIMANOVSKY

E.O. Paton Electric Welding Institute, NASU, Kiev, Ukraine

Effectiveness of application of a two-channel system of automatic stabilization in consumable-electrode pulsed-arc welding of aluminium alloys under the impact of disturbing factors has been established experimentally. It is shown that the mechanical properties of butt-welded joints of AMg6 alloy produced by pulsed-arc welding deteriorate with increase of electrode wire extension and lowering of the mains voltage. Use of a two-channel system of automatic stabilization of pulsed-arc process allows ensuring the mechanical properties of butt-welded joints on the level of those obtained in optimum modes without disturbances.

Keywords: pulsed-arc welding, consumable electrode, aluminium alloys, automatic stabilization, two-channel system, disturbing factors, average value of welding current, average value of arc voltage, geometrical dimensions of welds, defects, mechanical properties

Consumable-electrode pulsed-arc welding is one of the advanced processes of aluminium alloy welding. Unlike nonconsumable-electrode welding, this process allows solving many problems related to improvement of the quality of welded joints (by decreasing the number and dimensions of oxide inclusions and pores, improving the efficiency of the welding process, lowering welding deformations, etc.) [1–4]. Deviations of mode parameters from the rated values inevitably arise in welding, this being due to the impact of such disturbing factors, as variation of the feed rate, extension of electrode wire and gaps, and warping of edges being welded, fluctuations of mains voltage, tack welding, etc. The above factors lead to variation of the geometric parameters of welds, appearance of various defects, lacks-of-penetration and lacks-of-fusion, as well as lowering of welded joint mechanical properties.

The E.O. Paton Electric Welding Institute developed two-channel systems of automatic stabilization (SAS) of the main energy parameters of consumable-electrode pulsed-arc welding mode, namely average values of welding current $I_{w.av}$ and arc voltage $U_{a.av}$ [5, 6].

The purpose of this study is evaluation of the influence of the developed SAS of consumable-electrode pulsed-arc welding process on the quality of aluminium alloy welded joints.

Influence of the main disturbing factors, namely variation of electrode wire extension and mains fluctuations on the quality of joints of AMg6 alloy plates (GOST 4784–74) has been evaluated. Experiments were conducted using a welding head of GSU-7 type with its control system BARS-2V, pulsed power source of I-169 type, developed at the E.O. Paton Electric Welding Institute [7], and developed two-channel SAS for $I_{w.av}$ (with action on the power source pulse parameters) and $U_{a.av}$ (with action on the welding wire feed rate).

Influence of $I_{w.av}$ and $U_{a.av}$ on geometrical parameters of welds deposited on plates of AMg6 alloy 16 mm thick with 1.6 mm dia. Sv-AMg6 wire (GOST 7871–75) was evaluated. Obtained dependencies are shown in Figure 1.

It is established that in consumable-electrode pulsed-arc welding of an aluminium alloy of AMg6 type, change of $I_{w.av}$ is important, as its variation may lead to considerable deviations of penetration depth h and weld width B (Figure 1, a). Height of weld reinforcement a varies only slightly. Welding current $I_{w.av}$ has a greater influence on penetration depth of aluminium alloys than that of steel [8, 9], which is attributable to their different thermophysical properties. Change of $U_{a.av}$ values in the range of working currents does not have a noticeable influence on weld geometry (Figure 1, b).

Influence of extension L of electrode wire on $I_{w.av}$ and $U_{a.av}$ was evaluated in different consumable-electrode pulsed-arc welding modes (Figure 2). Optimum average values of $I_{w.av}$ and $U_{a.av}$ at initial electrode wire extension of 15 mm, were selected proceeding from the conditions of providing a controllable transfer of electrode metal by «1 pulse–1 drop» law and good formation of deposited welds. Figure 2 shows a change of $I_{w.av}$ and $U_{a.av}$ values, depending on electrode wire extension $L = 15–30$ mm at consumable-electrode pulsed-arc process without SAS and with application of a two-channel SAS.

It is established that with increase of extension L of electrode wire, $I_{w.av}$ and $U_{a.av}$ values change less significantly in aluminium alloy welding than in the case of steels [6]. However, such changes also lead to defect formation.

Results of investigation of metal macrostructure in welds produced by consumable-electrode pulsed-arc welding on a plate of alloy AMg6 10 mm thick suggest that increase of electrode wire extension leads to a non-uniform penetration, lack-of-fusion of the weld with the base metal, as well as formation of a central crystallite in the weld metal (Figure 3, a). Deposited metal consists of two layers, this being due to a different orientation of the crystals. The central crystallite consists of packs of crystals of the same

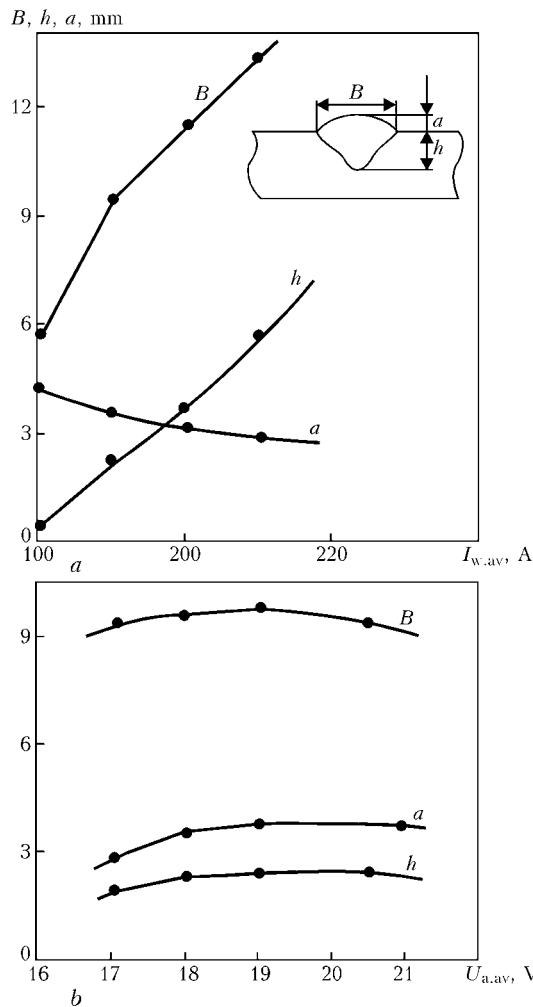


Figure 1. Influence of $I_{w.av}$ (a) and $U_{a.av}$ (b) on geometrical parameters of welds produced by consumable-electrode pulsed-arc process on AMg6 alloy plate with 1.6 mm dia. Sv-AMg6 wire in argon at the welding speed of 22 m/h and current pulse duration of 2.1 ms: a — $U_{a.av} = 18$ V; b — $I_{w.av} = 150$ –155 A

orientation (parallel or at a certain angle to weld axis). Formation of such a structure may lead to deterioration of the mechanical properties of weld metal and welded joint as a whole. Increase of electrode wire extension is accompanied by increase of arc length, this also increasing the number and size of pores from 0.2 to 1.0 to 1.5 mm (Figure 3, a). When SAS is used (Figure 3, b), a uniform melting is achieved, lacks-of-fusion with the base metal are absent, and individual fragments of the central crystallite and small-sized pores (up to 0.1 mm) may form.

Consumable-electrode pulsed-arc process was used for welding butt joints of plates of AMg6M alloy 6 mm thick with a V-shaped groove to evaluate the results of summary influence of disturbing factors, namely increase of the extension and lowering of mains voltage on the mechanical properties of butt welded joints of AMg6 alloy and effectiveness of two-channel SAS application under the conditions of such disturbances. Single-pass welding was performed with 1.6 mm dia. Sv-AMg6 wire in argon (GOST 10157–79) on a copper backing with a forming groove. The groove angle was 60°; root face being 1.5 mm (without a gap). Table 1 gives the parameters of consumable-electrode pulsed-arc welding modes.

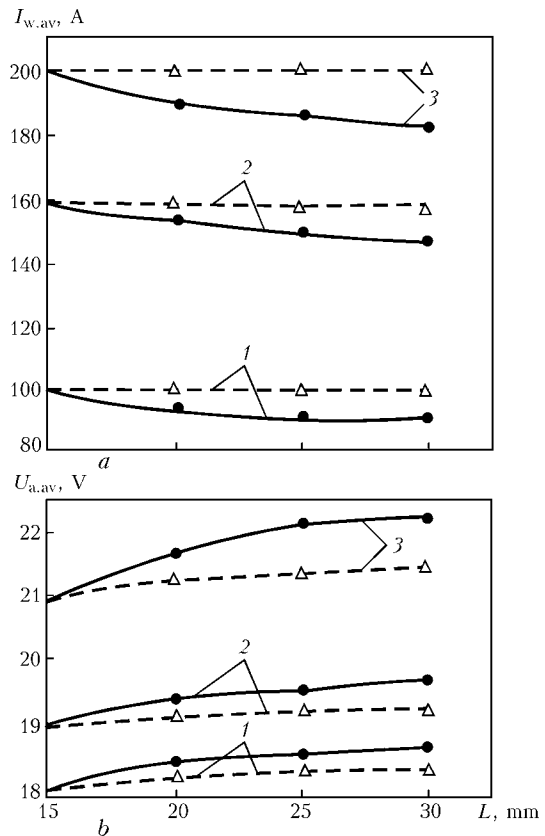


Figure 2. Dependence of $I_{w.av}$ (a) and $U_{a.av}$ (b) on extension L of electrode wire at consumable-electrode pulsed-arc welding of AMg6 sample with 1.6 mm dia. Sv-AMg6 wire in argon without (solid curves) and with (dashed curves) SAS. Peak values of welding parameters at $L = 15$ mm: 1 — $I_{w.av} = 100$ A, $U_{a.av} = 18$ V; 2 — $I_{w.av} = 100$ A, $U_{a.av} = 19$ V; 3 — $I_{w.av} = 200$ A, $U_{a.av} = 21$ V

Mode 1 was implemented with parameters optimum for 6 mm plates of alloy AMg6M without the action of the disturbing factors, mode 2 (without SAS) was used with the action of the disturbing factors, namely increase of electrode wire extension and lowering of mains voltage. This led to a change of $I_{w.av}$ values from 190 to 170 A and $U_{a.av}$ values from 21.4 to 18.5 V. Mode 3 was used with the same disturbances as mode 2, but with SAS application, when initial $I_{w.av}$ and $U_{a.av}$ values were the same as in mode 1. Results of mechanical testing of samples for tension, bending and impact toughness, which were conducted in keeping with GOST 6996–66, are given in Table 2.

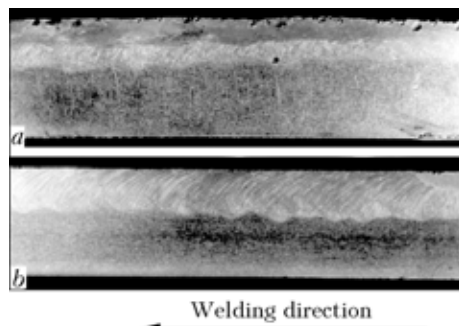


Figure 3. Macrosections of weld metal (longitudinal section) produced on a plate of AMg6 alloy by consumable-electrode pulsed-arc process with 1.6 mm dia. Sv-AMg6 wire in argon at $L = 15$ –30 mm without SAS (a) and with two-channel SAS (b)

**Table 1.** Consumable-electrode pulsed-arc welding modes for AMg6M alloy butt joint

Mode No.	Mains voltage, V	Electrode wire extension L , mm	Arc voltage $U_{a,av}$, V	Welding current $I_{w,av}$, A	Pulse frequency f , Hz	Wire feed rate v_f , m/h
1	376–400	14	21.4–21.8	190–195	117	372
2 (without SAS)	342–354	24	18.5–19.5	170–176	117	372
3 (with SAS)	342–354	24	21.4–21.6	190–191	Adjustable in the range of 140 to 156	Adjustable in the range of 355 to 372

Note. The following parameters are constant: welding speed --- 32 m/h; current pulse duration --- 2.1 ms and pulse amplitude --- 525 A.

Table 2. Mechanical properties of butt-welded joints of AMg6 aluminium alloy

Mode No.	σ_t , MPa	α , deg	KCV, J/cm ²
1	<u>318.0–328.0</u> 324.2	<u>40.0–52.0</u> 47.6	<u>18.0–20.7</u> 19.7
2	<u>190.0–220.0</u> 209.5	<u>13.0–55.0</u> 33.0	<u>13.3–14.6</u> 13.7
3	<u>308.3–332.3</u> 317.0	<u>25.0–48.0</u> 39.6	<u>19.2–20.6</u> 19.8

Note. Data of testing 3 to 5 samples are given.

It is established that compared to the optimum mode, increase of electrode wire extension and lowering of mains voltage lead to a lowering of ultimate tensile strength σ_t by 35.7 %, bend angle α by 30.6 % and KCV impact toughness by 30.5 %. Figure 4 gives macrosections of butt welded joints made in the modes given in Table 1. Action of the above disturbing factors led to initiation of various defects, for instance, lacks-of-fusion with the side wall, lacks-of-penetration (Figure 4, b), and impaired the mechanical properties of welded joints.

Use of a two-channel SAS of the consumable-electrode pulsed-arc welding process at the action of the above disturbances, enabled prevention of defects of the type of lacks-of-penetration and lacks-of-fusion. Mechanical properties of welded joints are on the level of those obtained in undisturbed modes (see Table 2 and Figure 4, a, c).

CONCLUSIONS

1. In consumable-electrode pulsed-arc welding of AMg6 aluminium alloy increase of electrode wire extension or lowering of the mains voltage lead to a change of $I_{w,av}$ and $U_{a,av}$ and initiation of defects of the type of pores, lacks-of-penetration, lacks-of-fusion, as well as structural inhomogeneity in the form of a central crystallite. Presence of disturbing factors lowers by 30 to 35 % the mechanical properties of butt joints produced by the consumable-electrode pulsed-arc process.

2. Application of two-channel SAS of consumable-electrode pulsed-arc welding of AMg6M alloy allows at simultaneous action of the disturbing factors ensuring the mechanical properties of welded joints on the level of properties obtained in undisturbed welding in the optimum modes.

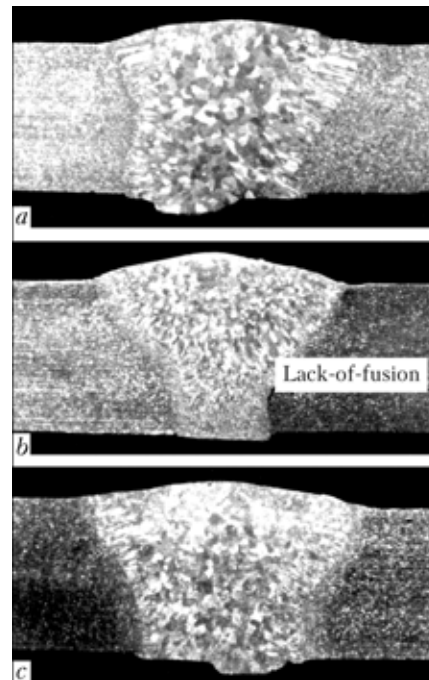


Figure 4. Macrosections of butt-welded joints of AMg6 plates 6 mm thick produced by consumable-electrode pulsed-arc welding: a --- mode without disturbances; b --- with disturbances by electrode wire extension and mains voltage without SAS; c --- with SAS application at disturbances action

- Mashin, V.S., Pavshuk, V.M., Dovbishchenko, I.V. et al. (1991) Influence of pulsed-arc welding parameters of aluminium ADO on the shape and porosity of welds. *Avtomatich. Svarka*, **4**, 57–60.
- Ghosh, P.K., Gupta, S.R., Gupta, P.C. et al. (1990) Influence of pulsed current welding on the microstructure and porosity content of Al–Zn–Mg alloy weldment. *Pract. Metallogr.*, **12**, 613–626.
- Ghosh, P.K. (1996) An analysis of weld characteristics as a function of pulse current MIG welding parameters. *Int. J. Joining of Materials*, **8**(4), 157–161.
- Kudryashov, O.N., Novikov, O.M., Alekseev, I.V. et al. (2001) Welding of thick aluminium alloy structures of flying vehicles. *Svarochn. Proizvodstvo*, **12**, 31–33.
- Paton, B.E., Shejko, P.P., Zhernosekov, A.M. et al. (2003) Stabilization of the process of consumable-electrode pulse-arc welding. *The Paton Welding J.*, **8**, 2–5.
- Shejko, P.P., Zhernosekov, A.M., Shimanovsky, Yu.O. (2004) Consumable-electrode pulsed-arc welding with automatic stabilization of mode parameters. *The Paton Welding J.*, **1**, 7–10.
- Pavshuk, V.M., Shejko, P.P. *Power supply for pulsed-arc welding*. USSR author's cert. 1682076. *Int. Cl. B 23 K 9/09*. Publ. 07.10.91.
- Rimsky, S.T., Svetsinsky, V.G., Shejko, P.P. et al. (1993) Consumable-electrode pulsed-arc welding of low-alloy steels in Ar + CO₂ mixture. *Avtomatich. Svarka*, **2**, 38–41.
- Mandal, A., Parmar, R.S. (1996) Effects of pulse parameters on weld bead geometry. *Int. J. Joining of Materials*, **8**(2), 69–75.



CHOICE OF OPTIMAL PARAMETERS OF EXTERNAL ELECTROMAGNETIC ACTION IN ARC METHODS OF WELDING

R.N. RYZHOV and V.D. KUZNETSOV

National Technical University of Ukraine «Kiev Polytechnic Institute», Kiev, Ukraine

Dependencies are given which allow optimizing the parameters of electromagnetic action. Adequacy of the derived dependencies to the actual welding conditions is confirmed by comparative analysis of the calculated and experimental data. Analysis is performed of the influence of both the welding parameters and thermophysical properties of materials on the optimum range of the mode of electromagnetic action.

Keywords: electromagnetic action, controlling magnetic fields, geometrical characteristics of welding pool, thermophysical properties of materials

Controlled regulation of forced movements of the pool melt flows in welding with electromagnetic action (EMA) allows considerably improving mechanical properties of welds, increasing their corrosion resistance and resistance to formation of hot and cold cracks, decreasing a level of porosity. Analysis of the data of different authors indicates that irrespective of the methods and conditions of welding there is a certain range of EMA parameters under which a maximal increase of technological and physicochemical properties of the welded joints are achieved. Therefore, regularities determining a condition for EMA optimality manifest themselves within this range.

The aim of this work is to establish physically justified criterion of EMA optimality and to develop with its help an engineering method for choosing the EMA parameters with regard to regularities determining the efficiency of its use.

Controlling magnetic field (CMF) in the welding pool (Figure 1) facilitates formation of flows whose movement from the head to the tail area proceeds by turns along each of the side solidification fronts with

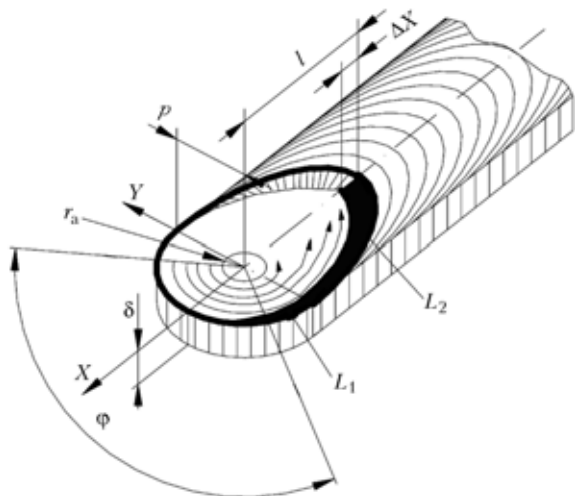


Figure 1. Diagram of welding pool in welding with EMA (for designations see the text)

a frequency corresponding to the CMF reverse interval. In this case solidification front relative to which the overheated melt moves from the head area of the welding pool fuses while the opposite one solidifies with maximal rates (darkened and lined areas in the surface of the pool, respectively). Stop and fusion of one side solidification front and, the other way round, accelerated movement of the opposite one are controlled by the temperature gradients before fronts with periodicity corresponding to the frequency of the changes in the direction of the movement of flows in the pool with reverse of the magnetic field. The work [1] makes a conclusion that a periodical reaching of the most far zone of the solidifying area of the pool by the heat front of the molten metal is a necessary and sufficient condition for the controlled periodicity of growth of crystallites on the whole interface and, thus, for formation of fine grain structure with minimal chemical heterogeneity. Condition of the EMA optimality is presented by the equality $S_{fl} = L_{sol}$, where S_{fl} is the path passed by the flow with its reverse movement; L_{sol} is the length of the side edge of the solidifying area of the pool.

Development of activities in this sphere allowed obtaining the data verifying a correlation between solidification rates and temperature gradients in the interface. It is shown [2] that in the full period of solidification there is a maximum of increase of the actual solidification rates, which falls on overcooling degree determined by the gradient in the conditions under which a time of the overheated melt existence in the tail area of the pool is minimal. Therefore, a path of the flow movement near solidification front for the length L_{sol} remaining necessary is not a sufficient condition of optimality. Extreme dependences of actual solidification rates on the EMA parameters manifest themselves in conditions when time of the flow movement limited by the distance L_{sol} agrees with the time of growth of the non-equilibrium overcooled zone in the solidification front. The indicated regularities predetermining formation of fine-crystal structures in EMA welding allow formulating a physically substantiated criterion of optimality in the form of the equality

$$\tau_{sol} = \tau_{fl}, \quad (1)$$



where τ_{sol} is the time of the non-equilibrium zone intergrowth by the solidification front with maximal rates; τ_{fl} is the time of flow movement for the length L_{sol} .

Components of the equality (1) may be determined by using the available notions about manifestation regularities of solidification peculiarities and forced movements of the flow of the pool melt in EMA welding.

For effective refining of the initial structure for the time of the reverse interval the solidification front should move to the distance equal to the width of the two-phase area ΔX (see Figure 1). Regarding this time the intergrowth of this zone by solidification front may be presented by a dependence

$$\tau_{sol} = \frac{\Delta X}{v_w \cos \alpha}, \quad (2)$$

where v_w is the welding speed; $v_w \cos \alpha$ is the average solidification rate of the considered section.

When determining τ_{fl} we proceed from the fact that in EMA welding the melt flows are formed in the head part of the pool with cross-section $\Delta S = (p - r_a)\delta$, where p is the half-width of the head part of the pool; r_a is the deviation radius of the arc of CMF cross component; δ is the thickness of the welding joint (see Figure 1). For the flow to achieve the solidification front point remote at a distance of $L_{fl} = L_1 + L_2$ and at the same time for a preset change of the temperature gradient for sure to take place regarding complexity of the pool hydrodynamic it is necessary to move the melt volume through the section ΔS :

$$V_{pr} = \Delta S L_{fl} = (p - r_a)\delta L_{fl}. \quad (3)$$

Rigorous calculation of the melt volume passing for the time τ_{fl} through the section ΔS is complicated by the presence of velocity field of its volume elements (parameters of the velocity field depend on distribution of the axial component of the CMF induction B_z and horizontal component of the current density in the welding pool). Preliminary processing of the experimental data showed that this parameter could be sufficiently accurately estimated using the dimension complex obtained on the basis of the Poiseuille formula:

$$\frac{V_{pr}}{\tau_{fl}} = 0.012 \frac{\delta(p - r_a)^2 B_z I_w}{L_{fl}^3 \eta}, \quad (4)$$

where I_w is the welding current; η is the dynamic viscosity of the melt.

Regarding (3) and the fact that when using EMA with reverse axial magnetic fields $\tau_{fl} = t_r$ between two consecutive changes in the polarity of the magnetizing current conducted through electromagnet of the generating device in the welding zone of CMF the dependence (4) may be transformed as follows:

$$B_z t_r = A = 83.3 \frac{L_{fl}^2 \eta}{(p - r_a) I_w}, \quad (5)$$

where $A = B_z t_r$ is the generalized EMA parameter.

In the general case

$$A = \int_0^{t_r} |B(t)| dt. \quad (6)$$

The value L_{fl} was determined regarding the following assumptions: a process of melting and solidification in welding is carried out in the plane; a form of the melting front is described by the circle equation while the solidification front --- by the ellipse equation (see Figure 1). Then

$$L_{fl} = L_1 + L_2 = \pi p(1 - \varphi/180)/2 + \pi(1.5(p + l) - \sqrt{p^2 + l^2})/4,$$

where p and l are the half-width and length of the solidifying part of the pool, respectively; φ is the central angle of the head part of the pool limiting the volume of the melt where the main part of I_w spreads (within the range $B_z = 12 - 25$ mT, $\varphi = 64 + 7.03(B_z - 12)$ [3]).

Geometrical parameters of the pool were determined by the dependences recommended in the work [4]:

$$p = (q\sqrt{2/(\pi e)}) / (n2v_w c \gamma \delta T_{melt}), \quad (7)$$

$$l = (q^2(e - 1)) / (m4\pi\lambda c \gamma v_w e \delta^2 T_{melt}^2), \quad (8)$$

where q is the power of the heat sources; λ , $c \gamma$ and T_{melt} are the thermal conductivity, specific heat capacity and melting temperature of the material in welding, respectively; n , m are the coefficients introduced by the author of the work [4] for consideration of differences between calculated and real sizes of the pool (they also were used for considering changes of the pool geometry caused by wash-out of edges with hot flows of the melt).

In the dependence (2) $\Delta X = l_s - l_l$. Lengths l_s and l_l were calculated using the dependence (8) substituting T_{melt} with the temperatures of solidus T_s and liquidus T_l of the materials to be welded.

A form of the dependence (5) objectively reflects physical processes typical for EMA welding. So, the increase of geometrical parameters of the pool and viscosity of the melt should be accompanied with increase of the EMA parameters. A speed of filling the volume V_{pr} with the melt decreases with increase of the deviation radius of the arc of the CMF radial component, which also requires correction towards increase of the EMA parameters. To a greater extent this regularity is observed while implementing the technology of welding with non-consumable electrode on AC or opposite polarity widely used in welding of aluminium and alloys on its base when deviation of the arc is facilitated by a round form of the non-consumable electrode end. With expansion of the temperature range $T_l - T_s$, which is typical for alloys with complex alloying systems a width of the concentrated overcooling zone increases, thus allowing a

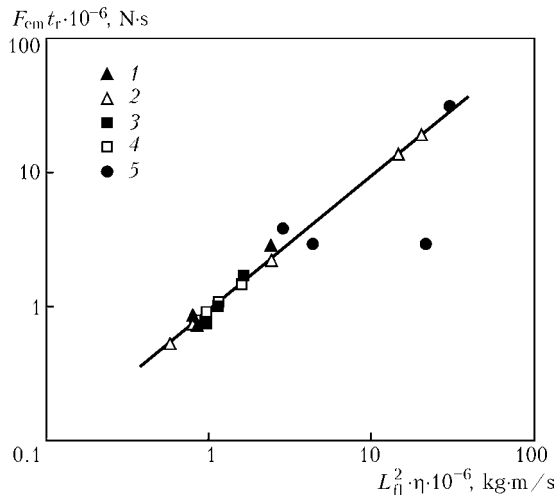


Figure 2. Dependence of pulse of electromagnetic force on square of a distance passed by the flow with viscosity η for the EMA period: 1, 2 — experimental and calculated values for stainless steels, respectively; 3, 4 — same for aluminium alloys; 5 — experimental values for commercial titanium and its alloys

small decrease of the EMA intensity. It is noteworthy that calculation of EMA parameters for materials with narrow temperature range $T_L - T_S$ by the dependence (5) leads to extremely high values of the parameter A , which, when used, may disturb stability of the welding process.

Correspondence of the developed calculation scheme to the real welding conditions was verified by comparison of calculated and experimental optimal values of CMF for stainless steels and alloys [5–10], aluminium [11–14] and titanium [15–19] alloys. Taking into consideration that the authors of the mentioned publications implemented both continuous CMF and CMF pulsing with different porosity the values of the generalized EMA parameter were determined by the dependence (6). Calculations of the pulse of electromagnetic force by using the dependence (5) showed that calculation error for the considered conditions of the welding of stainless steels and aluminium alloys does not exceed 10–15 % (Figure 2). In view of the adopted assumptions these results may be considered satisfactory.

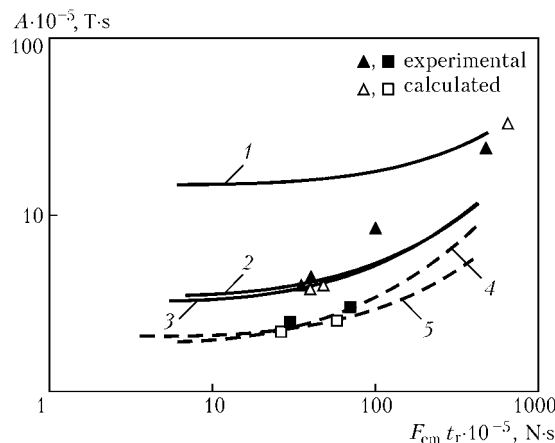


Figure 3. Dependence of parameter A on pulse of electromagnetic force: 1–3 — welding conditions for stainless steels with $q/v = 378, 524$ and 820 kJ/m, respectively; 4, 5 — same for aluminium alloys with $q/v = 310$ and 650 kJ/m, respectively

Verification showed considerable differences in calculated and experimental parameters of EMA conditions in welding of commercial titanium and alloys on its base. In this case excessively high calculated values of the parameter A are specified by a narrow temperature range $T_L - T_S$ and also by the fact that the welding pool has a larger length L_{fl} because of low thermal conductivity. Since according to the authors [15–19] experimental EMA conditions were optimal and allowed successfully solving problems of the pool degassing and increase of corrosion resistance of the weld metal, then they were used for analysis of the factors effecting the EMA parameters.

As a result of processing of calculated and experimental data it is established that high optimal values of the EMA parameters do not always correspond to large power consumptions of the weld in welding of specimens of similar thickness produced of the materials of one class (Figure 3). Such non-correspondence occurs because of large degree of intensification of the applied welding conditions. With unchanged values of running power q/v in case of I_w growth the length of the solidifying part of the pool increases. Simultaneous increase of the pulse of electromagnetic force does not allow achieving a maximal efficiency of the action, which requires a corresponding increase of the generalized EMA parameter. Precisely because of this one requires 2.75 times larger optimal value A with 1.5 lower value of q/v but with practically 3 times more intensive welding conditions (see Figure 3).

Optimal EMA parameters essentially depend on thermophysical properties of the welded materials. So, aluminium alloys have higher thermal conductivity but considerably lower specific mass and melting temperature than stainless steels. Therefore, optimal EMA parameters in welding of aluminium alloys 2 times lower than in welding of stainless steels (Figures 3, 4). Thermal conductivity of titanium alloys with higher specific mass and melting temperature is 4.5 times lower than that of aluminium alloys. Such differences of thermophysical properties with similar thickness of the joints require larger values of parameter A than in welding of aluminium alloy, which does not correspond to the published experimental

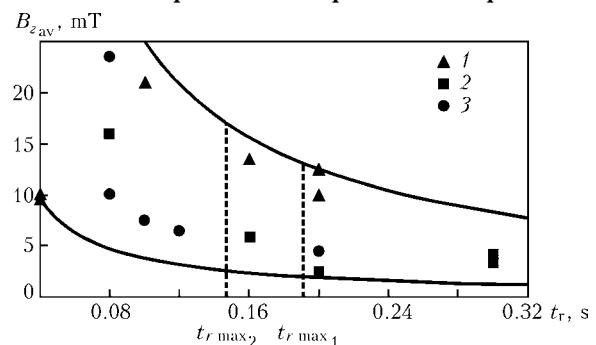


Figure 4. Choice of optimal EMA conditions: 1–3 — experimental EMA conditions for stainless steels, aluminium and titanium alloys, respectively; curves limiting the area of optimal values of CMF induction at preset duration of t_r ; $t_{r \max_1}$, $t_{r \max_2}$ — maximal durations of t_r for stainless steels and aluminium alloys



data. Such discrepancy is explained by the fact that more intensive conditions were used for welding of aluminium alloys in all considered cases.

After determination of the values of parameter A by means of the dependence (5) it is necessary to calculate the value of $B_z = A/t_r$. Considering that the known devices of EMA control are synchronized with the frequency of the power supply the dependence $B_z(t_r)$ with its exponential form analogous to the curves limiting the area of their values and most widely used in practice is constructed by changing t_r with a step of 0.01 s (see Figure 4). Under severe EMA conditions characterized with increased values of B_z and short-term t_r a ripple is formed on the surface of the weld as a result of periodical running of the melt on the solidification front. Therefore, such conditions are not used for multipass welding at the stage of producing top passes. However, under too soft EMA conditions a long-term movement of the melt along the side surface of the pool may cause its considerable melting, which may result in the instability of the form of the fusion line.

EMA parameters should be selected regarding the method of welding. So, increase of B_z higher than critical values in welding with consumable electrode causes increase of spattering. EMA conditions in AC welding of aluminium alloys are characterized with longer t_r and small B_z related to the stability of the arcing process. To provide good manipulation possibilities of the tool and view of the welding zone in manual welding methods the electromagnet for generating CMF located on the body of the torch should have the minimal coiling parameters and mass, which does not permit creating a wide range of B_z values. In this case the required value of the parameter A is achieved by increasing duration of t_r .

In case when EMA is carried out by the use of pulsing CMF with pauses of different duration between CMF pulses the most often $B_z = 5\text{--}25$ mT at $t_r = 0.08\text{--}0.20$ s (see Figure 4). In this situation increase of the porosity of CMF pulses is accompanied by a decrease of the average values of B_z requiring a proportional increase of the EMA parameters. More intensive action is achieved in the case when there are no pauses between the CMF pulses during t_r . This allows reducing B_z range to 5–15 mT and t_r ---- to 0.04–0.08 s. The above indicated differences in the range of values of the parameter A between stainless steels and aluminium and titanium alloys proceed in practice because of corresponding differences in the CMF induction with similar range of durations of the reverse intervals. As it was mentioned above, the EMA conditions would be optimal with performance of the equality (1). In this case if $\tau_{\text{sol}} > t_r$, then the melt may pass the remaining part L_{fl} by inertia. Otherwise it is impossible to achieve maximal effect by using

EMA. This circumstance restricts maximal values of t_r showed by vertical straight lines in Figure 4.

Therefore, the developed calculation scheme based on simultaneous consideration of the effect of geometrical characteristics of the pool and thermophysical properties of the welded material on the hydrodynamics of the melt allows optimizing parameters of electromagnetic action in welding of materials with a wide temperature range $T_L - T_S$ with accuracy sufficient for practical application.

1. Pakhareno, V.A. (1982) Calculation of optimal parameters of magnetic field in argon-arc welding with pool stirring. *Avtomatich. Svarka*, **7**, 39–41.
2. Korab, N.G., Kuznetsov, V.D., Chernysh, V.P. (1990) Evaluation of effect of controlling magnetic field on solidification in arc welding. *Ibid.*, **2**, 33–36.
3. Chernysh, V.P. (1977) Calculation of parameters of movement of weld metal pool in electromagnetic stirring. *Ibid.*, **10**, 12–16.
4. Prokhorov, N.N. (1968) *Physical processes in metals during welding*. Vol. 1. Moscow: Metallurgiya.
5. Ryzhov, R.N., Skachkov, I.O., Chernysh, V.P. (1997) Improvement of resistance of welds to hot cracking in manual nonconsumable electrode arc welding. *Avtomatich. Svarka*, **4**, 25–29.
6. Chernysh, V.P., Kuznetsov, V.D. (1971) Resistance of welds solidified in stirring conditions to hot cracks. *Svarochn. Proizvodstvo*, **6**, 41–42.
7. Chernysh, V.P., Popovsky, V.Yu. (1977) Peculiarities of movement of weld metal pool in electromagnetic stirring. *Avtomatich. Svarka*, **4**, 4–6.
8. Chernysh, V.P., Kuznetsov, V.D., Turyk, E. (1977) Effect of electromagnetic stirring of weld pool on temperature brittleness range of weld metal. *Ibid.*, **9**, 14–17.
9. Pakhareno, V.A. (1979) *Kinetics of solidification and formation of weld properties in electromagnetic stirring welding*. Syn. of Thesis for Cand. of Techn. Sci. Degree. Kiev: KPI.
10. Igumnov, V.P., Maltsev, S.N., Konkov, Yu.D. et al. (1983) Consumable electrode shielded-gas welding with electromagnetic stirring. *Avtomatich. Svarka*, **3**, 41–42, 59.
11. Chernysh, V.P., Syrovatka, V.V., Gritsenko, A.F. et al. (1972) Structure and properties of weld metal on AMg6 alloy in welding with electromagnetic stirring. *Ibid.*, **11**, 16–19.
12. Novikov, O.M., Kryukovsky, V.N., Zhandarev, A.P. (1975) Effect of electromagnetic stirring of weld pool on processes of degassing and destroying of oxide films in AMg6 alloy weld. *Svarochn. Proizvodstvo*, **11**, 14–15.
13. Sityavin, Yu.I., Zubrienko, G.L., Ejdelshitejn, A.E. (1978) Effect of controlling magnetic field on structure and tightness of AMg6 alloy weld. *Ibid.*, **9**, 33–35.
14. Chayun, A.G., Syrovatka, V.V., Matyash, V.I. (1981) Arc welding of 01420 aluminium alloy with electromagnetic stirring. *Avtomatich. Svarka*, **6**, 19–21.
15. Kuznetsov, V.D., Malinkin, I.V., Chernysh, V.P. et al. (1972) Effect of electromagnetic stirring on structure and properties of VT6S alloy. *Svarochn. Proizvodstvo*, **5**, 8–9.
16. Shelonkov, G.M., Troyanovsky, V.E., Briskman, A.N. et al. (1974) Effect of electromagnetic stirring on properties of thin-sheet titanium welded joints. *Ibid.*, **12**, 21–22.
17. Blashchuk, V.E., Gurevich, S.M., Onoprienko, L.M. et al. (1976) Effect of electromagnetic stirring of weld pool on properties of VT1-0 alloy joints. *Avtomatich. Svarka*, **8**, 40–43.
18. Shelonkov, G.M., Chernysh, V.P., Gurevich, S.M. et al. (1977) Peculiarities of weld formation in arc welding of titanium with electromagnetic stirring. *Svarochn. Proizvodstvo*, **3**, 24–25.
19. Abzalov, M.A., Abdurakhmanov, R.U., Iuldashev, A.T. (1978) Electromagnetic effect on process of primary solidification of titanium. *Ibid.*, **5**, 1–3.

STEEL AND WELDING IN CONSTRUCTION ENGINEERING

V.N. BERNADSKY

E.O. Paton Electric Welding Institute, NASU, Kiev Ukraine

In the paper modern civil engineering is presented as an independent sector in the economies of the world leading countries that is characterized by a growing application of steel metal products and welding equipment. Approximate scope of application of steel and steel metal products in the industrial and civil construction of several countries is evaluated. It is shown that welding and allied technologies are no-alternative processes of treatment and joining during fabrication and construction of steel building structures. Predicted tendencies of development of the sector of welding equipment in the world welding product market are outlined.

Keywords: welding, cutting, constructional metalwork, welding facilities, market, projection trends

• Modern industrial and civil engineering and construction industry occupy one of the leading places as an independent sector in the countries with developed economies. For example, total expenses for construction in the USA in 2004 made up 346 bln USD, which corresponds to the third place after such leading sectors of industrial production in the USA as motor industry (510.7) and manufacturing of tools and electronic devices (436.4 bln USD).

Active growth of consumption and processing of metalwork, first of all steel, is one of the peculiarities of modern construction engineering. Despite of appearance of such alternative structural materials as aluminium and plastic, steel remains the basic structural material and its world production exceeded 1 bln t in 2004. Transfer to a wide application of steel welded metalwork often instead of reinforced concrete for construction of industrial and commercial structures, high-rise buildings, sports structures, transport overpasses, sea platforms, tank batteries and others provides a decrease of the cost of construction and assembling works, increase of reliability and longevity of engineering structures with a decrease of their total mass.

Volumes of using steel metalwork in construction of objects and structures different in their purposes have specifics in every country. Figure 1 shows diagrams characterizing a share of steel structures in con-

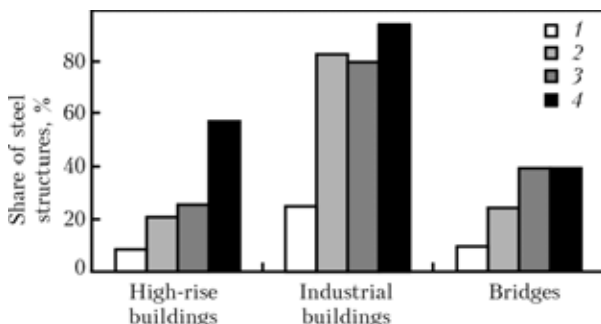


Figure 1. Share of steel structures in construction of different objects in certain EU countries: 1 — FRG; 2 — France; 3 — the Netherlands; 4 — Great Britain

struction of three groups of objects: high-rise buildings and architectural structures, industrial building and objects as well as bridges in a number of European countries. It is shown that steel structures are mainly used in industrial construction; construction of bridges and viaducts takes the second place. Use of steel structures in FRG is noticeably lower than in France and Great Britain (even though FRG produces steel in larger volumes than in France and Great Britain altogether). The study was carried out by the German metallurgists in the end of the 1990s that allowed determining large potentials for domestic supplies of steel products for construction engineering.

• The use of steel and steel metal products in construction engineering of specific countries depends on the number of factors, first of all, on the level of development of the national economy, scales of construction and total volume of steel application. The following data give the idea on the value of domestic consumption of steel in the leading countries in 2003 (mln t): China — 258.1; USA — 103.9; Japan — 77.0; FRG — 37.5; Italy — 33.6; Russia — 26.8; Ukraine — 16.5; Great Britain — 13.9.

Until recently the leading positions in application of steel metalwork were occupied by Japan, which (disregarding certain economical constrains and a decrease of construction volumes) consumes up to 25–30 % of the total steel consumption. In this case its larger share (about 4/5) is used for industrial construction, particularly for construction of bridges. In the middle of the 1990s the volume of using steel metalwork only in the industrial construction of leading countries of the European Union was 5–10 % of the total volume of steel consumption in the respective countries. In Russia in 2001 according to the data of the State Research Center of the RF «I.P. Bardin TsNII Chermet» consumption of steel rolled stock in construction exceeded 6 mln t or more than 20 % of the total domestic consumption.

Structures of industrial building and erections are the basis of the fund of metalwork in Ukraine, their share achieving 65 %. However, in the recent years the volumes of industrial construction and replenishment of the fund of steel structures in Ukraine sharply dropped.



Therefore, one can estimate that the construction engineering sector of different countries uses the steel metal products within 10–30 % of their domestic consumption. If to proceed from this index one can assume that at present the leading place in the world for application of steel and steel metal products in the civil engineering is held by China, which doubtlessly occupies the leading place in the world for production and consumption of steel. In 2003 consumption of steel in China exceeded 257 mln t, i.e. made up almost third of its global consumption. If to consider that only 10–20 % of the total steel consumption was used in China in 2003 for construction, then the volumes of completed structures and erections achieved 25–50 mln t.

- In modern construction industry and in construction and assembling works welding and related technological processes are the only basic technology for processing and joining of work pieces and elements of metal structures: severing, surfacing, application of special protection coatings and others. All steel constructional metal structures can be with a big probability considered welded construction structures. Total production expenses for welding in the sector of construction engineering of the leading countries are comparable with analogous expenses in machine-building sectors. For example, in the USA total expenses specifically on welding in construction engineering in 2000 were 11.3 bln USD, which in the absolute value exceeds welding expenses in leading industrial sectors of the USA. Particularly, expenses in machine-building amount only to 7.6 bln USD or 67 % of expenses for welding in the sector of construction engineering.

Practically all conventional technologies of electric arc pressure and fusion welding find their application in the construction engineering. Naturally, the technological processes of welding for construction-assembling conditions in the open sites, at great height and under sharp variations of the ambient temperature are adopted to these conditions due to special equipment, welding techniques and relevant welding-technological properties of the welding consumables. Expansion of the range of plates and sections as well as introduction of new steel grades used in construction facilitate continuous improvement of welding technology and methods providing required physical-mechanical properties of welds and high operational reliability of both welded joints and welded steel structures on the whole.

Technologies of severing are analogous to the technologies widely used in the industrial enterprises for production of work pieces (mainly gas-oxygen and plasma-arc cutting). In the recent time hydroabrasive cutting of high-alloyed steels, metal polymers and elements of combined systems of dissimilar materials is gaining its application. This process is characterized by the absence of the heat-affected zone, deformations as well as by a high quality of cut.

In conditions of commercial production of large-dimension work pieces and components of engineering structures the welding production has very little difference from the welding technologies applied in large machine-building or ship-building enterprises. Expansion of the use of large-thickness steels in struc-

tural elements (particularly for welding I-shaped columns and bridge beams labor-consuming in their manufacturing) creates demand for welding robotic systems in the construction engineering. This allows the producers of welded structures to solve the problem of providing high and stable quality of welded joints and in particular to partially settle the shortage of highly qualified welders.

It is noteworthy that the increase of the volume of construction and assembling works as well as the scope of welding in the construction is accompanied by a flow of the qualified welders from machine-building sectors where the level of automation and robotic applications in welding processes is increasing more intensively than in construction engineering. This tendency is most vividly exposed in the USA and Japan where the shortage of highly qualified welders is a long-standing problem.

- Producers and the world market of structural materials actively respond to the current demand of both receptive and potential consumer. First of all this concerns supplies of steel and steel structures as the basic material preserving its significance for a long-term perspective. Among materials steel possesses a perfect «price/quality» criterion and is highly ecology-friendly. Steel engineering structures after expiry of their service life are easily and comparatively cheaply exposed to recycling as against reinforced concrete. Creating new grades of steels, first of all, well welded low- and microalloyed steels of increased and high strength metallurgist in cooperation with construction engineers solve urgent problems of decreasing mass of the structures with simultaneous increase of operational loads and reliability of both specific elements and the structure as a whole.

Along with increase of volumes of supplies, continuous increase of physical-mechanical and technological indices of the mastered steel grades and production of new ones metallurgist together with construction engineers put a lot of efforts for expanding, optimization and improving the range of sheets and profiles. Production and supply of thin hot-rolled plates including steels of increased strength as well as long corrugated sheets with and without protection coating, thin-plate roll-formed sections as well as rolled-welded multilayer packages (sandwich type) for roofing and wall elements and also for the so-called light structures for construction are increasing. At the same time metallurgists are bringing to the commercial level production of thick plates and special thick-walled rolled stock of well welded structural steels including high-strength ones. This also includes non-standard heavy T-sections, wide-strip and non-symmetric rolled and rolled-welded bridge beams, bridge crossings and spans. Cooperation of German and Japan metallurgists resulted in supplying to the construction market long sketch plates of different geometry with small difference in the thicknesses (35–55 mm) with bevels, recesses and grades (in section).

It is cost-effective to produce at the enterprises of ferrous metallurgy steel half-products as the components of construction systems of the module type, particularly for thin-layer spans, combined ceiling systems with cell-shaped beams for commercial buildings as well as for module steel frames for rapid as-

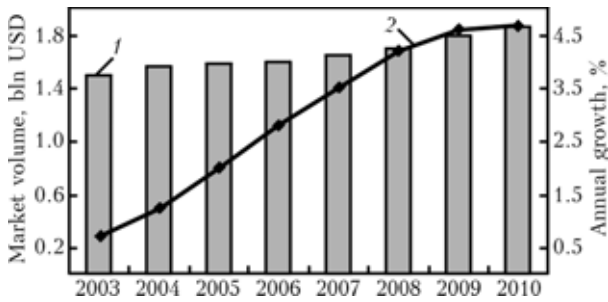


Figure 2. Projection of developments in world market of welding equipment and accessories for construction (the Frost&Sullivan Report B 199): 1 — market volume; 2 — annual growth

sembling of supporting structure of houses in the mass individual construction. The latter products have gained practical development in the housing construction in the USA and Australia. Application of these products as well as industrialization of production of welded structures leads to a decrease of assembling, the scope of welding operations in construction and increase of their quality.

- Growth of activity in construction is accompanied by an increase of demand for welding facilities, particularly for high-productive welding consumables and specialized welding equipment considering peculiarities of welding operations in the open sites, in the conditions of assembling and others. The world welding market is very responsive to the increased demand of the construction sector. Market supplies of high production electrodes with iron powder in the coating, with cellulose coating, electrodes for vertical-downward welding, universal electrodes for welding in all spatial positions as well as electrodes for welding of low-alloyed steels of increased strength and special electrodes for welding of alloyed steels are increasing. Regarding requirements of the constructors a supply of new grades of solid and flux-cored wire for mechanized gas-arc welding in plant and assembling conditions is increasing.

Structure of the world market of welding facilities is determined by sales volumes of its two main components — the market of welding consumables (70 %) and the market of welding equipment (30 %). The general tendency of the last year is a decrease of the cost of welding consumables and increase of the cost of welding equipment. The latter is related to the growth of prices for the modern welding equipment (as a rule with electronic systems of regulation and control) as well as with development of production of specialized welding equipment for new advanced technologies of welding, which do not need filler materials and others. It is the growth of construction volumes and application of new steel grades and a range of rolled stock as well as new designs in industrial and civil engineering that has led to an increase of the share of welding equipment and keen demand for innovation technologies and equipment for welding in construction engineering.

In compliance with calculations of the international society of producers the experts of the world-known Frost&Sullivan Company predict the growth of sales volumes of welding equipment for construction from 1.5 in 2004 up to 1.86 bln USD in 2010. Information on the total turnover of sales of welding equipment and construction accessories in 2003 and

the forecast for its growth until 2010 is given in Figure 2. Curve in the same Figure characterizes rather moderate rates of annual growth of the sales volumes for this equipment, which do not exceed 0.7–0.8 % and somewhat decrease by 2008–2010.

There are also changes in the regional markets of welding equipment and accessories specifically for welding in construction. So, industrially developed countries of the Northern America and Western Europe until recently consumed considerable quantities of welding equipment for construction, however due to a high degree of saturation of construction enterprises with this equipment, the further perspectives are rather negative. Such decrease of the demand in the world market of welding equipment is partially offset by growing sales volumes in the countries of the South-Eastern Asia (first of all China) and in the countries of the Eastern Europe where one can observe a noticeable increase of industrial and housing construction. The total growth of the market of welding equipment for construction should be partially attributed to the growth of the share of China in the market. Swift economical development of China, its welding production and industry for welding machinery is accompanied by a growing share of China in the world market of welding equipment from 10 % in 2003 up to 19 % in 2010. After accession of Poland to the EU one expects growth of the volumes of its industrial production including the welding sector.

The experts explain small growth rates of the market of welding equipment in part by a number of reasons. Construction industry with its traditions is characterized by a rare renovation of welding equipment and rather conservative attitude to new technologies and technical innovations of the modern welding systems. Besides, growing cost of equipment is not always compensated by increased efficiency of its application.

Market of welding equipment despite of some difficulties is on the whole based on the newest technical achievements, which meet the interests of the final consumers and intensively growing sphere of its application. For example, volumes of using mechanized gas-shielded welding with solid and flux-cored wire in the plant and assembling conditions in construction are growing. In this case innovations are mainly aimed at decreasing mass and achieving small size of the welding current sources and semi-automatic machines, furnishing of the welding equipment with integrated control systems of power supplies and wire feed mechanisms. Specialized inverter power supplies for mechanized gas-arc welding in construction-assembling conditions have started to be supplied to the welding market. It is significant that gas-arc welding with inverter power supplies permits decreasing requirements to qualification of the welder while the welding may be carried out in any weather conditions without considerable deterioration of the weld quality.

Equipment and consumables for mechanized (semi-automatic) gas mixture and gas-shielded welding in construction have confidently occupied the second place after equipment, electrodes and accessories for manual welding.

HIGH-EFFICIENCY WIDE-LAYER SURFACING USING ELECTRODE WIRES AND STRIPS (REVIEW)

I.A. RYABTSEV

E.O. Paton Electric Welding Institute, NASU, Kiev, Ukraine

Main methods for high-efficiency wide-layer surfacing using electrode wires and strips are described. Their advantages and drawbacks are considered. Examples of commercial application are given.

Keywords: arc surfacing, electroslag cladding using strips, electrode wires, electrode strips, penetration depth, deposition efficiency

One of the key goals of surfacing operations is to achieve high efficiency of the process (as to the mass of metal or surface area of layer deposited per unit time). The efficiency can be increased by two methods: direct method, i.e. through raising quantitative indicators of deposition, and indirect method, i.e. through decreasing the content of base metal in the deposited one, thus reducing the quantity of deposited layers needed to provide the required composition of deposited metal.

High-efficiency wide-layer surfacing (cladding, hard-facing) using electrode wires or strips allows both methods to be used to address the problem of raising the deposition efficiency.

High-efficiency surfacing using electrode wires.

Multi-electrode surfacing (surfacing using split electrode) is performed with two or more electrode wires used simultaneously, sharing the welding current conductor. The method provides high efficiency of the process, reduction in specific heat input and decrease in penetration and buckling of workpieces. Drawbacks of multi-electrode surfacing include complexity of the mechanisms used for feeding a large number of electrode wires. This problem is solved in the simplest way for two-electrode surfacing. In this case no upgrading of the feed mechanisms used in standard surfacing automatic devices A-874N, AD-231, A-1406, etc. is required. Only a special nozzle for feeding two wires is employed. In a case of three or more electrode wires, it is necessary to use both special feed mechanisms and nozzles [1]. Furthermore, multi-electrode surfacing involves difficulties associated with mounting of a large number of wire spools on the surfacing machine. Some difficulties arise also in connection with the technological process. The matter is that the surfacing wire bundles have different weight, and every time to replace one of the finished bundles it is necessary to stop the surfacing process.

Because of these difficulties, the two- and, less often, three-electrode surfacing process has gained the increasingly wide commercial acceptance [2]. Report-

edly [1], there are designs of equipment where 15 electrode wires are used simultaneously. In a case of 2 electrode wires with a diameter of 3.6 mm, the deposition efficiency amounts to 14 kg/h, and in a case of 15 electrodes --- 100 kg/h. The content of base metal in the deposited one reaches 20--25 % [1, 3]. Additional possibilities are opened up in the case of feeding powder additives to the weld pool. The use of such additives leads to decrease in excessive heat in the pool, allows the process to be performed under the forced conditions, assures the high quality of metal, and provides formation of the required compositions of alloys of initial components directly on the surface of workpiece during the surfacing process. Composition of the deposited metal can also be adjusted by feeding different compositions of wires to the common weld pool.

In multi-electrode surfacing the distance between the electrode axes should be equal to 3--4 electrode diameters. At a large width of the layers (more than 100 mm) and a large quantity of electrodes, it is recommended to vary the distance between them along the front of the deposited layer: at the ends the electrodes should be placed at a distance of 1--2 diameters, and at the centre --- at a distance of 3--4 diameters [1]. This arrangement of electrodes provides good formation of deposited layers and guarantees the absence of lack of fusion.

Important feature of multi-electrode surfacing using a common current supply is an alternate (pulsed) melting of electrodes. With the properly selected values of voltage and electrode wire feed speed, electrodes in the multi-electrode system are spontaneously melted in a pulsed mode using no special devices. Pulsed melting of electrodes at the front leads to dissipation of heat input into the base metal and decreases the penetration depth [1].

Surfacing with electrode weaving opens up extra capabilities [4], as it allows width of the deposited layer to be flexibly varied from 12--15 to 120--140 mm, thus ensuring a sufficiently high efficiency and good formation. Forward inclination of electrode at an angle of 50--65° to the surface treated and high weaving speed (150--300 m/h) minimise penetration of base metal. Available are the weaving mechanisms that allow deposition of a layer with a total width of up



to 300 mm, providing simultaneous weaving of 2–4 electrodes and adjustable distance between them [5].

Both DC and AC power supplies can be applied for multi-electrode surfacing. Advantages of using DC power supplies include a high consistency of electrode melting, reduced spattering and high quality of deposited metal. And drawbacks include an increased power consumption and probability of arc blow at a deposited layer more than 100 mm wide.

Advantages of using AC power supplies are a good consistency of electrode melting and absence of arc blow at width of the deposited layer equal to or more than 600 mm, as well as decreased power consumption. A drawback is a worse formation of the deposited layer.

Arc surfacing using flux-cored strips. The E.O. Paton Electric Welding Institute pioneered the use of flux-cored strips for surfacing [6]. And up to now the Institute is a leader in development and manufacture of these surfacing consumables. The method is characterised by high deposition efficiency (up to 70 kg/h when using two strips with a section of 3×45 mm [7]) and relatively low penetration (content of base metal in the deposited one is 15–30 %). The fill factor of flux-cored strips amounts to 70 %, i.e. they provide deposited metal with a high alloying degree, much higher than in flux-cored wire surfacing. Flux-cored strips are made using special machines equipped with proportioning devices and rollers for forming, curling of a strip sheath and compacting of core of the formed flux-cored strip. The process of drawing is absent in manufacture of flux-cored strip, which greatly reduces production costs.

Surfacing flux-cored strips are 3–4 mm thick and 14–45 mm wide. Characteristic peculiarity of the majority of the developed flux-cored strips is their versatility. They can be applied for surfacing both by the submerged-arc and open-arc methods. Reported [8] is an experience with CO_2 surfacing using flux-cored strips. Flux-cored strip surfacing provides sufficiently high homogeneity of deposited metal [9], although a bit inferior to that provided by other electrode materials [10].

Hard-facing by the automatic arc method using self-shielding flux-cored strips is most widely applied in manufacture of blast furnace bells and hoppers [11–13]. To raise the productivity, hard-facing is performed with two self-shielding strips used simultaneously (voltage from a separate power supply is fed to each of the strips), the width of weaving of which amounts to 400 mm. To minimise the amount of cracks formed along the generating line of a bell and having a negative effect on wear resistance of deposited metal [14], hard-facing is performed by continuously depositing individual beads along the generating line and moving a workpiece by a deposition pitch. This method is called «deposition of stringer beads». At present it is a key method for hard-facing of blast furnace bells and hoppers. Movement by a deposition pitch is provided by a special control device.

Intermediate and protective bands of bells and hoppers are deposited with flux-cored strips PL-Np-300Kh25S3N2G2 and PL-Np-120Kh22R3G2S. Deposition of a contact band is performed primarily with flux-cored strips PL-Np-500Kh40N40S2R and PL-Np-400Kh20B7M6N5V2F [12, 13]. Components of blast furnace loading devices that use no bells are also deposited by the automatic method using self-shielding flux-cored strips PL-Np-450Kh20B7M6V2F, PL-Np-500Kh40N40S2RTs and PL-Np-550Kh44N34GSR [15].

The E.O. Paton Electric Welding Institute suggested that cladding on thin plates should be done using self-shielding flux-cored strips PL-AN101, PL-AN171, PL-AN179, etc., to deposit layers characterised by high wear resistance under abrasive and gas-abrasive wear conditions [16]. Hardness of the deposited layer is *HRC* 55–64. The equipment and process developed provide finished plates 2600×1400 mm in size with a treated surface 2500×1250 mm in size. Thickness of base metal can be varied from 5 to 12 mm, and that of the deposited layer — from 3 to 17 mm. The deposition efficiency amounts to 25 kg/h, and the penetration depth is no more than 4 mm.

Wear-resistant bimetal plates can be used to make hoppers, conveyers, chutes, cyclones, smoke exhausters, dump truck bodies and other parts and structures subjected to intensive abrasive wear during operation.

Experience is available in application of cladding using flux-cored strip PL-AN150 for critical parts of power generation and petrochemical gates Dn700, Dn1000 and Dn1200 [17], as well as parts of construction and road machines [7]. In the latter case the cladding process is carried out using flux-cored strip PL-U30Kh30G3TYu with a cross section of 3×45 mm. Cladding with one or two strips provides a layer 50 or 100 mm wide, respectively, deposited in one pass. The deposition efficiency in this case amounts to 70 kg/h.

Arc surfacing using sintered strips. The E.O. Paton Electric Welding Institute and I.N. Frantsevich Institute for Problems in Materials Science of the NAS of Ukraine developed technologies for manufacture and application of sintered (cermet) strips to be used as electrode materials for cladding by the submerged-arc method [18]. Sintered iron-base strips are made by the powder metallurgy methods using cold rolling and subsequent sintering of mixtures of metal powders, ferroalloys, graphite and other materials with a particle size of 70–200 μm in shielding atmosphere at a temperature of 1200–1300 °C. Sintered strips have the following characteristics: tensile strength is not less than 60 MPa, porosity is not more than 30 %, and density — not lower than 6 g/cm³. Sintered strips are produced with thickness of 1.0 ± 0.2 mm and width of 30–100 mm (with an interval of 5 mm). The deposition rate is 40–45 g/(A·h) (deposition efficiency — up to 30 kg/h). The content of base metal in the deposited one is no more than



15 %. Cladding using sintered strips by the submerged-arc method provides good formation of the deposited metal and good detachability of the slag crust [19, 20].

Owing to porosity, sintered strips have increased electrical resistance, resulting in enhanced heating of electrode extension during the deposition process [21]. This leads to a 20–30 % increase in productivity compared with cold rolled strips of an identical cross section and composition. Uniform distribution of components of the charge particles across the section of a sintered strip provides deposited metal with a more homogeneous chemical composition, compared with the use of flux-cored strip. In turn, this leads to improvement in its performance [22, 23]. Another advantage of sintered strips is the possibility of manufacturing them from super pure powders.

The experience is available in cladding by the submerged-arc method using two sintered strips, where one strip is used as an electrode, and the other strip is used as a filler [24]. In this case the deposition efficiency almost doubles and penetration decreases, which makes it possible to achieve the required composition of deposited metal even in the first layer.

In the 1980s, the output of sintered strips amounted to 600 t/year [25, 26]. Sintered strip LS-70Kh3MN was applied for treatment of spring-loaded supports of KamAZ trucks [27]. At the Kalkomansk (Kazakhstan) and Bryansk (Russia) factories DOR-MASH strips LS-U10Kh7GR and LS-70Kh3MN were applied for hard-facing of knives of bulldozers and grading machines [28]. Cherepovetsk Metallurgical Plant used up to 100 t of sintered strips for hard-facing of roll-table rollers, reel blocks, etc. [29].

Arc surfacing using cold-rolled strips. Cladding by the submerged-arc method using cold-rolled strips was applied for the first time for treatment of hydraulic turbine blades [30, 31]. Strip of steel 10Kh18N9T with a cross section of 0.5×70 mm was used for this purpose. Since then the method of arc cladding using cold-rolled stainless steel strips has been widely accepted in industry [32]. Depending upon the process parameters and strip sizes, the deposition efficiency ranges from 10 to 35 kg/h, and the content of base metal in the deposited one is 10–25 %. To impart desirable properties to the deposited metal, it is necessary to deposit two layers or more. This method was employed for deposition of corrosion-resistant layers on parts of nuclear power station equipment [33]. Cladding was performed in two layers by the submerged-arc method using flux 48-OF-10. The first layer was deposited using electrode strip Sv-07Kh25N13, and the second layer — using strip Sv-04Kh20N10G2B. Total thickness of two layers was 9–11 mm. To treat internal surfaces, it is necessary to continuously remove the slag crust. Moreover, to avoid overheating of a workpiece, the cladding process should be interrupted or the outside surface should be cooled with water. To eliminate these drawbacks, it was suggested using the two-start cladding method,

i.e. first the individual beads are deposited with a certain pitch, and then, with the second start, the gaps between them are filled in. This cladding process was employed also for hardening of work surfaces of forming drums used in lines for production of coiled plastics. The cladding consumables were electrode stainless steel strip Sv-20Kh13 with a cross section of 0.4×50 and 0.5×60 mm, and flux 48-OF-10. Hardness of deposited metal in the second and subsequent layers was *HRC* 40–43 [34]. High-efficiency cladding by the submerged-arc method using cold-rolled strip 08kp (rimming), etc. is used to restore dimensions of different parts or as a bond coat in deposition of high-alloy materials.

The Priazovsky State Technical University developed the method for wear-resistant hard-facing with cold-rolled strip of steel 08kp by the submerged-arc method using alloying ceramic fluxes [35–38]. Hard-facing of parts operating under conditions of friction of metal on metal at normal and increased temperatures, thermal cycling and high contact loads (rollers of continuous casting machines) is performed by the submerged-arc method using flux ZhSN-5, whereas flux ZhSN-6 is used for hard-facing of parts operating under conditions of thermal cycling, impact loading and high specific pressure (knives for hot cutting of metal, etc.).

To raise productivity, it was suggested that hard-facing should be performed with increased electrode strip extension [35]. The productivity can be raised by a factor of 1.5 through heating the electrode extension with a current flow. As hard-facing is carried out using thin strip, the required stiffness is imparted to the strip by profiling, i.e. flanging of its edges. Profiling of strips is done directly in a feed mechanism of the welding automatic device. The optimal shape of edges flanged on radius also allowed improvement of quality of the deposited metal formation.

Reported [39] is another example of arc cladding of rolling mill support rollers using electrode strip of tool steel 25Kh5FMS. Production of this strip for in-house needs was mastered at the Metallurgical Plant SEVERSTAL.

Submerged-arc surfacing with cold-rolled strips is performed, as a rule, by using the DC power supplies. In the case of strip more than 100 mm wide, this leads to the effect of arc blow and dramatically deteriorates the deposited metal formation. However, providing that this effect is suppressed by using special devices, strips of a much larger width can be used for surfacing.

Electroslag surfacing using strips. As noted above, in the case of arc cladding with strips the required composition of deposited metal can be achieved only in the second layer. To avoid this drawback, it was suggested that two strips should be used for cladding, i.e. electrode and filler [24, 40]. The patent of the Austrian inventor P. Scherl [41] provides for feeding two or more electrode strips, which are «melted in the common weld pool due to formation of the electric arc». The process of cladding with two



parallel strips at a certain gap turned out to be most promising in this respect [42]. Because cold flux does not get into the gap, liquid slag heats up heavily and shunts the current flowing through the strips. According to the estimate made by the authors, the current flow through the slag amounts to about 60 %, while that through the arc constitutes 40 %. For strips 60 mm wide the recommended size of the gap is 8–10 mm. In cladding with two strips 60 × 0.5 mm in size, the process productivity reaches 26 kg/h, and the content of base metal in the deposited one is not in excess of 9 %. In the 1970s, the E.O. Paton Electric Welding Institute conducted experiments to convert this process into the fully electroslag one [43]. Cladding was performed with two cold-rolled (Sv-08Kh19N10G2B) or sintered (LS-07Kh23N12G) strips. Good results were obtained with fluxes AN-26P and 48-OF-10. Application of these fluxes provided a stable electroslag process and excellent formation of the beads. Under the pinch effect, the liquid slag goes up to a significant height in the gap between the strips. Heating and melting of the strips occur exclusively as a result of heat transfer from the slag melt. The efficiency of heating and productivity of melting of the strips are higher compared with the combined arc-slag processes. The arc-free character of the process is confirmed by the oscillography data.

The gap size has a high effect on the process. If a gap is too small, the slag pool becomes overheated and boils, thus leading to the arc process. Whereas with a gap which is too large the slag pool surface area increases, its temperature falls, resistance rises, and the process is converted into the arc one. At low power the process is performed using small gaps, and at high power the gap is made larger. In cladding with two sintered strips LS-07Kh23N12G 60 × 0.8 mm in size the deposition efficiency is over 40 kg/h, and the base metal content of the deposited one is 5–8 %. Increasing the strip width to 100 mm allows the deposition efficiency to be increased to more than 60 kg/h. Like in the arc process, the effect of arc blow shows up in electroslag cladding with strips more than 100 mm wide. And again, if this effect is suppressed, cladding can be performed with wider strips.

The primary application of electroslag cladding using strips is in nuclear and power engineering [44–48]. Internal surfaces of equipment made from low-alloy pearlitic steels (15Kh2NMFA, 10G2N2MFA, etc.) are clad with a layer of chrome-nickel austenitic steels to ensure high corrosion resistance of materials in contact with coolant of the primary system of a nuclear power plant. As noted above, anticorrosion arc cladding with strips requires deposition of two layers. One-layer electroslag cladding is performed using a specially developed cold-rolled strip Sv-03Kh22N11G2B, which provides deposited metal with the required anticorrosive and mechanical properties [46, 47].

Attempts were made to employ the electroslag process for cladding with sintered strips to provide deposited metal of the type of wear-resistant carbon steels [49, 50]. The electroslag process was stable and consistent at an up to 0.1 % C content of strip, whereas at a higher carbon content the process alternated with the arc one. At a fixed content of deoxidisers (manganese and silicon) in strip, increase in the content of carbon is accompanied by its intensive oxidation to evolve a large amount of CO. This causes intensive boiling of the pool and violation of the electroslag process. Oxidation of carbon is enhanced at high amounts of FeO, MnO and SiO₂ present in slag. This explains a lower stability of the cladding process in the case of using high-silicon fluxes. When strips are alloyed with strong deoxidisers, the cladding process can be stabilised, and in this case electroslag cladding can be performed with sintered strips LS-5Kh4V3F and LS-45Kh4V2M2FS containing up to 0.5 % C.

Low dilution of base metal with the deposited one in electroslag cladding with strips allows the quantity of deposited layers to be reduced, which leads to decrease in strains, sensitivity of deposited metal to cracking and labour intensiveness of cladding.

Therefore, different high-productivity methods are available now to perform wide-layer surfacing using electrode wires and strips, which have been tried out to advantage in commercial production. Wide variety of surfacing methods allows a factory specialist to select the most rational method out of them, based on availability of equipment and surfacing consumables in the market, as well as their affordability and price.

1. Melikov, V.V. (1988) *Multi-electrode surfacing*. Moscow: Mashinostroenie.
2. Malikin, V.L., Oparin, L.I., Gladky, P.V. et al. (1988) Surfacing of rolls of continuous casting machines. In: *Theoretical and technological principles of surfacing. Surfacing in metallurgical and mining industry*. Kiev: PWI.
3. Melikov, V.V. (1973) Multi-electrode surfacing and some of its capabilities. In: *High-productivity surfacing processes and consumables*. Kiev: PWI.
4. Yuzvenko, Yu.A., Kirilyuk, G.A. (1973) *Flux-cored wire surfacing*. Moscow: Mashinostroenie.
5. Levin, V.V., Shel, M.M., Asalkhanov, V.N. et al. (1980) Machines for mechanized surfacing with electrode weaving. In: *Theoretical and technological principles of surfacing. Surfacing of parts of metallurgy and power equipment*. Kiev: PWI.
6. Yuzvenko, Yu.A. (1970) Flux-cored strip. *Avtomatich. Svarka*, 2, 23–26.
7. Kuznetsov, L.D., Kortelev, G.A., Nikolaenko, M.R. (1982) Specific features of the process of flux-cored strip surfacing of parts of building and road machines under forced conditions. In: *Theoretical and technological principles of surfacing. Current surfacing methods and their application*. Kiev: PWI.
8. Patskevich, I.R., Solovskoj, V.M., Khejsets, L.A. (1973) Experience of application and prospects of development of flux-cored strip surfacing. In: *High-productivity surfacing processes and consumables*. Kiev: PWI.
9. Yuzvenko, Yu.A., Gorpenyuk, B.N., Shimanovsky, V.P. (1977) Chemical macroheterogeneity of metal deposited by the open arc method using flux-cored strip. In: *Theoretical and technological principles of surfacing. New processes of mechanized surfacing*. Kiev: PWI.
10. Eremeev, V.E., Strelyany, Yu.V., Korbut, V.A. et al. (1979) Chemical macroheterogeneity of metal deposited with different electrode materials. In: *Theoretical and tech-*



- nological principles of surfacing. Properties and tests of deposited metal.* Kiev: PWI.
11. Yuzvenko, Yu.A., Shimanovsky, V.P., Gavrish, V.A. (1972) Arc surfacing of blast furnace hoppers. *Avtomatich. Svarka*, **2**, 59–64.
 12. Shimanovsky, V.P., Danilchenko, B.V., Voronchuk, A.P. (1982) Surfacing of blast furnace hoppers. In: *Theoretical and technological principles of surfacing. Current surfacing methods and their application.* Kiev: PWI.
 13. Shimanovsky, V.P., Voronchuk, A.P., Zvezdin, S.M. (1990) Consumables and equipment for surfacing of blast furnace bells and hoppers. In: *Surfacing equipment and consumables.* Kiev: PWI.
 14. Shimanovsky, V.P., Yuzvenko, Yu.A. (1971) Effect of cracks on gas-abrasive wear of deposited metal. *Avtomatich. Svarka*, **2**, 61–62.
 15. Shekhter, S.Ya., Piankov, V.V., Lazarenko, Yu.N. et al. (1986) Surfacing in production of modern blast furnace hoppers. In: *Surfacing in production of machinery parts and equipment.* Kiev: PWI.
 16. Danilchenko, B.V., Shimanovsky, V.P., Terpilo, V.N. (1986) Equipment and technology for high-productivity cladding of wear-resistant alloys on thin sheets. In: *Surfacing in production of machinery parts and equipment.* Kiev: PWI.
 17. Ereemeev, V.B., Strelyany, Yu.V., Lopukhov, Yu.I. (1980) Flux-cored wire surfacing of large-sized formed-welded gate valve seats. In: *Theoretical and technological principles of surfacing. Surfacing of parts of metallurgy and power equipment.* Kiev: PWI.
 18. Oparin, L.I., Frumin, I.I., Otrok, A.I. (1968) Mechanized cladding of steel layer using cermet strip. *Avtomatich. Svarka*, **12**, 58–61.
 19. Malikin, V.L., Oparin, L.I. (1981) Effect of surfacing conditions using sintered electrode strip on productivity of the process and formation of deposited layer. *Ibid.*, **5**, 45–47.
 20. Malikin, V.L., Oparin, L.I., Fortunatova, N.N. (1986) Productivity of the process and geometric sizes of deposited beads in electric arc and electroslag cladding using sintered electrode strips. In: *Surfacing in production of machinery parts and equipment.* Kiev: PWI.
 21. Frumin, I.I., Oparin, L.I., Malikin, V.L. (1973) New cermet strips for mechanized submerged-arc surfacing of special steels and alloys. In: *High-productivity surfacing processes and consumables.* Kiev: PWI.
 22. Malikin, V.L., Frumin, I.I., Oparin, L.I. et al. (1979) Study of performance of wear-resistant metal deposited with sintered electrode strips. In: *Theoretical and technological principles of surfacing. Properties and tests of deposited metal.* Kiev: PWI.
 23. Malikin, V.L., Frumin, I.I., Satsunkevich, V.D. (1982) Effect of chemical homogeneity of deposited metal on thermal fatigue resistance. *Avtomatich. Svarka*, **11**, 12–14.
 24. Malikin, V.L., Oparin, L.I. (1974) Increasing the productivity of strip electrode surfacing. *Ibid.*, **8**, 58–60.
 25. Oparin, L.I. (1981) Some results and prospects of application of sintered electrode strip surfacing. *Ibid.*, **8**, 61–64.
 26. Oparin, L.I., Malikin, V.L. (1985) Application of wear-resistant surfacing using sintered electrode strips. In: *Surfacing. Experience and efficiency of application.* Kiev: PWI.
 27. Oparin, L.I., Frumin, I.I., Malikin, V.L. et al. (1980) Increasing wear resistance of KamAZ truck spring-loaded supports by sintered electrode strip hard-facing. *Avtomatich. Svarka*, **3**, 36–37.
 28. Oparin, L.I., Malikin, V.L., Akimova, A.G. et al. (1980) Wear-resistant hard-facing of road-building machine knives using sintered electrode strip. In: *Theoretical and technological principles of surfacing. Surfacing in machine-building and repair.* Kiev: PWI.
 29. Oparin, L.I., Malikin, V.L. (1985) Application of wear-resistant hard-facing using sintered electrode strips. In: *Surfacing. Experience and efficiency of application.* Kiev: PWI.
 30. Khomusko, F.A. (1957) Automatic strip-electrode surfacing. *Avtomatich. Svarka*, **5**, 71–77.
 31. Khomusko, F.A., Rabotnov, B.A. (1957) Hard-facing of blades of rotary-blade water turbines by the automatic submerged-arc electrode-strip method. *Ibid.*, **5**, 62–71.
 32. Kravtsov, T.G. (1978) *Electric arc electrode-strip surfacing.* Moscow: Mashinostroenie.
 33. Belov, Yu.M., Trofimov, I.F., Evtushenko, A.S. (1986) Improvement of technology for mechanized surfacing of nuclear power plant equipment. In: *Surfacing in production of machinery parts and equipment.* Kiev: PWI.
 34. Belov, Yu.M., Smorchkov, P.I., Pryanik, N.I. et al. (1982) Strip surfacing of large-size thin-walled forming drums. In: *Theoretical and technological principles of surfacing. Current surfacing methods and their application.* Kiev: PWI.
 35. Leshchinsky, L.K., Tarasov, V.V., Belousov, Yu.V. (1973) Heating of electrode strip extension with molten slag. *Avtomatich. Svarka*, **2**, 71–72.
 36. Belousov, Yu.V., Bagryansky, K.V., Leshchinsky, L.K. (1974) Peculiarities of metal formation in arc electrode-strip surfacing. *Svaroch. Proizvodstvo*, **12**, 32–34.
 37. Belousov, Yu.V., Leshchinsky, L.K. (1977) Main peculiarities of surfacing with profiled strip electrode. In: *Theoretical and technological principles of surfacing. New processes of mechanized surfacing.* Kiev: PWI.
 38. Leshchinsky, L.K., Belousov, Yu.V., Matvienko, V.N. (1980) Improving the productivity and quality of wide strip-electrode surfacing. In: *Theoretical and technological principles of surfacing. Surfacing of parts of metallurgy and power equipment.* Kiev: PWI.
 39. Danilov, L.I., Skorokhvatov, N.B., Sobolev, V.F. et al. (2004) Extension of service life of support rolls of hot strip mill 2000 at Open Joints Stock Company SEVERSTAL. *Chyorn. Metallurgiya: Bull. NTIEI*, **8**, 68–69.
 40. Johnson, W.C. *Overlay welding.* Pat. 3271554 USA. Fil. 24.06.65. Publ. 06.09.66.
 41. Scherl, P. *Lichtbogenschmelzschweißverfahren.* Pat. 313026. Fil. 24.12.69. Publ. 25.01.74.
 42. Neff, F., Scherl, P., Ornig, H. (1974) Neue Verfahren zum Schweißplattieren dickwandiger Stahlbleche und Behälter. *Schweisstechnik*, **7**, 139–146.
 43. Frumin, I.I., Kalensky, V.K., Panchishin, Yu.A. et al. (1977) Development of the process and investigation of some technological peculiarities of electroslag strip cladding. In: *Theoretical and technological principles of surfacing. New processes of mechanized surfacing.* Kiev: PWI.
 44. Frumin, I.I. (1975) Surfacing in nuclear power machine-building. *Avtomatich. Svarka*, **10**, 21–24.
 45. Kalensky, V.K., Panchishin, Yu.A., Shekhter, S.Ya. et al. (1980) Application of electroslag cladding with sintered strip for production of two-layer sheet billets. In: *Theoretical and technological principles of surfacing. Surfacing of parts of metallurgy and power equipment.* Kiev: PWI.
 46. Ignatov, V.A., Murzin, V.V., Rokhlin, E.A. et al. (1980) Study of the process of anticorrosive electroslag cladding using two strip electrodes. *Ibid.*
 47. Zalinov, A.V., Runov, A.E., Starchenko, E.G. et al. (1980) Investigation of anticorrosive layer deposited with strips by the two-electrode method on steel 15Kh2NMFA. *Ibid.*
 48. Kalensky, V.K., Panchishin, Yu.A. (1985) Efficiency of anticorrosive electrode-strip surfacing. In: *Surfacing. Experience and efficiency of application.* Kiev: PWI.
 49. Malikin, V.L., Oparin, L.I. (1977) Electroslag cladding of some wear-resistant steels using sintered electrode strips. In: *Theoretical and technological principles of surfacing. New processes of mechanized surfacing.* Kiev: PWI.
 50. Malikin, V.L. (1982) Development of consumables and technology for wear-resistant anticorrosive electroslag cladding using sintered electrode strips. In: *Theoretical and technological principles of surfacing. Current surfacing methods and their application.* Kiev: PWI.

SURFACING OF TRAIN WHEEL FLANGES AFTER ANNEALING OF THE TREAD SURFACE IN CAR-REPAIR PLANTS OF UKRAINE

V.V. MATVEEV
VILTRANS, Ltd., Kiev, Ukraine

Features of wear of railway wheels and applied technologies of wheel flange reconditioning by surfacing are considered. Experience of reconditioning the wheel flanges after annealing of the tread surface is described. Advantages of such a technology of flange reconditioning are noted.

Keywords: arc surfacing, train wheels, tread surface, high-frequency annealing, hardness, microstructure, increase of efficiency

At braking a number of defects develop on the wheel tread surface because of plastic deformations, namely metal pressing out to the tread surface periphery, metal delamination, cracks, fatigue-type damage in the zone of contact of the wheel rim with the rail [1]. In 60 to 70 % of the cases such defects as flats, dents, scale on the tread surface, are the cause for cutting of freight cars for current repair of wheel pairs (WP). The main cause for the observed in 1990s increase in the number of wheels with defects of contact fatigue origin is lowering of the quality of the metal of wheels made in the metallurgical plants [2]. During operation the defects may propagate to the depth of 20 mm or more into the region of tensile stresses in the wheel, which is promoted, in particular, by shock loads. Cracks can initiate at the depth of 15 to 20 mm from the tread surface, in the locations of defects of metallurgical origin in wheel metal, which develop under the impact of cyclic loads. Such defects usually propagate in parallel to the tread surface and end on the outer surface of the flange. Development of a crack in the flange region metal may lead to metal spallation on up to 200 to 250 mm length and loss of guiding functions of the wheel. Presence of non-metallic inclusions in wheel steel and its lower deformability may also lead to cracks in the wheel discs [3]. Defects of fatigue origin are characterized by small microcracks, propagating for approximately 10 mm in-depth the metal from the tread surface and at the flange base. These microcracks are oriented at an angle of 45° to the direction of rolling, and usually do not develop to dangerous dimensions. On the whole, action of shock loads, and hydrogen penetration into steel under the conditions of a high humidity may result in lowering of the surface and fatigue strength, ductility, impact toughness and endurance [4].

To recondition 1 mm of a worn flange of train wheels (producing a standard profile with flange width of 33 mm at 18 mm distance from flange tip) the rim thickness is to be reduced by 2 mm. To preserve

the rim thickness after train wheel turning, the railway transportation enterprises of CIS countries, in particular, of Ukraine, as well as Germany, Czechia, Bulgaria, Poland, India, Sweden, etc., use the technology of submerged-arc surfacing of worn flanges [5, 6].

According to technical documentation, flange surfacing can be performed on wheels after complete elimination of defects by turning. Wheels with a hardened tread surface (with work hardening and flats) are machined with 2 to 3 mm of the metal being turned off («cut off») from the wheel rim. Right now practically all the wheels, going into repair, have 2 to 3 flats of not more than 2 mm depth, about 25 % of the wheels have flats with more than HRC 50 metal hardness on the tread surface. In the last years it is recommended to use surface annealing of the tread surface hardened in operation, to reduce the thickness of the removed chips before turning [7].

The purpose of this study is generalization of the experience of surfacing the train wheel flanges after annealing of tread surface, gained by VILTRANS Company in the enterprises of Ukraine. Use of annealing before surfacing of the worn tread surface of the wheels [8] was proposed by us for the first time for introduction in the surfacing sections of VILTRANS in a number of car-repair plants of Ukraine.

Multiple pulsed annealing of the surface layer of the metal of the wheel rim and flange was performed in TI2-100/10M units, made by VILTRANS. Surface induction annealing is performed by 10 Hz currents on a rotating wheel by heating at 150–160 °C/s rate up to temperature above $\dot{A}_{\bar{n}_1}$ (810 ± 20 °C), cooling to the temperature below \dot{A}_{r_1} (630 ± 20 °C) for 5 to 6 s, repeated heating for 5 to 6 s to a temperature below $\dot{A}_{\bar{n}_1}$ point (680 ± 20 °C) and natural cooling. Critical point $\dot{A}_{\bar{n}_1}$ of 60G steel close in its properties to typical wheel steel, is equal to 730 °C. Modes of multiple pulsed annealing corresponded to recommendations, given in [9].

TI2-100/10M unit (Figure 1) consists of two heating stations, inductor displacement mechanism, WP rotation mechanisms, cooling system, power source

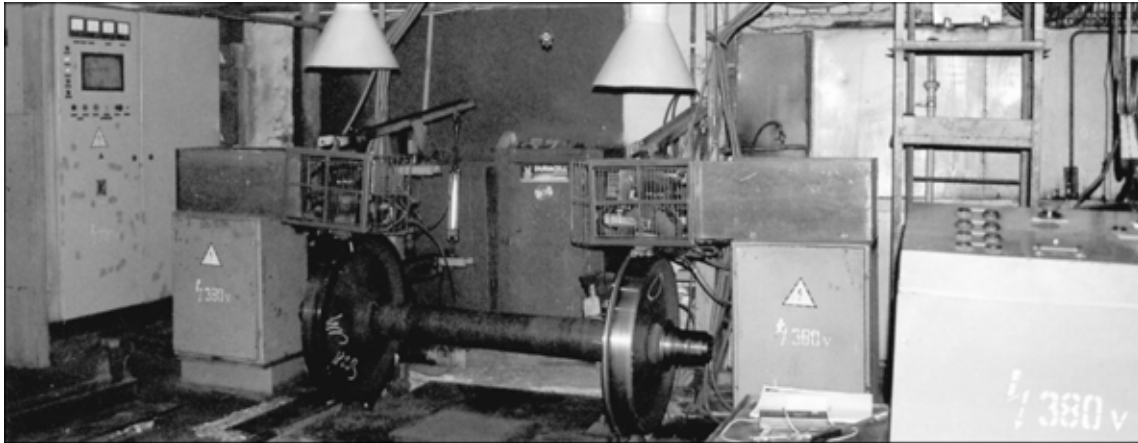


Figure 1. Induction unit TI2-100/10M for annealing of train wheel tread surface

(SChG9-100/10 generator of 100 kW power). Heating station consists of inductor-transformer and capacitor block. Inductor-transformer is designed for creating two narrow spots of induction heating, which enable implementation of the required parameters of heating and cooling. It is welded of a copper tube, bent to suit the wheel profile, with radiator plates soldered to it. The gaps are filled by plates of electrical engineering steel, forming the magnet core. Soldered to the tube ends are copper plates, forming a flange for fastening the inductor to the transformer. Inductor-transformer and generator are made with water-cooling. Cooling system is original and contains a two-section tank for distilled water (condensate) with an inner partition, two pumps and two heaters. Wheel rotation is ensured, using an AC motor and reduction gear. Linear speed of WP rotation is 20 mm/s.

Metallographic investigations have been conducted of a wheel sample (Figure 2) with worn tread surface on the rim and the flange, defects on the rim surface (flat, crack), traces of thermal impact at braking on the flange. Analysis of the sample structure was performed at the E.O. Paton Electric Welding Institute after their etching in a solution of chloric iron with subsequent lightening in ammonium persulphate solution (macrostructure), after chemical etching in 4% alcohol solution of nitric acid (microstructure). Rockwell metal hardness was measured in TK-2M instrument, Vickers microhardness ---- in the LECO instrument M-400 at 100 g load.

Sample macrostructure shows that in the flange upper part the etched strip depth is up to 4 to 5 mm (*HRC* 24–25). Microstructure of wheel flange metal in the zone of thermal impact due to slipping against the rail head is that of bainite (Figure 3, *a*). Metal microhardness in the subsurface zone is equal to *HV*1-3080–3060 MPa, in the thermal impact zone *HV*1-2850–2970 MPa, in the base metal (away from the thermal impact zone) *HV*1-2740–2850 MPa. Figure 3, *b* gives metal microstructure of wheel rim with a flat. At $\times 1000$ -magnification it is established that the microstructure of the subsurface layer (light layer in Figure 3, *b* of 0.8 to 1.0 mm thickness) consists predominantly of martensite (Figure 3, *c*) with *HV*1-6400–6800 MPa hardness. In addition to an acicular

martensite structure, also dark regions of nodular bainite with *HV*1-3660–4010 MPa hardness are observed. Lying deeper is a gray layer 0.5 to 0.6 mm thick, the structure of which (Figure 3, *d*) consists predominantly of nodular bainite of *HV*1-3090–3390 MPa hardness, and large light regions with *HV*1-4640–6650 MPa hardness. Still farther from the surface the second gray layer is observed (Figure 3, *b*) of 0.5 to 0.6 mm thickness. Its structure is granular bainite (Figure 3, *e*) with microhardness *HV*1-3250 MPa. It is followed by the wheel metal proper, where the structure consists of sorbite-like pearlite (Figure 3, *f*) with microhardness *HV*1-2540–2650 MPa and thin interlayers of ferrite. The polished unetched surface of a wheel sample with a flat revealed light-gray inclusions, elongated in the deformation direction (*HV*1-2750 MPa microhardness), which are identified as sulphides. In addition, individual inclusions of a complex composition of a high hardness of *HV*1-2750 MPa are observed.

Comparison of microhardness of the wheel rim metal before (Figure 3) and after HF current annealing of the tread surface (Figure 4) led to the conclusion that:

- metal microstructure in the zone with acicular martensite (6400–6800 MPa), as well as a region with nodular bainite structure (hardness *HV*1-3660–

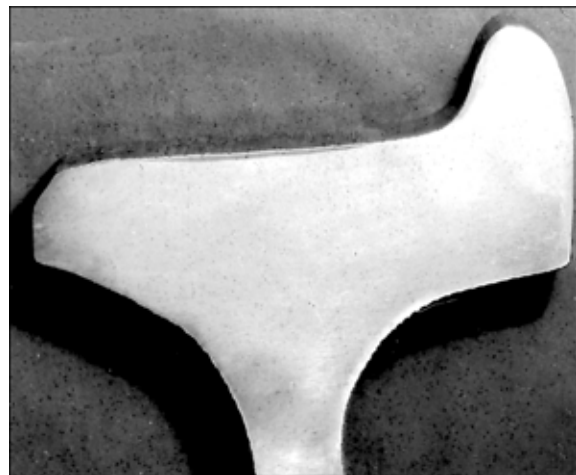


Figure 2. Macrosection of a wheel fragment with a worn tread surface

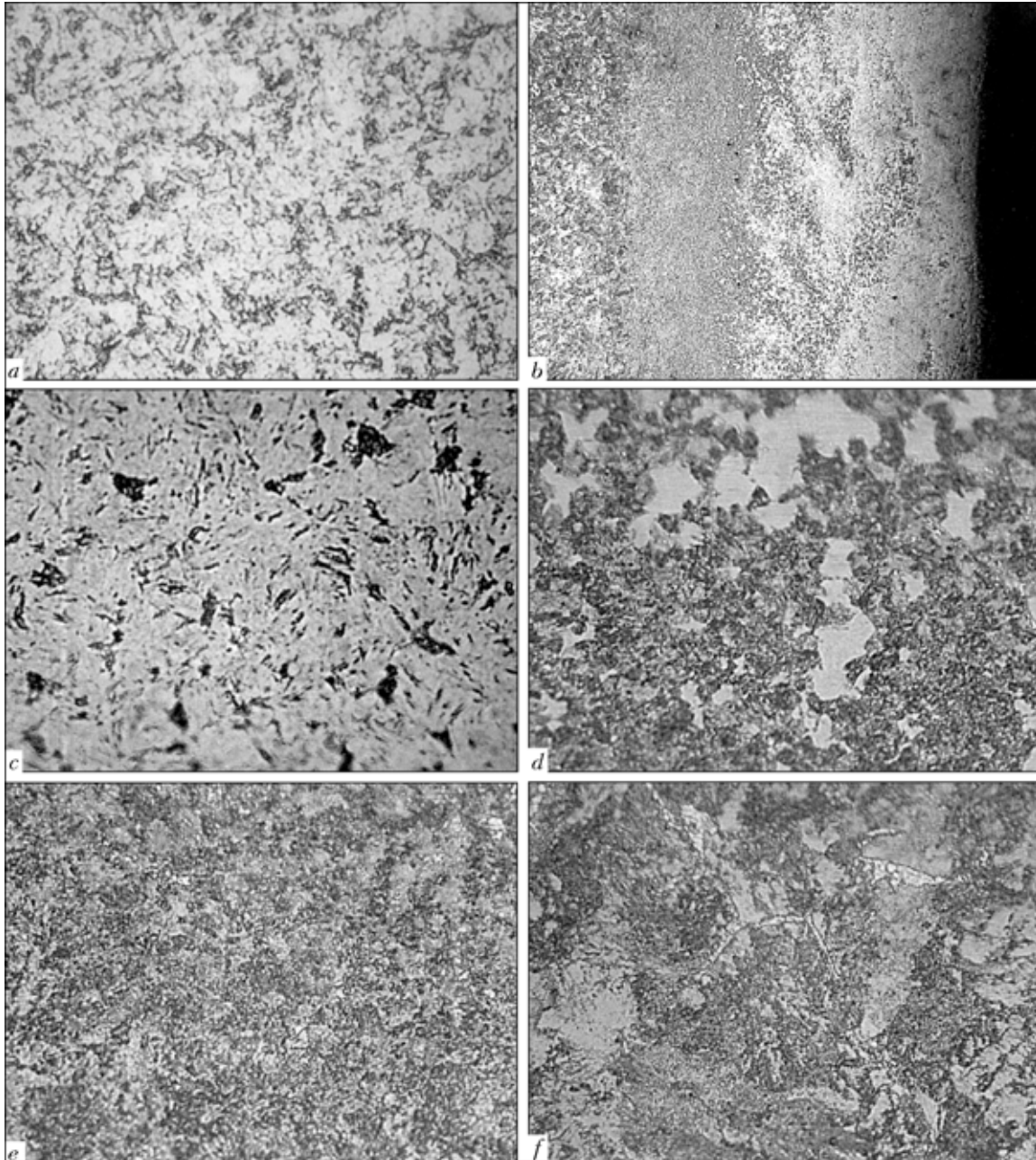


Figure 3. Metal microstructure in different surface regions of the wheel: *a* — flange HAZ ($\times 1000$); *b* — wheel rim ($\times 40$); *c* — subsurface light layer of the rim ($\times 1000$); *d* — first subsurface gray layer ($\times 100$); *e* — second subsurface gray layer ($\times 1000$); *f* — wheel base metal ($\times 1000$)



Figure 4. Microstructure of metal of wheel rim subsurface regions after HF current annealing ($\times 40$)

4010 MPa) after HF current annealing undergoes a transformation with formation of fine-grained bainite of about $HV1-2970-3090$ MPa hardness at up to 2.4 mm depth from the tread surface;

- after HF current annealing the structure of the subsurface layer of the wheel becomes more uniform;
- influence of HF current annealing on the structure by depth is limited (microstructure and microhardness at the depth greater than 2.4 mm practically do not change).

Therefore, surface annealing before surfacing promotes transformation of martensite structure in this zone into bainite structure, and grain refinement, thus lowering the probability of cold cracking in surfacing. Annealing changes the level of residual stresses in the wheel rim, arising at hardening, and increases the

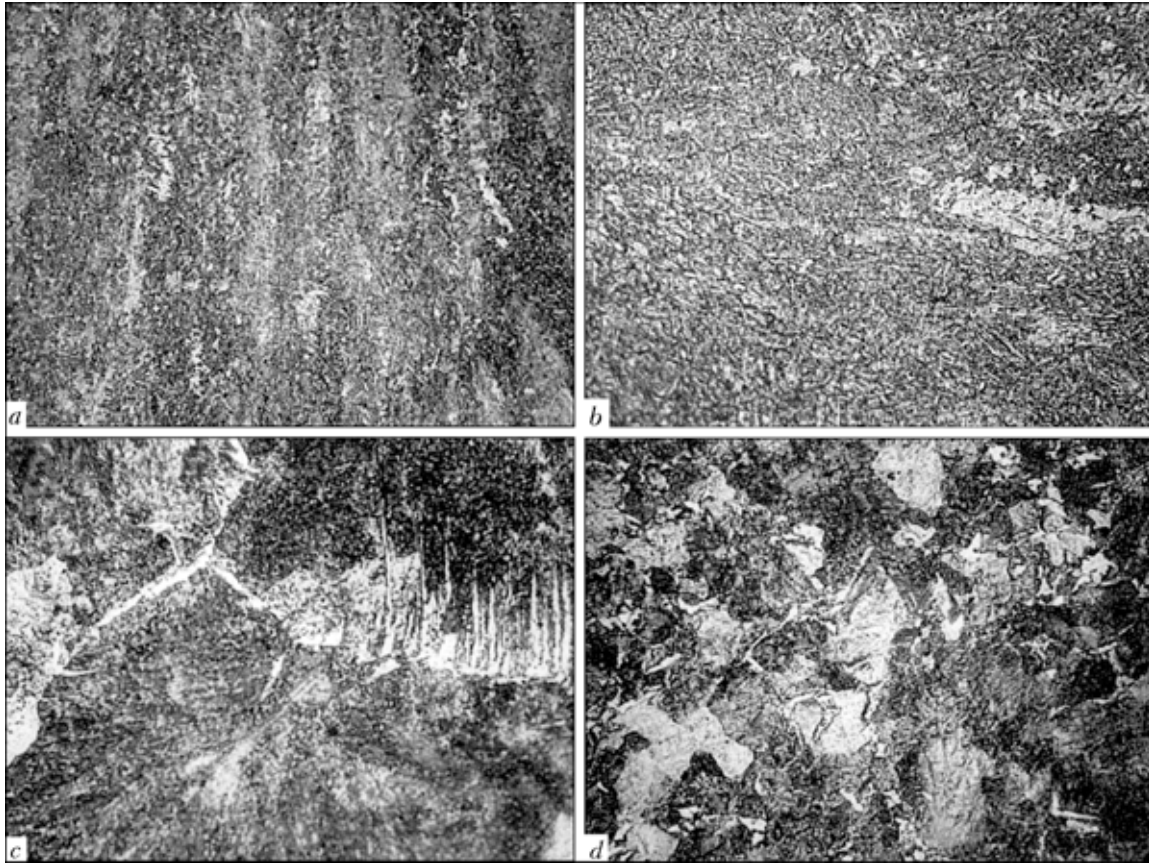


Figure 5. Microstructure of deposited flange metal and the HAZ: *a* — upper layer of deposited flange metal ($\times 200$); *b* — intermediate (recrystallized) layer of the deposited metal ($\times 200$); *c* — region of coarse grain in the flange metal HAZ after single-pass surfacing ($\times 1000$); *d* — region of recrystallized metal of multipass deposit ($\times 1000$)

level of tensile stresses in it. The latter promotes opening of defects (microcracks) on the wheel surface up to detectable sizes. Toe out of the wheel ends from the wheel tread surface after annealing and cutting up is equal to +1 mm. According to item 1.9 of GOST 10791-89 «All-Rolled Wheels» and ISO 1005/6 the toe-in of the wheel rim ends after radial cutting up (in as-delivered condition) should be not less than 1 mm, no toe-out is allowed.

Single-electrode multilayer submerged-arc surfacing of the flange (after surface annealing) with AN-348AM flux and Sv-08KhM wire of 3 mm diameter (surfacing rate of 26 to 28 m/h) does not lead to cold cracking in the HAZ metal.

Rockwell hardness of the deposited metal of the flange varies from *HRC* 31 in the upper layer metal to *HRC* 21-23 in the lower-lying beads. Microhardness of the HAZ metal of the flanges under the lower and central layers of the deposit is equal to *HV*1-3220-3090 MPa, under the upper ones *HV*1-2740-3510 MPa. Processing the data of process charts of train wheel flange surfacing after annealing of the hardened metal on the tread surface shows that the tread surface hardness decreases almost 2 times. After rim turning, flange surfacing, wheel cooling in the thermostat and deposited layer turning by the profile (average cooling rate of not more than 50 °C/h), hardness of the metal of wheel tread surface increases and becomes not lower than that of the base metal.

Figure 6 gives the sequence of wheel repair with flange surfacing after annealing of the tread surface in the currently used repair cycle of 18335 WP in the case of Darnitsa section of flange surfacing of VIL-TRANS Company. These wheel pairs went into repair at Darnitsa Car-Repair Plant (Kiev) in the period from June 2003 to May 2004. Analysis of this data shows that:

- wheels reveal wear and defects after service due to reduction of the rim thickness in repair to the depth of 2 to 25 mm;
- after annealing of the tread surface, as well as after annealing and surfacing during repair cracks were detected in the rim, which enabled rejecting 38 WP (0.2 % of all the WP going into repair);
- annealing of the tread surface of train wheels reduced the hardness of the wheel surface hardened in service, which allowed reducing the cost of power, cutting tools, turning time, cost of machine tool repair, and, this being important, reducing the thickness of the layer removed in turning by 1.4 mm on average (for comparison $L_1 = 6.7$ and $L_3 = 5.3$ mm in Figure 6);
- probability of hot cracking in the deposited metal and cold cracking in the HAZ metal is lowered. The temperature of heating of the flange metal before surfacing can be reduced considerably.

Flange surfacing after local surface heating and cooling of wheels during annealing lead to develop-

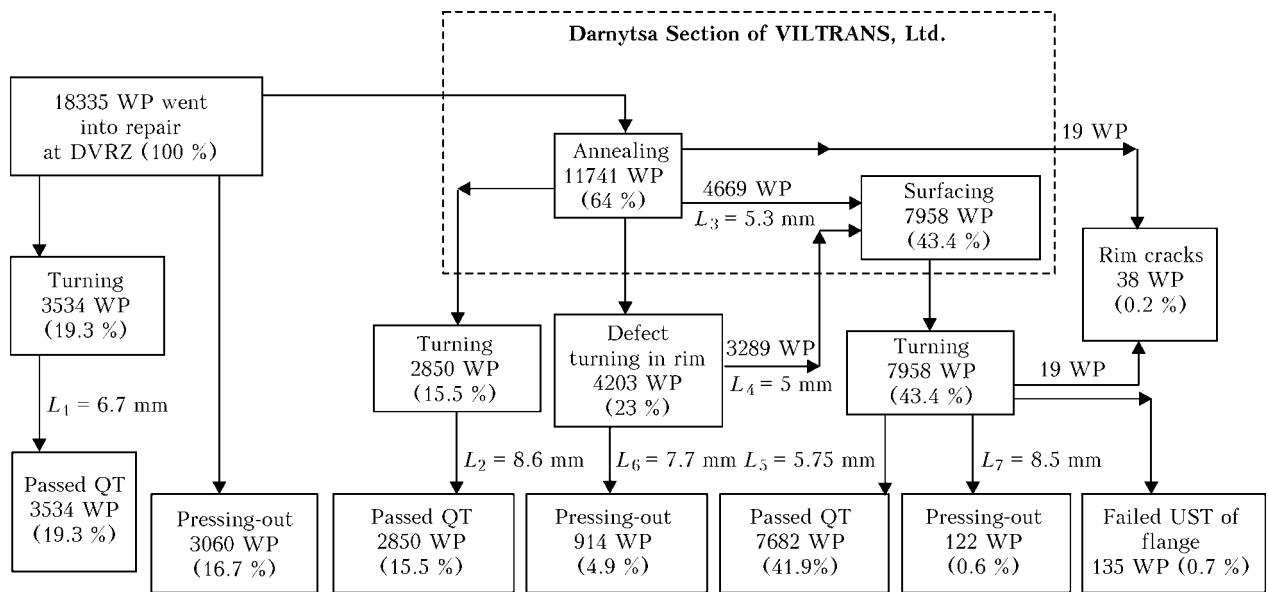


Figure 6. Map of the process of surfacing train wheel flanges after annealing of hardened tread surface (L — average decrease of rim thickness after turning)

ment of residual stresses, which apply tension to the wheel (0.2 % rejects). Wheel toe out after annealing and surfacing of flanges is equal to +2.5 mm. Microcracks in the wheel rim, which arose in operation, «open» up to the level of UST sensitivity, which allows revealing the «weak» wheels. Turning of wheel rim (before flange surfacing) to the depth of the revealed defects after surface layer anelaing, increases the wheel reliability. As shown by observation, during 5 months of the year 2003 in the Darnytsa (DVRZ), Popasnyansk (PVRZ), Stryjsk (SVRZ) car-repairing plants (Figure 7), after annealing of the tread surface before flange surfacing, about 65 % of the wheels were turned with the specified chip thickness below 4 mm. Other wheels were turned up to 6 times with reduction of rim diameter to 23 mm. Average reduction of rim diameter was equal to 5.1 mm. During the surveyed period about 35 % wheels were turned on average before surfacing the flanges.

At UKRSPETSVAGON, where no annealing of the tread surface was performed starting from May 2002, 25 % of wheels were turned with chip thickness of 3 to 4 mm, the other wheels were turned several times with rim reduction to 25 mm. Average reduction of the rim was 6.5 mm. Reduction of the distribution maximum 2.6 times and shifting of the histogram to

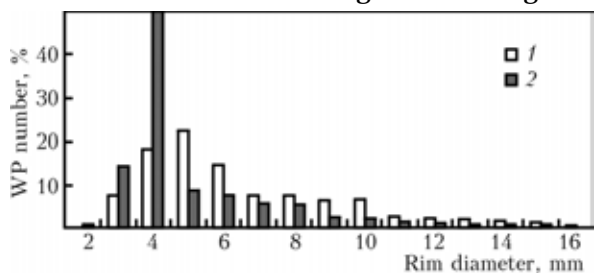


Figure 7. WP distribution in the sections of VILTRANS, Ltd. depending on the size of rim diameter reduction: 1 — UKRSPETSVAGON (without annealing or turning of rim defects); 2 — average value for SVRZ, DVRZ, PVRZ (after annealing and defect turning on the rim)

the right, compared to the results of turning in car-repair plants for 1.4 mm, is related to absence of annealing of the tread surface before flange surfacing.

After annealing of the tread surface and defect turning, the amount of expenses for flange surfacing (welding consumables, time, power) decreases by 30 to 40 %. Introduction of control of wheel flange and rim thickness after defect turning allows evaluation of the cost and effectiveness of surfacing the flanges for each wheel. The necessary heating of wheel rim to the required temperature before surfacing is achieved directly by HF current annealing of the tread surface. Therefore, there is now room for improving the efficiency of a section with one annealing unit and two surfacing units, namely reconditioning of up to 60 wheels in an 8 h shift.

At present the admissible rim thickness after shop repair is not less than 27 mm, and after depot repair — not less than 25 mm. Accordingly, wheels with not less than 35 and 30 mm rim thickness are taken in for repair without annealing. After annealing of the tread surface before flange surfacing, turning wheels with flange thicknesses of 29 and 26 mm, respectively, became possible in a number of cases. Therefore, the technology of repair using annealing before flange surfacing is particularly urgent, when carriages with «thin» wheels go into repair at the plants. Figure 8 shows a rim thickness distribution for 13445 WP, which went into flange surfacing in the period from June to December, 2003 (DVRZ — 4292, PVRZ — 4270, SVRZ — 4883).

Tread surface annealing before flange surfacing was conducted according to «Technological Instructions on Induction Annealing of the Tread Surface of Wheel Pairs by the Rolling Stock Repair Plants of Ukrainian Railway», which was introduced by an Act of Ukrzaliznitsa #208-Ts of June 7, 2000. SC TSC SEPROZ of Ukraine issued a certificate of compliance #UA1/012/0096713-04 on the technology of sur-

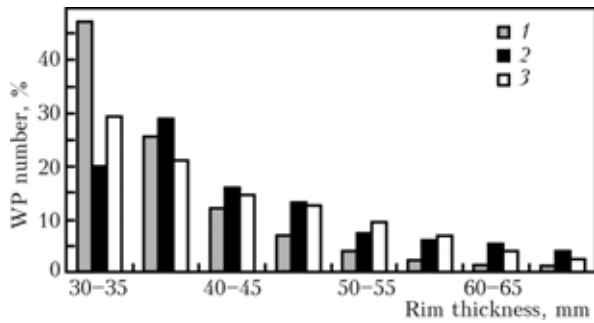


Figure 8. Distribution of WP going into flange surfacing sections, depending on rim thickness: 1 — DVRZ; 2 — PVRZ; 3 — SVRZ

facing the wheel flanges of freight cars in UNG units with prior annealing of the tread surface.

From May 1996 up to 31.12.2004 VILTRANS performed annealing of tread surface of 215178 WP and surfacing of 256327 flanges of train wheels at DVRZ, SVRZ, PVRZ and at UKRSPETSVAGON. During this period these plants did not receive a single reclamation from the railways after wheel operation, concerning surfacing of flanges with annealing of the tread surface.

The possibility has been studied of surfacing a flange with two electrode wires into one common weld pool from one power source after HF current annealing of the wheel tread surface. The two electrodes were located at 4 mm distance from each other with connection to one power source (VDU-1600). Average values of welding mode were: $I_w = 550$ A, $v_{surf} = 28-30$ m/h. It was anticipated that the consumption of power, welding consumables and labour per 1 kg of deposited metal will decrease compared to single-electrode welding [10]. Experiments showed that a more sound formation of the deposited layer is achieved in two-electrode surfacing and the surfacing efficiency is increased by 30 to 40 %. Microstructure of metal deposited with two electrodes (3 mm dia. Sv-08KhM wire, AN-348AM flux, 28 to 30 m/h surfacing speed), is that of bainite with a small fraction of ferrite (Figure 9), as in the case of single-electrode surfacing. The deposited metal hardness is within HRC 22–24 (upper layer of the deposit) and HRC 20–21 (lower lying layers).

In conclusion it should be noted that the residual tensile stresses, arising after HF current annealing on the tread surface, are beneficial for revealing the defects and rejecting the wheels during their repair. Annealing before flange surfacing will allow reducing the surface layer hardness, this permitting decrease of chip thickness in reconditioning, increasing the surfacing efficiency, changing the metal structure before surfacing, and reducing the probability of defects in the deposited layer and in the HAZ.

- (1977) *MPS Instruction on inspection, examination, repair and formation of train wheel pairs TsV/3429*. Moscow: Transport.
- Tsyurenko, V.N. (2002) Service reliability of wheel pairs of freight cars. *ZhD Transport*, **3**, 24–28.
- Mamykin, S.M. (1999) Analysis of effect of humidity on wear of wheel pairs of passenger cars. *Effekt. Bezopasnosti i Tribotekhniki*, **1**, 46–47.

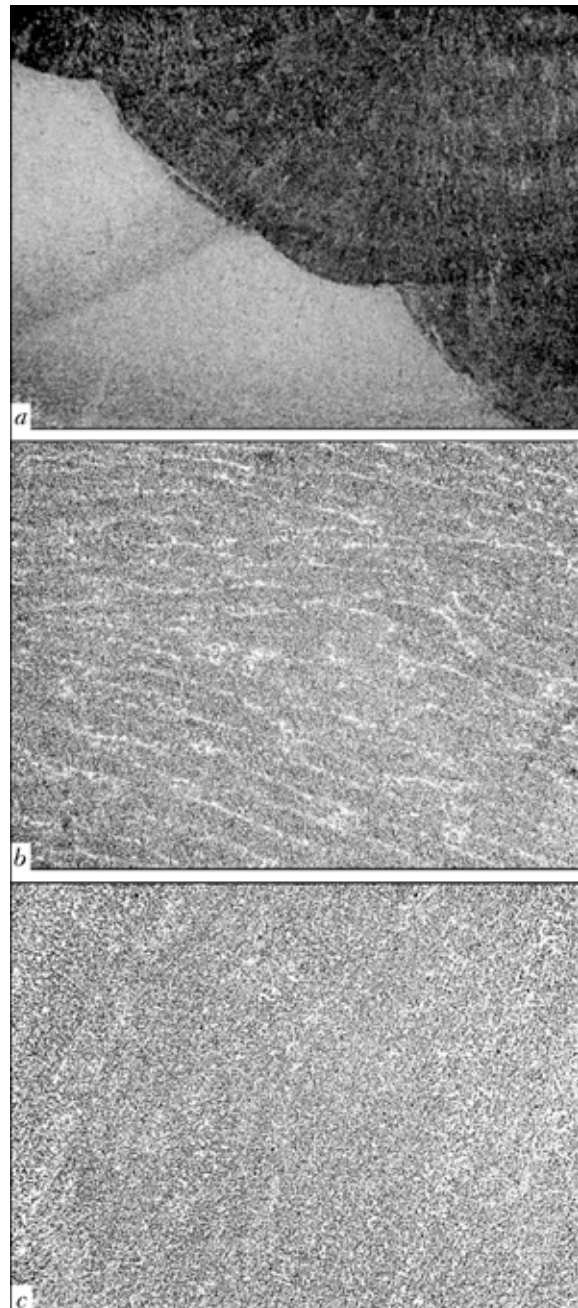


Figure 9. Microstructure of a wheel sample after two-electrode surfacing of flange by Sv-08KhM wire (a — $\times 25$), upper- (b — $\times 200$) and lower-lying (c — $\times 200$) layer

- Shanurin, A.M., Komlev, D.G., Kravchenko, G.I. et al. (2002) New approach to control of wheel disks of railway cars. *Defektoskopiya*, **9**, 90–95.
- Asnis, A.E., Gutman, L.M. (1948) Repair of worn-out band flanges by surfacing. In: *Transact. on automatic submerged-arc welding*. Kiev: PWI.
- Pavlov, N.V., Kozubenko, I.D., Byzova, I.E. et al. (1993) Surfacing of flanges of train wheel pairs. *ZhD Transport*, **7**, 37–40.
- Ivanov, I.A., Urushev, S.V. (1998) On improvement of life of solid wheels. *Ibid.*, **7**, 25–26.
- Matveev, V.V. *Method of reconditioning of tread surface of rail transport wheels*. Pat. 44373 Ukraine. Publ. 15.02.02.
- Alyokhin, S.V., Bogdanov, F.Ya., Bogdanov, A.F. et al. *Method of repair of wheel tread profile*. USSR author's cert. 433222. Int. Cl. C 21 D 9/34 and 1/32. Publ. 25.06.74.
- Melikov, V.V. (1988) *Multiple-electrode surfacing*. Moscow: Mashinostroenie.

FILLER MATERIALS FOR AUTOMATIC SUBMERGED-ARC WELDING OF HEAT-RESISTANT 9 % Cr STEELS*

V.Yu. SKULSKY and S.I. MORAVETSKY
E.O. Paton Electric Welding Institute, NASU, Kiev, Ukraine

Developed filler materials for mechanized submerged-arc welding of heat-resistant steel with 9 wt.% Cr are described. It is shown that the mechanical properties of weld metal and welded joints of the above steel produced using the proposed welding consumables, meet the specified requirements.

Keywords: submerged-arc welding, heat-resistant steels, welded joints, martensite structure, flux-cored wire, highly basic flux, mechanical properties

New heat-resistant 9 % Cr steels of martensitic class have become widely accepted in power engineering over the last years. These steels are designed for manufacture of high-temperature components of power generating units of thermal power plants [1, 2]. Their use allows increasing the working parameters of steam, namely temperature up to 610 °C and pressure up to 25–30 MPa. The power unit efficiency can be up to 45 %.

For steels (12Kh1MF, 15Kh1M1F, 20KhMFL) traditionally used in thermal power engineering the limit (critical) values of the steam working parameters are not higher than $T = 565$ °C and $P = 24$ MPa at up to 36 % efficiency, this eliminating their application in high-temperature components of new generation units with supercritical parameters. Under the conditions, when the design life is over, the actual values of the working parameters drop below the admissible limits, this leading to lower efficiency, ineffective utilization of fuel and increase of the amount of harmful evolutions into the atmosphere. This resulted in the need to replace the used power generating equipment in Ukraine by new and more perfect one. The problem of development of local welding consumables for welding heat-resistant 9 wt.% Cr steels

(of P91 steel type) becomes highly urgent. These steels have the following composition, wt. %: 0.06–0.12C; 8.0–9.5Cr; 0.85–1.05Mo; 0.2–0.5Si; 0.3–0.6Mn; 0.1–0.4Ni; 0.18–0.25V; 0.06–0.10Nb; 0.03–0.07N; not more than 0.02 S and P.

In power engineering high requirements are made of piping and thick-walled casing equipment as regards the weld quality, indices of physico-mechanical properties of weld metal, and its resistance to cold cracking. It is also necessary to ensure the minimum degree of the deposited metal contamination by non-metallic inclusions and maximum low content of diffusible hydrogen and impurities in it.

The E.O. Paton Electric Welding Institute developed a system of flux and flux-cored wire (PP-08Kh9NMAFB type), which allows producing by automatic submerged-arc welding the 9 wt.% Cr steels joints, having strength properties not lower than those of the base metal. The highly-basic flux is manufactured by a process of solid-phase synthesis of the initial charge components [3]. The charge is based on oxides of various metals and calcium fluoride, forming MgO–CaF₂–Al₂O₃–SiO₂ slag system. The flux developed for welding 9 wt.% Cr steels was designated SFT-9.

Butt welded joints of 16 mm thick plates with a V-shaped groove were welded to evaluate the composition of the deposited metal produced with application of the developed welding consumables and to

Table 1. Mode of welding butt joints of 9 wt.% Cr steel

Pass number	Welding process	I_w, A	U_a, V	$v_w, \text{m/h}$
1 (root)	Manual nonconsumable-electrode argon-arc	90	13	–
2–3	Automatic submerged-arc	240–280	40–42	24.6
4–8		290–320	40–42	21.7

Note. Filler and electrode wire diameter is 2 mm.

* Based on materials of a presentation made in the 3rd International Conference on Welding Consumables of CIS countries (Dnepropetrovsk, June 1–4, 2004).

**Table 2.** Deposited metal composition, wt. %

Welding consumables (flux-cored wire + flux)	C	Cr	Mo	Si	Mn	Ni	V	Nb	N	S	P
PP-08Kh9NMAFB + SFT-9	0.07	8.5	0.8	0.28	0.8	0.65	0.2	0.057	0.048	0.009	0.019
C9MV-UP + BB910	0.11	9.0	1.0	0.30	0.7	0.70	0.2	0.05	--	--	--
OK-Tubrod 15.3 S + OK-FLUX 10.63	0.10	9.0	1.0	0.30	1.0	0.50	0.2	0.05	0.04	--	--

Note. Two last chemical compositions are taken from catalog-directory of Boehler and ESAB companies.

determine its mechanical characteristics. Welding was conducted with preheating up to 250 °C in the mode, given in Table 1. The steel being welded corresponded to the following composition, wt. %: 0.085C; 8.85Cr; 1.0Mo; 0.33Si; 0.43Mn; 0.12Ni; 0.25V; 0.069Nb; 0.045N; 0.015S; 0.013P.

Welded joints were subjected to post-weld heat treatment (high tempering at 760 °C for 2 h). After that samples for mechanical tests to GOST 6996-66 and sections for metallographic studies were cut out of the welded joint metal.

Table 2 gives the composition of the deposited metal, produced using welding consumables with 9 wt. % Cr. As is seen from the Table, the developed welding consumables provide the deposited metal composition, which is practically the same as that of welding consumables of other manufacturers.

Content of residual gases in the weld metal was as follows, wt. %: 0.042[O]; 0.00035[H]. Concentration of diffusible hydrogen, determined by alcohol method [5] at sample soaking for 24 h, was equal to 0.22 cm³ per 100 g of deposited metal.

As shown by metallographic analysis, the deposited metal contains non-metallic inclusions of oxide, oxisulphide and silicate type, as well as highly fine-dispersed nitrides. Relative share *C* of non-metallic inclusions of different dimensions *d* in the deposited metal, obtained using the developed wire-flux system, is shown below:

<i>d</i> , μm	0.5-1.0	1.0-1.5	1.5-2.0	2.0-2.5	2.5-3.0	3.0-4.0
<i>N</i> , wt. %	26.90	49.08	17.25	4.93	1.23	0.62

In this case, the total volume fraction of non-metallic inclusions is equal to 0.194 % in the weld metal and 0.101 % in the base metal. The above data show that fine (*d* = 0.5-1.5 μm) non-metallic inclusions prevail in the weld metal.

Results of mechanical tests in Table 3 show that the strength and ductility values meet the requirements made of welded joints on steel of P91 type.

Table 3. Results of mechanical testing at *T* = 20 °C

Object of study	σ_t , MPa	$\sigma_{0.2}$, MPa	δ , %	ψ , %	KCV, J/cm ²
Weld metal	709	600	17.7	52.4	$\frac{46.0-69.5}{57.0}$
Welded joint metal	641-652*	--	--	69.7-67.8	$\frac{138-177^{**}}{164^{**}}$
Base metal	696	547	21.6	72.7	$\frac{217-224}{220}$
Requirements to DIN 32525 [4]					
Weld metal	585-850	≥ 415	≥ 17	--	≥ 51

*Sample fracture point --- base metal at 4-5 mm distance from the fusion line. **Notch along fusion line.

Thus, it is established that the welded joints of new heat-resistant 9 wt. % Cr steels of martensitic class made by mechanized submerged-arc welding with synthetic flux in combination with the proposed flux-cored wire feature a high quality and have the required mechanical properties. The deposited metal is characterized by a low content of impurities (less than 0.02 wt. % of sulphur and phosphorus), sufficient purity as to non-metallic inclusions (total volume fraction is 0.192 %) and low concentration of diffusible hydrogen (less than 1 cm³ per 100 g of deposited metal).

1. Olkhovsky, G. (1999) Technology for thermal power stations. *Gazoturb. Tekhnologii*, **2**, 4-7.
2. Skulsky, V.Yu., Tsaryuk, A.K. (2004) Problems of selection of weldable steel for high-temperature components of TPS power units (Review). *The Paton Welding J.*, **3**, 2-6.
3. Kasatkin, B.S., Tsaryuk, A.K., Vakhnin, Yu.N. et al. (1994) Synthetic welding fluxes: fabrication and field of application. *Avtomatich. Svarka*, **3**, 62-66.
4. (1993) Filler metals for the steel X10CrMoVNb91 W.-Nr.I-4903 and grade P91/T91 according to ASTM/ASME. In: *Boehler welding: Product informations*. Duesseldorf: Boehler Schweisstechnik.
5. Kozlov, R.A. (1986) *Welding of heat-resistant steels*. Leningrad: Mashinostroenie.



FLUX-CORED WIRE FOR WELDING IN SHIPBUILDING

L.N. ORLOV, A.A. GOLYAKEVICH, V.N. UPYR and S.P. GIYUK
TM. VELTEK, Ltd., Kiev, Ukraine

Self-shielded flux-cored wire for a wide application in shipbuilding is described. Composition and mechanical properties of the deposited metal, as well as delivery conditions are given.

Keywords: arc welding, flux-cored wire, shipbuilding, delivery conditions

Analysis of the state of welding in the world shipbuilding has shown a steady and dynamic growth of the use of mechanized and automatic welding with flux-cored wire. Shipyards of the largest shipbuilding companies of Japan, South Korea, Finland perform about 80 % of the whole volume of welding operations by the gas-shielded flux-cored wires of small diameter (1.0–1.2 mm). Advantages of using flux-cored wire include high productivity of works, marketable style of the weld and high welding-technological characteristics; simplification of the welding technique in different spatial positions and easiness of its mastering; a possibility to provide necessary mechanical properties.

Efficiency of the flux-cored wire application should be estimated not by separate stages but by an increase of the total productivity of the technological process of production of the metalwork. Manual welding with coated electrodes and mechanized gas-shielded welding with solid wire prevail in shipbuilding of the CIS countries. A noticeable growth of using import flux-cored wires of small diameter is observed in the recent years. The latter is connected first of all with the absence of the equivalent domestic analog and the presence of the number of factors making it difficult to apply domestic flux-cored wire. These factors include the lack of a reliable specialized welding equipment; a probability of the appearance of porosity; a problem of feed by hoses; increased release of welding aerosol; insufficient mechanical properties of welds.

Table 1. Welding conditions with wire PPs-TMV7 for producing fillet and butt welds (shielding gas is CO₂ or Ar + 18 % CO₂ mixture)

Spatial position	Welding current	Arc voltage	Wire feed rate, m/h	Deposition efficiency, kg/h
Vertical	160–210	23–27	270–500	2.0–3.5
Downhand	260–350	28–32	690–960	4.5–6.1
Horizontal	160–250	23–26	270–650	2.0–3.9

Note. Wire utilization factor is 1.15.

Welding technologies in the shipbuilding of Russia and Ukraine are subject to revision in the last years: a noticeable growth of the use of gas-shielded flux-cored wires instead of coated electrodes and solid wire of grade Sv-08G2S is observed. Demand of shipbuilding is met by import of flux-cored wires of the leading world producers: ESAB (Sweden), Welding Alloys (England), Filarc (the Netherlands), Kobeko (Japan), Hyundai (South Korea) and others. At the same time production capacities of domestic producers of flux-cored wire allow completely meeting the demand of the domestic shipbuilding in flux-cored wire of small diameter (1.2 mm).

Problems on creation of flux-cored wire on par with the best foreign specimens as to its technical data and provision of the domestic shipbuilding with gas-shielded wires of small diameter are solved by TM. VELTEK Company, one of the leading producers of flux-cored wire in Ukraine. In 1994–1996 a comprehensive research was carried out, which allowed developing and mastering production of gas-shielded flux-cored wire of new generation (grade PPs-TMV7) 1.0–2.5 mm in diameter (TUU 19369185.008–96). The flux-cored wire PPs-TMV7 and its production were adopted by the Russian Marine Navigation Register and Lloyds Register.

The latest achievements in the sphere of arc welding metallurgy were employed in developing a wire composition. Quickly setting rutile slag of increased basicity allows performing welding in all spatial positions. An alloying system provides mechanical properties of the deposited metal corresponding to the type E7T1 according to the standard AWS A5.20–95. The use of PPs-TMV7 wire is especially effective in welding of fillet and butt welds in vertical, horizontal and overhead positions with CO₂ or Ar + 18 % CO₂ mixture. In this case the deposition efficiency achieves 3.5 kg/h (Table 1).

The use of this flux-cored wire is highly effective in making root pass of the butt joints in all spatial positions using ceramic backing. Typical chemical composition of the deposited metal has the following content, wt.%: 0.05C; 0.32Si; 1.45Mn; 0.015S; 0.015P. Implementation of the gas-slag shielding of the welding pool leads to the minimal sensitivity of porosity caused by the grounds. Complex alloying of weld metal in combination with a low content of harmful impurities provides the required strength and



plastic properties with high level of impact strength of the weld metal (Table 2).

The improved production technology provides a stable quality of flux-cored wire. It is easily adapted to any types of semi-automatic machines for mechanized gas-shielded welding, characterized by an easy feed by hoses of semi-automatic machines. The flux-cored wire PPs-TMV7 is certified by UkrSEPRO. Tests of the manufactured products are controlled by the quality system TUF at the Open Joint Stock Company «Dneprometiz». The wire is supplied in bundles in the calcinated state in the standard cassettes K200 and K300 fully ready for application. The wire is packed in metallic drums 50–70 kg in mass by the GOST 26101–84. As requested by the consumer it may be packed in the paperboard boxes with one bun-

Table 2. Mechanical properties of deposited metal at the testing temperature $-20\text{ }^{\circ}\text{N}$

Index	Mechanical properties			
	σ_t , MPa, at least	σ_y , MPa, at least	δ , %	KCV, J/cm ²
Requirements of specifications	490–600	375	22	47
Testing results	560–620	440–500	23–25	80

dle or cassette in the box with preliminary packing into polyethylene package.

The TM. VELTEK, Ltd. Company delivers flux-cored wire on the following conditions: free carrier FCA or through its dealers in the Russian Federation.

THESIS

FOR A CANDIDATE OF TECHNICAL SCIENCES DEGREE



E.O. Paton Electric Welding Institute of the NAS of Ukraine

Ya.P. Chernyak (PWI) defended on 6 April 2005 his thesis for a candidate of technical sciences degree on the subject «Development of Consumables and Technology for Cladding of Worn-out Rails on an Active Tram Track»

The most important results of the thesis author are as follows.

Sparsely-alloyed flux-cored wire of the austenitic grade and fundamentally new flux-cored wire of the ferritic grade were developed for cladding of parts of high-carbon steels without preheating. The new wire has in its core a strong carbide forming element, i.e. titanium, which fully eliminates formation of martensite in deposited metal. Availability of these two wires with different alloying systems provides substantial widening of technological capabilities of cladding and ranges of parts of high-carbon steels to be repaired by the arc cladding methods without preheating.

It is shown that deposition of the first bead with the austenitic wire should be performed at increased energy input $Q = 28\text{--}30\text{ kJ/cm}$ to prevent formation of cracks of the spalling type. In this case, the HAZ structure is composed of a more ductile pearlitic-bainitic mixture, instead of martensite. Subsequent beads can be deposited under optimal conditions with an

energy input of $10\text{--}15\text{ kJ/cm}$. As opposed to this, deposition of all the beads with the ferritic wire is performed under the same optimal conditions.

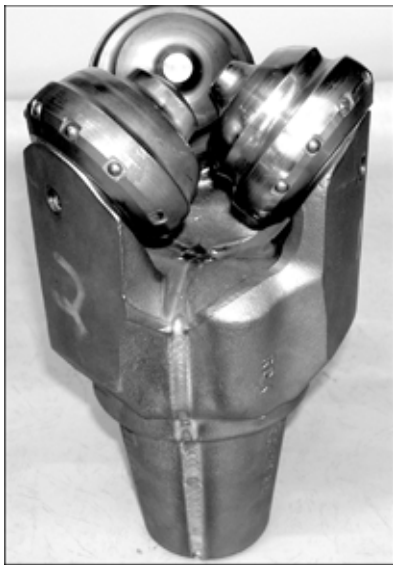
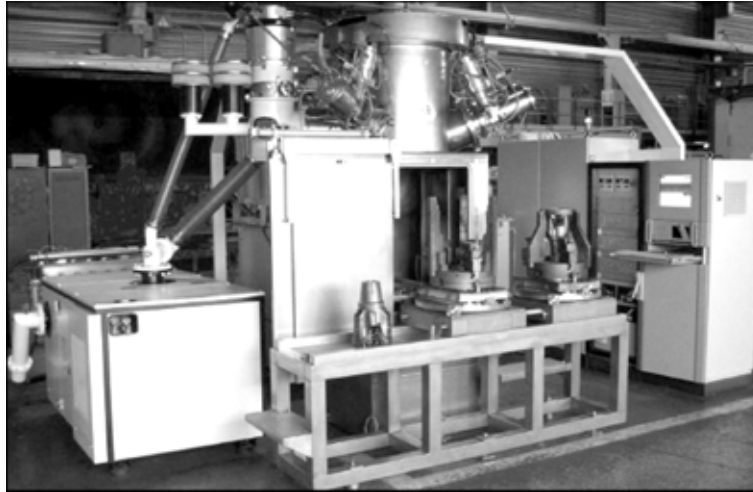
Tribological properties of deposited metal of the ferritic and austenitic grades in friction pairs with samples of high-carbon rail steel M76 were studied. The best wear resistance and lowest friction coefficient were exhibited by the austenitic deposited metal G13Kh13N2MF + steel M76 friction pair. Among the ferritic materials, the best tribological properties were exhibited by the deposited metal T3SGM + steel M76 friction pair.

Sanitary-hygienic and technological-welding evaluation of the developed flux-cored wires of the ferritic (PP-AN203) and austenitic (PP-AN202) grades was made for cladding of worn-out tram rails without preheating. These wires are included into TU 28.7.05416923.066–2002 of Ukraine, which makes it possible to apply them on a commercial scale.

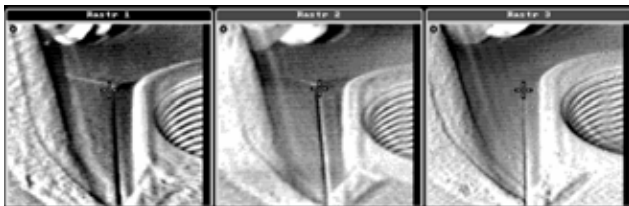
The technology was developed for cladding of tram girder rails without their dismantling, i.e. on an active tram track. The package of equipment for cladding of worn-out tram rails was developed and manufactured to implement the new technology. The technology, consumables and equipment passed the experimental-industrial verification at State Enterprise «Kievpasstrans» in cladding of region of a curve on the active tram track.

Repair of tram rails directly on the track does not only simplify and accelerate repair operations, but also allows saving of about 340 UAH per running metre of the rails. Service life of the repaired rails will be extended 2–5 times, compared with the new ones.

3-GUN MACHINE KL-117 FOR ELECTRON BEAM WELDING OF DRILL BITS



✓ Machine is intended for electron beam welding of drill bits up to 17.5" diameter with simultaneous performance of three welds, thus increasing both accuracy of drill bits dimensions and welding output.



✓ Application of a powerful control electronic tube in the accelerating voltage source prevents the arc processes in the welding gun by a short interruption of accelerating voltage, which does not lead to weld formation defects.

✓ The RASTR system, functioning on the principles of raster electron microscope, enables following the welding process and automatic coquidance of each of three electron beams to the butts of groove faces in the real time. The clear picture of the welding process is displayed on the monitor screen and is not exposed to the welded metal vapors, which is characteristic for traditional optical observing systems.

✓ Machine is provided with the electron beam diagnostic system allowing an operator:

- to define the beam focusing plane position prior to welding;
- to periodically evaluate changes in space and energy beam parameters in order to define the necessity of the welding gun cathode replacement.

✓ Lanthanum hexaboride cathode as a tablet has service life of not less than 40 h in the welding mode at beam power of 20 kW, and the beam axis position does not change at changes in beam focusing.

✓ Control of all equipment subsystems by means of CNC + PLC.

✓ The computer system of electron beam scanning stabilizes the molten pool state and improves the quality of face and root surfaces formation of the weld.

E.O. Paton Electric Welding Institute of NASU
11, Bozhenko Str., 03680, Kiev, Ukraine; Tel./ fax: (38044) 525 4319
E-mail: nazarenko@technobeam.com.ua www.nas.gov.ua/pwj/beam/index.html



FORTHCOMING BOOK INFORMATION

Vladimir I. Makhnenko, Viktor E. Pochynok. STRENGTH CALCULATION OF WELDED JOINTS WITH CRACK-LIKE IMPERFECTIONS.

Approx. 300 pp., 165 × 235 mm, hardback. November 2005. US\$ 90

In this manuscript, the idea of the fitness-for-purpose concept is used to improve strength calculations of welded joints with crack-like imperfections caused by structural or technological factors. These include welded joints with fillet, spot, slot and butt welds having sharp fissures brought by geometry of the elements welded and limited sizes of the weld sections. Such joints are widely encountered in modern general-purpose welded structures used in civil building, shipbuilding, automobile industries, etc.

The welded joints just mentioned do not usually cause problems for structures of relatively ductile materials with small-to-medium thicknesses of component sections, and operating under predominantly static loading. However, the use of new structural materials, especially high-strength steels and aluminum alloys, etc., large cross sections of structural elements, and loading with alternate loads, requires a certain caution to be taken. Nonetheless, the technological advantages that these joints produce attract an interest in their use, of course, when it does not cause any harm to the structure safety and its residual service life.

Performing strength calculations based on the fitness-for-purpose criterion for the joints encountered in general-purpose structures, allows ensuring the requirements concerning the service life-time. However, there is a difficulty of implementing such calculations in wide engineering practice. As shown by the authors, a successful implementation of the mentioned concept for general-purpose welded joints and for wide range of users is possible only when it is based on the use of corresponding computer systems with friendly user interface, which do not require a user to have a special knowledge in fracture mechanics, deformation mechanics, numerical methods, etc. Such systems are to be portable and efficient, i.e. calculations of appropriate section sizes or verification of strength of specific joints should be done promptly. In turn, it requires development of numerical procedures and creation of specialized databases that simplify and accelerate calculations.

Viktor Ya. Kononenko. TECHNOLOGIES OF UNDERWATER WET WELDING AND CUTTING.

Approx. 140 pp., 140 × 200 mm, softback. December 2005. US\$ 40

The book deals with the features of arcing, metal transfer and joint formation in consumable-electrode wet underwater welding. Principles of development of coated electrodes and self-shielded flux-cored wires for underwater welding and cutting are established. Characteristics of welding consumables and mechanical properties of weld metal are given. Some types of joints, procedure of preparation and fit-up for welding, possible defects of the joints and methods to prevent their formation are described.

Information on characteristic damage to the underwater metal structures is generalized, and technological solutions are given, which have been implemented during restoration of their performance, using wet processes of underwater welding and cutting. The book gives the characteristics of the equipment for implementation of underwater arc welding process.

The main processes of thermal underwater cutting are presented, and characteristics of consumable materials and equipment for its implementation are described. Examples of work performance using underwater cutting are given.

The book is designed for scientific and engineering-technical personnel, qualified welders-divers involved in design, fabrication and repair of underwater constructions.

The book is written by a specialist, who is developing electrode materials and technologies and has a vast experience of practical work under the water.

TITANIUM: Titanium and its alloys. Technologies. Equipment. Production. Electrometallurgy. Welding**Approx. 180 pp., 200×290 mm, softback. December 2005. US\$ 50**

The collection presents papers on electrometallurgy and welding of titanium and its alloys published between 2002 and 2005 in «Advances in Electrometallurgy» and «The Paton Welding Journal» journals. The authors of the papers are scientists and specialists in the field of titanium and its production, known in Ukraine and abroad. The collection is designed for a broad range of readers dealing with the problems of production, processing and use of titanium.

ORDER FORM

Please return to:

International Association «Welding»,
 11, Bozhenko str., Kiev, 03680, Ukraine
 Tel.: (38044) 287 6757, 287 6049, 529 2623
 Fax: (38044) 287 4677
 E-mail: journal@paton.kiev.ua; tomik@mac.relc.com

Please send me:

- Vladimir I. Makhnenko, Viktor E. Pochynok «Strength Calculation of Welded Joints with Crack-Like Imperfections». US\$ 90, postage included
- Viktor Ya. Kononenko «Technologies of Underwater Wet Welding and Cutting». US\$ 40, postage included
- «Titanium». Collection of Scientific Paper. US\$ 50, postage included

How to Pay and Payment Details

- By bank transfer (or mail a cheque) into our account
 № 2600801283433
 UKREXIMBANK, Kiev, Ukraine
 S.W.I.F.T.: EXBSUAUX
 CORR. ACC. #04-094-227
 Bankers Trust Company,
 New York, U.S.A.
 S.W.I.F.T.: BKTR US 33

 Please Invoice Your Details

Name _____

Organization _____

Address _____

Signed _____ Date _____

